CONTRACTOR REPORT
SAND94–0187 • UC–523
Unlimited Release
Printed August 1994

Evaluation of Conservatisms and Environmental Effects in ASME Code, Section III, Class 1 Fatigue Analysis

DOE
Plant Lifetime
Improvement Program

EPRI
Life Cycle Management
Program

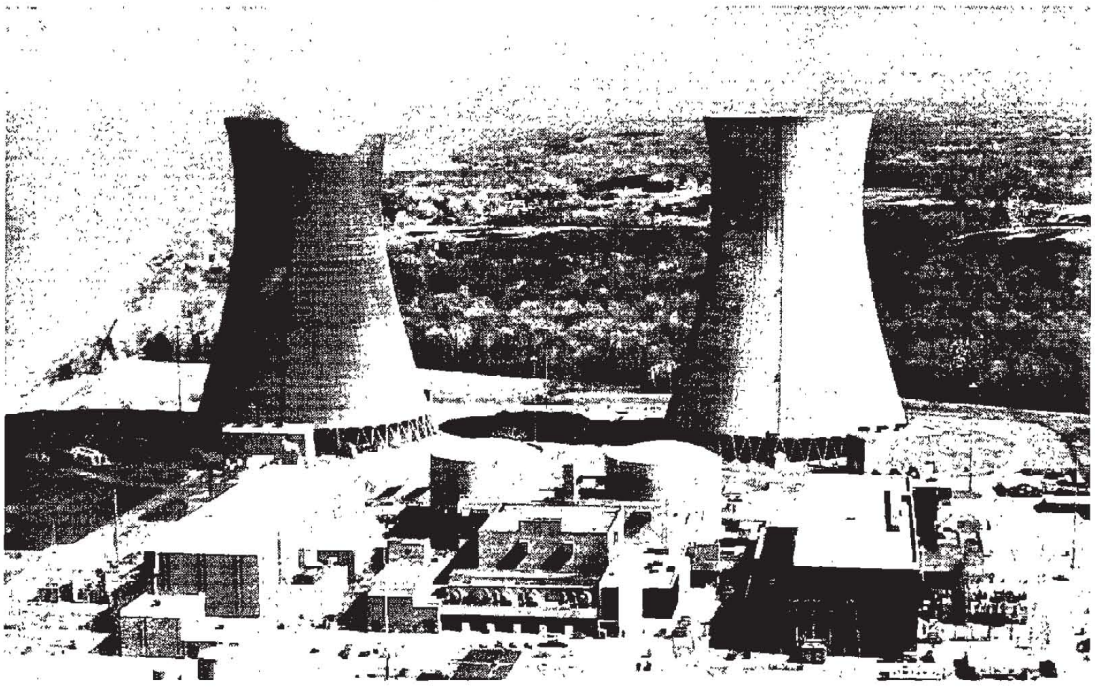

Prepared by Structural Integrity Associates, Inc., 3150 Almaden Expressway, Suite 145, San Jose, CA 95118, under contract to Sandia National Laboratories for the U.S. Department of Energy, in cooperation with the Electric Power Research Institute.

Funded by the U.S. Department of Energy under Contracts DE-AC04-76DP00789 and DE-AC04-94AL85000.

Issued by Sandia National Laboratories, operated for the United States Department of Energy by Sandia Corporation.

Available to DOE and DOE contractors from
Office of Scientific and Technical Information
PO Box 62
Oak Ridge, TN 37831

Prices available from (615) 576-8401, FTS 626-8401

Available to the public from
National Technical Information Service
US Department of Commerce
5285 Port Royal Rd
Springfield, VA 22161

NTIS price codes
Printed copy: A07
Microfiche copy: A01

SAND94-0187
Unlimited Release
Printed August 1994

Distribution
Category UC-523

EVALUATION OF CONSERVATISMS AND ENVIRONMENTAL EFFECTS IN ASME CODE, SECTION III, CLASS 1 FATIGUE ANALYSIS

Prepared by:

Structural Integrity Associates, Inc.
3150 Almaden Expressway, Suite 145
San Jose, CA 95118

Sandia Contract No. AF-1039

Authors:

Arthur F. Deardorff and Jay K. Smith

Under Contract to:

Sandia National Laboratories
Albuquerque, NM 87185
for the
U.S. Department of Energy

Project Manager:

James T. Nakos

Abstract

This report documents the results of a study regarding the conservatisms in ASME Code Section III, Class 1 component fatigue evaluations and the effects of Light Water Reactor (LWR) water environments on fatigue margins. After review of numerous Class 1 stress reports, it is apparent that there is a substantial amount of conservatism present in many existing component fatigue evaluations. With little effort, existing evaluations could be modified to reduce the overall predicted fatigue usage. Areas of conservatism include design transients considerably more severe than those experienced during service, conservative grouping of transients, conservatisms that have been removed in later editions of Section III, bounding heat transfer and stress analysis, and use of the "elastic-plastic penalty factor" (K_e). Environmental effects were evaluated for two typical components that experience severe transient thermal cycling during service, based on both design transients and actual plant data. For all reasonable values of actual operating parameters, environmental effects reduced predicted margins, but fatigue usage was still bounded by the ASME Section III fatigue design curves. It was concluded that the potential increase in predicted fatigue usage due to environmental effects should be more than offset by decreases in predicted fatigue usage if re-analysis were conducted to reduce the conservatisms that are present in existing component fatigue evaluations.

Acknowledgments

This report was prepared by Structural Integrity Associates, Inc., under the direction of the Department of Energy Light Water Reactor Technology Center at Sandia National Laboratories, Advanced Nuclear Power Technology Department 6471. Funding for this report was provided by the Department of Energy Light Water Reactor Safety and Technology Branch, NE-451, Dennis Harrison, Program Manager. Assistance of the Electric Power Research Institute Life Cycle Management Subcommittee is gratefully acknowledged. Review and comments were provided by members of the Nuclear Energy Institute (NEI, formerly NUMARC) Fatigue Ad Hoc Advisory Committee (AHAC) and other expert reviewers. Cover photograph of the Perry Nuclear Power Plant provided courtesy of Cleveland Electric Illuminating Company.

Contents

Contents

Figures

Figures (continued)

Tables

Nomenclature

α	=	Coefficient of thermal expansion.
E	=	Modulus of Elasticity (Young's modulus).
F_c	=	Factor of safety on cycles in the fatigue design curves.
F_s	=	Factor of safety on stress in the fatigue design curves.
K_e	=	Elastic-plastic penalty factor (See Section 2.4).
N	=	Allowable number of cycles obtained from design fatigue curve.
m,n	=	Material parameters defined in Table 2-2 which are used to calculate K_e.
P_b	=	Bending stress (primary)
P_e	=	Expansion stress (secondary)
P_L	=	Local membrane stress (primary)
P_m	=	General membrane stress (primary)
Q	=	Membrane plus bending stress (secondary)
S_{alt}	=	Amplitude of stress used to enter the design fatigue curve. Also called S_a in some sections of the Code.
S_m	=	Design stress intensity value.
$3S_m$	=	Allowable stress intensity for primary plus secondary stresses.
S_n	=	Primary plus secondary stress in piping components as calculated using Equation 10 of NB-3650.
S_p	=	Peak stress in piping components as calculated using Equation 11 of NB-3650.
S_y	=	Yield stress of material.
S_u	=	Ultimate stress of material.
T_a - T_b	=	Difference between ranges of average temperatures on side a and side b of a structural discontinuity, when the component goes from one load set to another.
U	=	Cumulative usage factor.
ΔT_1	=	Range of the temperature difference for each load set pair between the temperature of the outside surface and the temperature of the inside surface of the piping component assuming a moment generating equivalent linear temperature distribution.
ΔT_2	=	Range for that portion of the nonlinear thermal gradient through the wall thickness not included in ΔT_1.

Executive Summary

Metallic fatigue of Light Water Reactor (LWR) materials is a Generic Safety Issue (GSI) for commercial nuclear power plants. U.S. Nuclear Regulatory Commission (NRC) concerns about fatigue led to the issuance of a draft branch technical position (BTP) on fatigue for license renewal (BTP PLDR D-1). This draft BTP has since been withdrawn, and has been replaced by a generic regulatory evaluation plan of the fatigue issue for operating plants ("Fatigue Action Plan"). NUMARC Industry Reports and other industry studies contend that the current licensing basis (CLB) for fatigue is adequate. The only potential exceptions are components with geometric discontinuities (e.g., socket welds) and components with severe, step change thermal transient loadings. Although the original NUMARC position was formulated for license renewal, fatigue remains a concern due to the potential negative effects of the LWR environment on the fatigue life of components, and other issues (e.g., plants designed under ANSI B31.1 rather than ASME Section III).

The purpose of this study was to document the types and extent of conservatisms present in the overall ASME Section III, Class 1, fatigue design/analysis process. This report documents the results of this study. The types of conservatisms present in ASME Section III Code fatigue evaluations of Class 1 components are described. In addition, the report describes an evaluation of the effects of the LWR environment on two typical components based on both design transients and typical plant data.

After reviewing numerous Class 1 stress reports, it was apparent that there is a substantial amount of conservatism in many of the fatigue evaluations. There were two areas of conservatism: those inherent in the ASME Code, Section III fatigue design rules and those added by the analyst. Although the fatigue usage reported in many stress reports does approach the allowable of 1.0, this does not necessarily mean that the component is fatigue sensitive. As long as it was possible to show that the fatigue usage was less than 1.0 with a simplified, bounding analysis, the Section III fatigue requirement was met. Often, no additional analysis was performed to show that requirements could be met by a larger margin. Because of this, the analysis of record for many components contains conservative assumptions which reduced the amount of work required to perform the evaluation.

One area of conservatism in Class 1 fatigue evaluations concerns the operating pressure and temperature transients which were defined in the component Design Specifications. It was found in this study that fatigue usage for actual plant transients obtained from in-plant monitoring systems was significantly less than that calculated for the design-basis transients. Analytical techniques have become more sophisticated and less conservative since the time when many of the stress evaluations were performed (late 1960s and early 1970s). Use of these more sophisticated techniques reduced conservatisms in predicted fatigue usage. Also, there were conservatisms inherent in the ASME Code, some of which were removed in later editions.

Environmental effects on two components known to be affected by severe thermal transients were also investigated in this study. Based on evaluations of both design-basis transients and actual plant data, it was found that environmental effects are clearly bounded by ASME Code fatigue curve margins. Whereas this margin is approximately 20 (on cycles) for low cycle (less than 50,000 cycles) fatigue, it was concluded that a margin of 10 remains even when

environmental effects are included. Several key issues were identified that need to be resolved with respect to application of environmental fatigue data to design of actual components.

Based on the overall findings of the report, it is concluded that the reductions in margin due to environmental effects are more than offset by the conservatisms found in typical ASME Code fatigue evaluations.

This page intentionally left blank.

EVALUATION OF CONSERVATISMS AND ENVIRONMENTAL EFFECTS IN ASME CODE, SECTION III, CLASS 1 FATIGUE ANALYSIS

1. INTRODUCTION

1.1 Background

Metallic fatigue of Light Water Reactor (LWR) materials is a Generic Safety Issue (GSI) for commercial nuclear power plants. U.S. Nuclear Regulatory Commission (NRC) concerns (e.g., LWR environmental effects, ANSI B31.1 vs. ASME Section III designed plants, what to do when the cumulative usage factor is greater than 1, etc.) about fatigue led to issuance of a draft branch technical position (BTP) on fatigue for license renewal (BTP PLDR D-1 [1.1]). This draft BTP has since been withdrawn, and has been replaced by a generic regulatory evaluation plan of the fatigue issue for operating plants ("Fatigue Action Plan") [1.2]. NUMARC Industry Reports and other industry studies contend that the current licensing basis (CLB) for fatigue is adequate; design requirements (e.g., ANSI B31.1 [1.3, 1.4], or ASME Section III, Class 1 [1.5]), inservice examination requirements (e.g., ASME Section XI [1.6]) and licensing commitments related to fatigue (e.g., monitoring of operating transients) are adequate with a few exceptions. Two exceptions were identified. The first was components with geometric discontinuities (e.g., socket welds). The second was components with step change thermal transient loadings (e.g., reactor coolant system nozzles for the emergency core cooling system (ECCS)).

In order to provide quantitative information regarding fatigue issues in nuclear power plants, the U.S. Department of Energy, through its LWR Technology Center at Sandia National Laboratories (SNL), in cooperation with the Electric Power Research Institute (EPRI), has initiated several efforts regarding fatigue evaluation of nuclear power plant components. A companion study sponsored by EPRI [1.7] compared the results of fatigue evaluation methods for piping designed to the ANSI B31.1 Code to those of ASME Section III, Class 1. ASME Section III fatigue analyses were performed for two fatigue sensitive locations in reactor coolant piping systems, which were originally designed to ANSI B31.1. These evaluations showed that the B31.1 designed systems had limited areas with high fatigue usage. In both systems, the locations of high fatigue usage were those with geometric (or material) discontinuities that were also affected by severe step change thermal design transients. The evaluations also showed that a stress analysis based on the requirements of the current version of the ASME Code produces significantly less fatigue usage than the earlier Code versions used for design of most domestic plants in service today, with the reduced usage due to the reclassification of through-wall thermal gradients.

1.2 Purposes and Objectives

The purpose of this study was to document the types and extent of conservatisms present in the overall ASME Section III, Class 1, fatigue design/analysis process. These conservatisms could be implicit in the ASME Code itself, in the application of the ASME Code, or in the plant design transients that generate most of the fatigue usage. The conservatisms identified can then be compared to any nonconservatisms that might be due to "environmental effects" (oxygen content, water chemistry, strain rate, etc.). This evaluation was accomplished by reviewing existing stress reports for Class 1 components for Westinghouse, General Electric (GE), Babcock & Wilcox (B&W), and Combustion Engineering (CE) designed plants. The conservatisms in design transients were evaluated by comparing the actual transients, as collected by fatigue transient monitoring systems installed in operating plants, with the design transients. The effects of LWR environment (oxygen content, strain rate, and temperature) were considered by incorporating the available fatigue test data for the LWR environment into the fatigue monitoring system, then recalculating usage factors that incorporate environmental effects for both the actual and design transients.

Considering that fatigue evaluations for plants provided by four different designers were to be reviewed, there were a large number of Class 1 components that could be considered in this study. The components for this study were chosen based on several criteria. They were:

1. A "broad base" of the Class 1 components were considered. In other words, components such as Reactor Pressure Vessel (RPV) nozzles, RPV internal structures, RPV head bolts and flanges, RPV supports, pressurizers, steam generators, piping systems, and containment penetrations were components included in this study.

2. "Problem areas" (i.e., areas with high predicted usage factors) were included. For each plant, only the components with the highest usage factors were considered. The Class 1 components were not "screened" to find usage factors that could easily be reduced.

3. An area of potential nonconservatism, LWR water environmental effects on fatigue usage, was also considered. The possibility of this potential nonconservatism offsetting conservatisms found in other areas was evaluated.

For the purpose of providing sufficient background regarding ASME Class 1 fatigue evaluations, Section 2 describes the historical development of the ASME Section III fatigue evaluation. The process of performing an ASME Code design and fatigue evaluation is also described on a step-by-step basis. ASME Code fatigue requirements are discussed for vessel components and piping, along with changes that have occurred in the Code over the past 20 years. For those readers who already have sufficient understanding of ASME Section III fatigue evaluation methodology, skipping to Section 3 may be appropriate.

Section 3 provides a description and discussion of each of the potential conservatisms. Section 4 describes the results of the plant specific evaluations of the conservatisms. Section 5 describes fatigue monitoring methodology, and existing in-plant monitoring results are presented. In-plant monitoring results are compared with simulated transient results based on the transients

defined in the plant Design Specification. In Section 6, LWR environmental effects on the ASME Code fatigue curves are discussed. Actual plant data are evaluated to show the effects of the LWR environment on the usage factors. Conclusions are summarized in Section 7.

Although actual ASME Section III, Class 1 fatigue evaluations are used, the plant names are not included in this report at the request of the utilities that have allowed their plants to be included in this study.

1.3 References

1.1 Letter from J.W. Craig (USNRC) to E.P. Griffing (NUMARC), "Fatigue Evaluation in NUMARC License Renewal Industry Reports and NUMARC Industry Report Status Sheets," (TAC No. M80644), with attached Branch Technical Position, PLDR D-1, "Fatigue Evaluation Procedures," December 12, 1991.

1.2 Letter from W.T. Russell (USNRC) to W. Rasin (NUMARC), "NRC Staff Action Plans Concerning the Issue of Environmental Requalification and Fatigue Analysis of Components," July 30, 1993.

1.3 "Code for Pressure Piping," ASA B31.1-1955, American Society of Mechanical Engineers, New York, NY.

1.4 "Power Piping," USAS B31.1.0-1967, American Society of Mechanical Engineers, New York, NY.

1.5 "Rules for Construction of Nuclear Power Plant Components," Section III, Division 1, 1992 ASME Boiler and Pressure Vessel Code, American Society of Mechanical Engineers.

1.6 "Rules for Inservice Inspection of Nuclear Power Plant Components," Section XI, 1992 ASME Boiler and Pressure Vessel Code, American Society of Mechanical Engineers.

1.7 "Comparison of Piping Designed to ANSI B31.1 and ASME Section III, Class 1," Prepared for Electric Power Research Institute by Structural Integrity Associates, Inc., EPRI Report No. TR-102901, August, 1993.

This page intentionally left blank.

2. BACKGROUND*

2.1 History of Fatigue Evaluation in the ASME Section III Code

In the early 1900s boiler explosions in the United States occurred at the approximate rate of one per day [2.1]. This situation was almost completely remedied by the publication of design rules for boilers in the ASME Boiler Code in 1914. The design rules in this code were based on an allowable value for membrane stress due to internal pressure equal to one-fifth of the ultimate tensile strength of the material used to fabricate the boiler. Simple rules guided the design of regions in the vessel that had relatively complex geometries where membrane stresses could not easily be calculated. During World War II, the factor of safety against ultimate tensile failure was reduced from five to four as a wartime measure to reduce the amount of steel used in construction of boilers [2.2]. Because of this reduction in factor of safety and the introduction of new design technology and high strength materials, it was felt that consideration of additional failure modes was necessary. Specifically, failure due to fatigue cracking caused by localized stresses needed to be considered.

Section III of the ASME Boiler and Pressure Vessel Code ("Section III") was first published in 1963 and contained rules for design and construction of Reactor Pressure Vessels. A design by analysis concept was utilized which differed completely from the design by formula concept utilized in the Section I (Power Boilers) and Section VIII (Pressure Vessels) Codes. The 1963 Edition of Section III was the first of the ASME Codes to require explicit evaluation of non-membrane stresses, such as self-limiting (secondary) and localized stresses. It also recognized that the allowable stresses for the secondary and local stresses should be higher than for membrane stresses. There have been many revisions and additions to the requirements of the ASME Section III Code since 1963. The 1971 Edition of Section III was expanded to include requirements for design of piping, metal containment systems, valves, and pumps. It should be noted that the rules for Class 1 piping were an outgrowth of the ANSI B31.7 Nuclear Power Piping Code [2.3], which was eventually replaced by Subsection NB of ASME Section III. An additional important change regarding fatigue evaluations was made in the 1971 Edition. This was the inclusion of a methodology to perform a simplified elastic-plastic analysis if it could not be shown that the primary plus secondary stresses would "shakedown" to purely elastic behavior after several cycles of loading. Another important change which affected ASME Section III Code fatigue evaluations was the extension of fatigue curves for austenitic steel, nickel-chromium-iron alloys, nickel-iron-chromium alloys, and nickel-copper alloys from 10^6 to 10^{11} cycles in 1982.

2.2 ASME Code Design Process

The ASME Code [2.4] design process begins with preparation of a Design Specification. From NCA-3250 of the ASME Code, it is the responsibility of the Owner of the nuclear power plant to "provide, or cause to be provided, Design Specifications for components, appurtenances,

* Because Section 2 describes the ASME Section III Code related to fatigue design, those familiar with the Code may choose to skip to Section 3.

and component and piping supports." The contents of the Design Specification must include the following:

1. The functions, configuration (basic dimensions), and boundaries of the items covered;

2. The design requirements, which include temperatures, pressures, and mechanical loads to which components and supports are subjected to in consequence of plant or system operating and test conditions;

3. The environmental conditions, including radiation;

4. The code classification of the items covered;

5. Material requirements, including impact test requirements;

6. Operating requirements of the component (if applicable); and

7. The effective Code Edition, Addenda, and Code Cases to be used for construction.

Code classification of components is the Owner's responsibility. The Owner must decide whether a component should be designed according to the rules of Class 1, Class 2, Class 3, Class MC (Metal Containments) or Class CS (Core Support Structures). Guidance for this classification is not specifically provided by the ASME Code but can be found in engineering standards or in the requirements of regulatory and enforcement authorities having jurisdiction at the nuclear power plant site. Typical Class 1 components include pressure retaining components in contact with reactor coolant such as the RPV, RPV nozzles, piping directly attached to the RPV nozzles, and internal structures integrally attached to the RPV. Of particular importance to Class 1 fatigue evaluations is the definition of operating pressure and temperature transients and mechanical loads. This definition must include the time history of each event (startup, shutdown, safety relief valve (SRV) discharge, etc.) and the number of cycles associated with each event.

Based on the geometry, material, loading and Code classification information presented in the Design Specification, the thicknesses of plate, piping and nozzles can be calculated by use of formulas in Section III. For the case of components designated as Class 1, Subsection NB-3000 provides rules which limit calculated stresses in the components to the basic allowable stress provided by Section III. Guidelines are provided in this subsection for calculation of minimum wall thicknesses. It should be noted that these are minimum wall thicknesses, and serve as a starting point in the design process. The following are examples of the "initial design by formula" approach:

1. NB-3133 describes formulas which, when used in conjunction with figures included in the Appendices to Reference 2.4, define the minimum plate thicknesses for cylindrical and spherical shells, tubes, fittings, and pipes when these components are subjected to external pressure loadings;

2. NB-3324 provides formulas as an "aid to the designer for determining a tentative thickness" for cylindrical and spherical shells which are loaded by internal pressure loadings; and

3. NB-3641 gives formulas for the minimum required thickness of the wall of a straight pipe loaded by internal pressure.

The internal or external pressures used in these formulas are Design Pressures, as opposed to operating pressures. The Design Pressures and Temperatures are defined in the Design Specification. The Design Pressure is taken as the maximum difference in pressure between the inside and outside of the component which can exist during normal operation, including allowances for pressure surges, control system error and system configuration effects such as static pressure heads.

The next step in the design process of a Class 1 component is a detailed stress analysis. For most Class 1 components, analytical models based on the finite element method have been employed to perform the stress analysis. The finite element method [2.5] is a numerical method in which the component to be analyzed is subdivided into a large number of "finite elements." There are a number of different formulations, but most finite elements are based on assumed displacement shapes over the area or volume which is occupied by that element. The finite elements can be two dimensional (plane stress, plane strain or axisymmetric) or three dimensional (solid "brick" elements or thick shell). Stress analysis of vessels and nozzles are normally accomplished by use of the finite element method. The finite element method can also be used to perform heat transfer analyses for the purpose of calculating temperatures in the component of interest. Finite difference methods have also been used for this purpose. Vessels and nozzles have sometimes been analyzed by thin shell theory. Within the limitations of thin shell theory regarding geometry and loading, "exact" stress results are obtained from closed form solutions. Piping systems are modeled by one dimensional beam and truss elements. The displacement functions for these elements are theoretically exact, so they are not finite elements in the classical sense of the term, although beam models of piping systems are sometimes referred to as finite element models.

Class 1 RPVs, RPV nozzles, and RPV internal structures are evaluated based on the "design by analysis" rules of NB-3200. Certain piping components, such as flued heads, are also evaluated according to these rules. Figures 2-1 and 2-2, which are taken directly from NB-3200, summarize the allowable stress requirements for the various types of stresses. The stresses basically fall into three categories; primary, secondary and peak. These various types of stresses are calculated by use of the analytical models described in the above paragraph. Primary and secondary stresses can normally be calculated with a reasonable degree of accuracy by these models, but it is sometimes difficult to capture the maximum peak values of stress. This is particularly true in the presence of local structural discontinuities such as fillet welds, where NB-3200 requires the use of fatigue strength reduction factors to account for stress concentration effects.

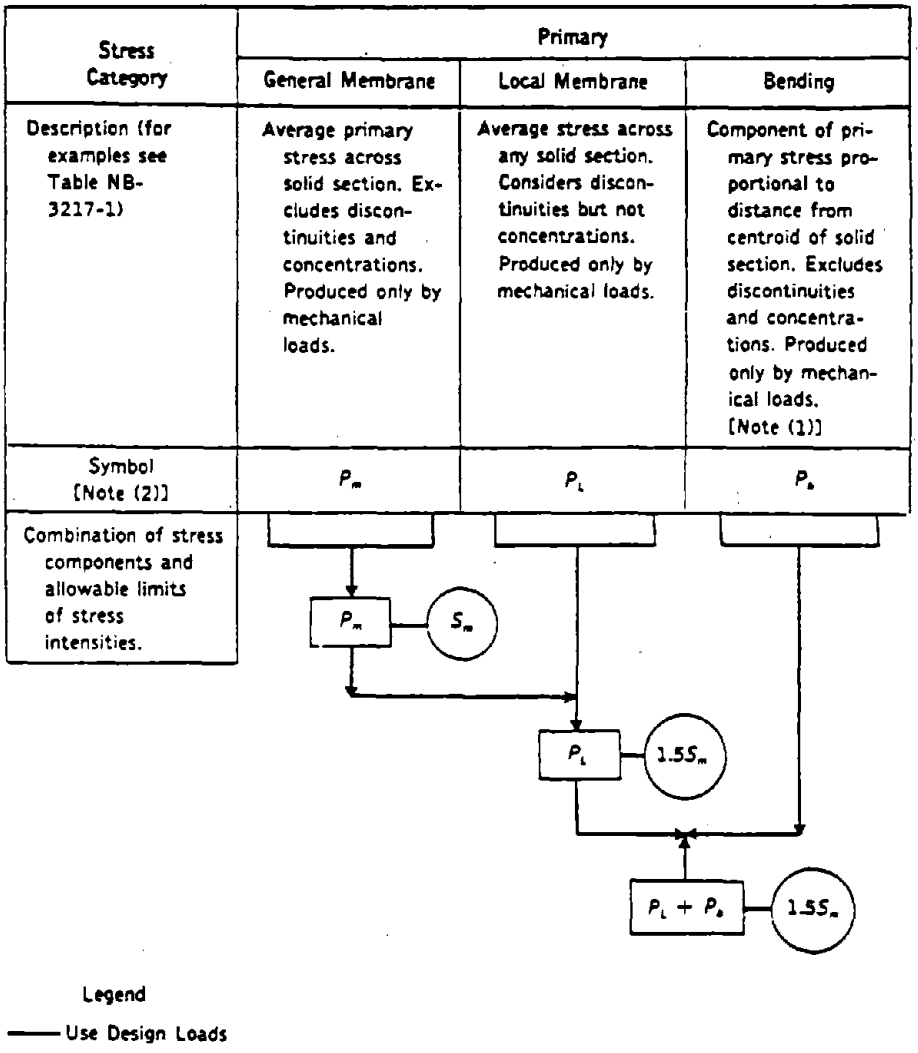

NOTES:
(1) Bending component of primary stress for piping shall be the stress proportional to the distance from centroid of pipe cross section.
(2) The symbols P_m, P_L, and P_b do not represent single quantities, but rather sets of six quantities representing the six stress components σ_t, σ_l, σ_r, τ_{tl}, τ_{lr}, and τ_{rt}.

Figure 2-1. Stress Categories and Limits of Stress Intensity for Design Conditions (Figure NB-3221-1 of Reference 2.4).

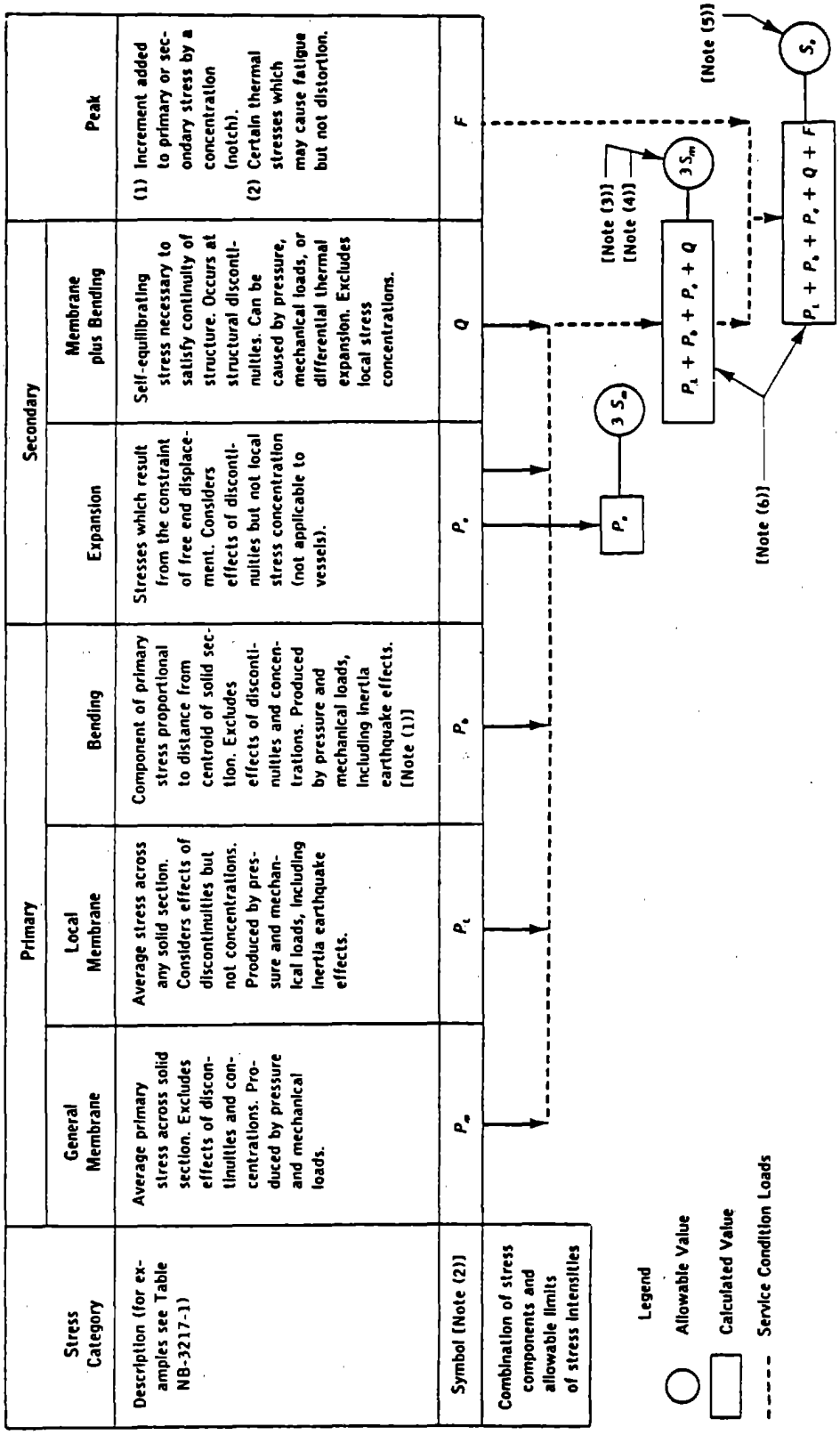

NOTES:
(1) Bending component of primary stress for piping shall be the stress proportional to the distance from centroid of pipe cross section.
(2) The symbols P_m, P_L, P_b, P_e, Q, and F do not represent single quantities, but sets of six quantities representing the six stress components σ_x, σ_y, σ_z, τ_{xy}, τ_{yz}, and τ_{zx}.
(3) When the secondary stress is due to a temperature transient at the point at which the stresses are being analyzed or to restraint of free end deflection, the value of S_m shall be taken as the average of the tabulated S_m values for the highest and the lowest temperatures of the metal during the transient. When part or all of the secondary stress is due to mechanical load, the value of S_m shall not exceed the value for the highest temperature during the transient.
(4) Special rules for exceeding $3S_m$ are provided in NB-3228.5.
(5) S_r is obtained from the fatigue curves, Figs. I-9.0. The allowable stress intensity for the full range of fluctuation is $2S_r$.
(6) The stresses in category Q are those parts of the total stress that are produced by thermal gradients, structural discontinuities, etc., and they do not include primary stresses that may also exist at the same point. However, it should be noted that a detailed stress analysis frequently gives the combination of primary and secondary stresses directly and, when appropriate, the calculated value represents the total of $P_m + P_e + Q$, and not Q alone. Similarly, if the stress in category F is produced by a stress concentration, the quantity F is the additional stress produced by the notch over and above the nominal stress. For example, if a point has a nominal stress intensity P_m and has a notch with a stress concentration factor K, then $P_m \leq S_m$, $P_e = Q$, $Q = 0$, $F = P_m(K - 1)$, and the peak stress intensity equals $P_m + P_m(K - 1) = KP_m$. However, P_L is the total membrane stress that results from mechanical loads, including discontinuity effects, rather than a stress increment. Therefore, the P_L value always includes the P_m contribution.

Figure 2-2. Stress Categories and Limits of Stress Intensity for Level A and Level B Service Limits (Figure NB-3222-1 of Reference 2.4).

Assuming that the primary stresses and primary plus secondary stresses meet the allowable stress requirements shown in Figures 2-1 and 2-2, the total stress range due to the combined primary plus secondary plus peak stresses is then calculated. As will be explained in detail in Section 2.3, the total stress amplitudes for all significant load set pairs are then used to enter the fatigue curves in the Section III, Appendices (Figures I-9.1 through I-9.5 of Reference 2.4). A load set is defined as a combination of pressure, temperature and force/moment loadings. A load set pair is two load sets that are compared to form a total stress range. Three of the fatigue design curves are shown in Figures 2-3, 2-4, and 2-5. The allowable number of cycles are obtained from these curves. The Design Specification defines the number of cycles for each loading condition. Knowing the number of design cycles and allowable number of cycles, usage factors, the ratio of the number of design cycles to the allowable number of cycles for each load set pair (so called "Palmgren-Miners Rule"), can be calculated. The summation of the individual usage factors for all of the significant load set pairs is called the cumulative usage factor. If the cumulative usage factor is less than or equal to 1.0, the ASME Section III Code requirements for fatigue are satisfied.

Rules for fatigue evaluation of Class 1 piping are presented in NB-3650. The rules are presented as equations, which are discussed in detail in Section 2.4. The philosophy is fundamentally the same as that used in NB-3200. Using the bending moment results obtained from the piping analytical models for the mechanical and thermal loadings defined in the Design Specification, and through-wall temperature ranges corresponding to the significant load set pairs, peak stress ranges are calculated. The cumulative usage factor is then calculated in the same manner as described above, using the same fatigue curves, with the goal being to demonstrate a cumulative usage factor of less than 1.0.

If, for any component, the calculated usage factor is greater than 1.0, two options are available. One option would be to redesign the component so that stresses would be reduced. As an example, a thermal sleeve could be installed inside of an RPV nozzle to protect the inside surface of the nozzle from thermal cycling due to cold water being injected into the RPV from the attached piping. The second option involves the "fine tuning" of the fatigue analysis to remove unnecessary conservatisms from the analysis while continuing to meet the fatigue requirements in Section III.

2.3 NB-3200 Fatigue Rules

The major goal of the design rules in Section III, Subsection NB-3000 is to provide protections against two different types of failure:

1. Protection against membrane or catastrophic failure;

2. Protection against fatigue or leak-type failure.

NB-3213 defines a number of terms that are related to stress analysis which are used in Section III. Membrane stress is the component of normal stress equal to the average value of stress across the section under consideration. Bending stress is the variable component of normal stress which may or may not be linear across the section thickness. Primary stress is any normal stress or shear stress developed by an imposed loading which is necessary to satisfy the laws of

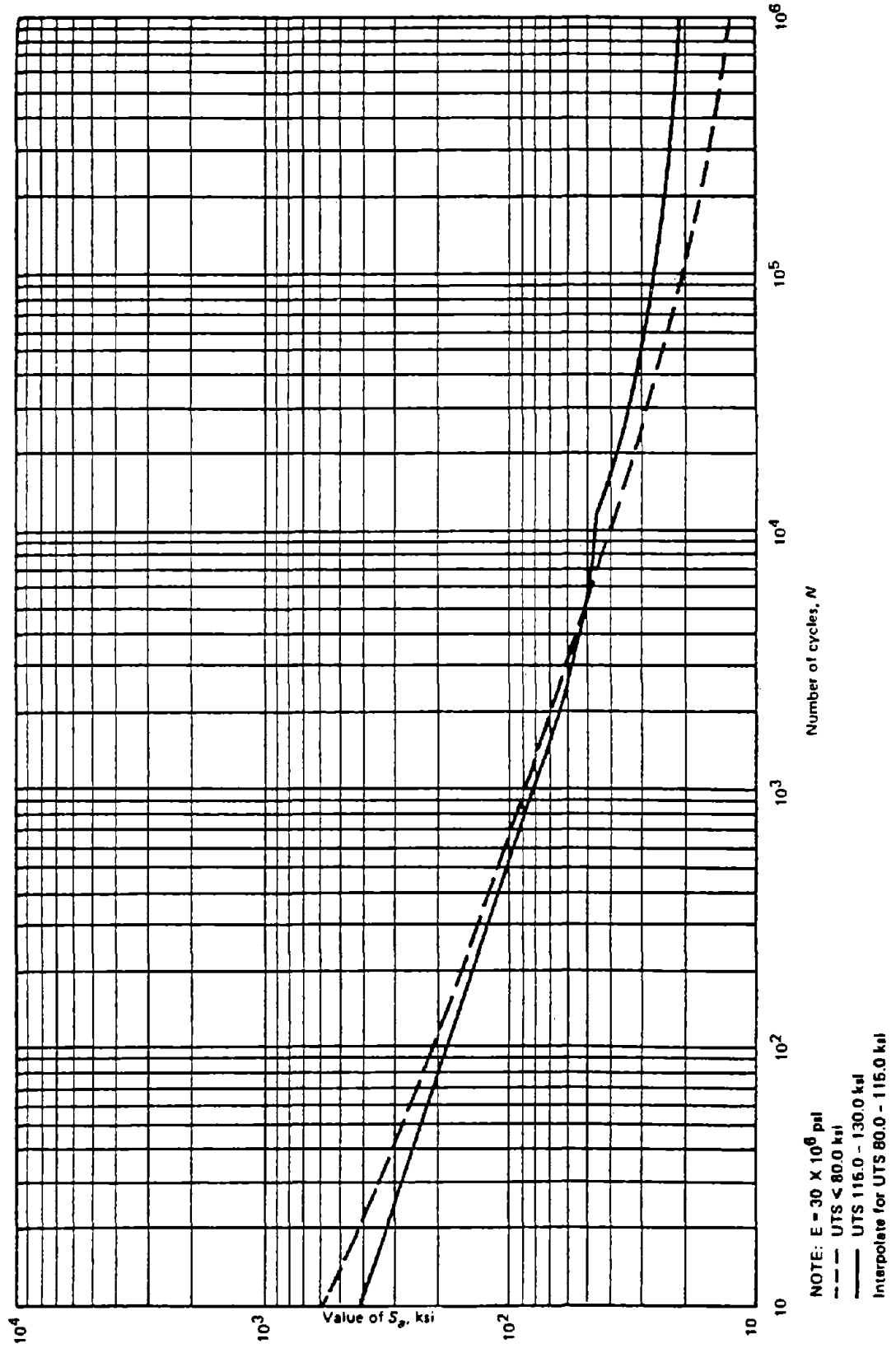

Figure 2-3. Design Fatigue Curves for Carbon, Low Alloy, and High Tensile Steels for Metal Temperatures Not Exceeding 370°C [700°F] (Figure I-9.1 of Reference 2.4).

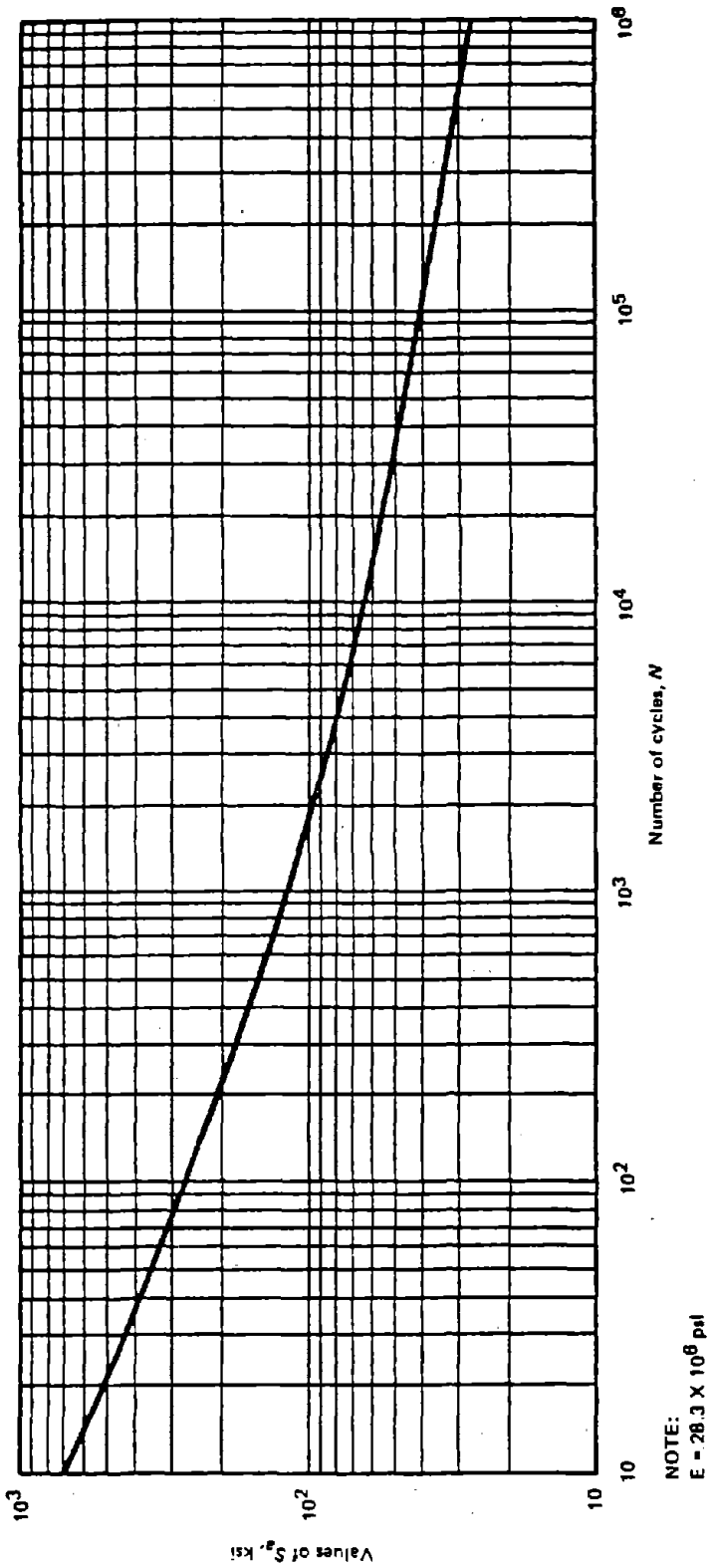

Figure 2-4(a). Design Fatigue Curve for Austenitic Steels, Nickel-Chromium-Iron Alloy, Nickel-Iron-Chromium Alloy, and Nickel-Copper Alloy for S_a > 194.4 MPa [28.2 ksi], for Temperatures Not Exceeding 427°C [800°F] (Figure I-9.2.1 of Reference 2.4).

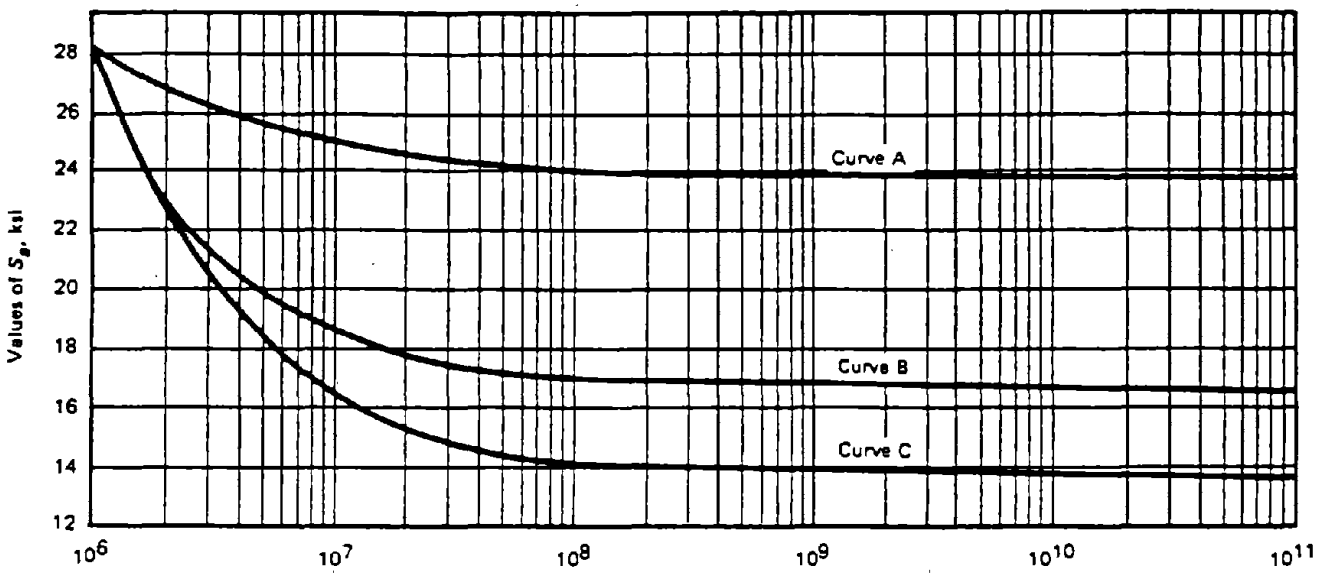

Criteria for the Use of the Curves in This Figure
[Notes (1)–(5)]

Curve	Elastic Analysis of Material Other Than Welds and Adjacent Base Metal	Elastic Analysis of Welds and Adjacent Base Metal
A	$(P_L + P_b + Q)_{Range} \leq 27.2$ ksi	. . .
B	$(P_L + P_b + Q)_{Range} > 27.2$ ksi and S_a is corrected for applied mean stress	$(P_L + P_b + Q)_{Range} \leq 27.2$ ksi
C	$(P_L + P_b + Q)_{Range} > 27.2$ ksi	$(P_L + P_b + Q)_{Range} > 27.2$ ksi

NOTES:
(1) Range applies to the individual quantities P_L, P_b, and Q and applies to the set of cycles under consideration.
(2) Thermal bending stresses resulting from axial and radial gradients are excluded from Q.
(3) Curve A is also to be used with inelastic analysis with $S_a = \frac{1}{2} \Delta \epsilon_t E$, where $\Delta \epsilon_t$ is the total effective strain range.
(4) The maximum effect of retained mean stress is included in Curve C.
(5) The adjacent base metal is defined as three wall thicknesses from the center line of the weld.

Figure 2-4(b). Design Fatigue Curve for Austenitic Steels, Nickel-Chromium-Iron Alloy, Nickel-Iron-Chromium Alloy, and Nickel-Copper Alloy for $S_a \leq 194.4$ MPa [28.2 ksi], for Temperatures Not Exceeding 427°C [800°F] (Figure I-9.2.2 of Reference 2.4)..

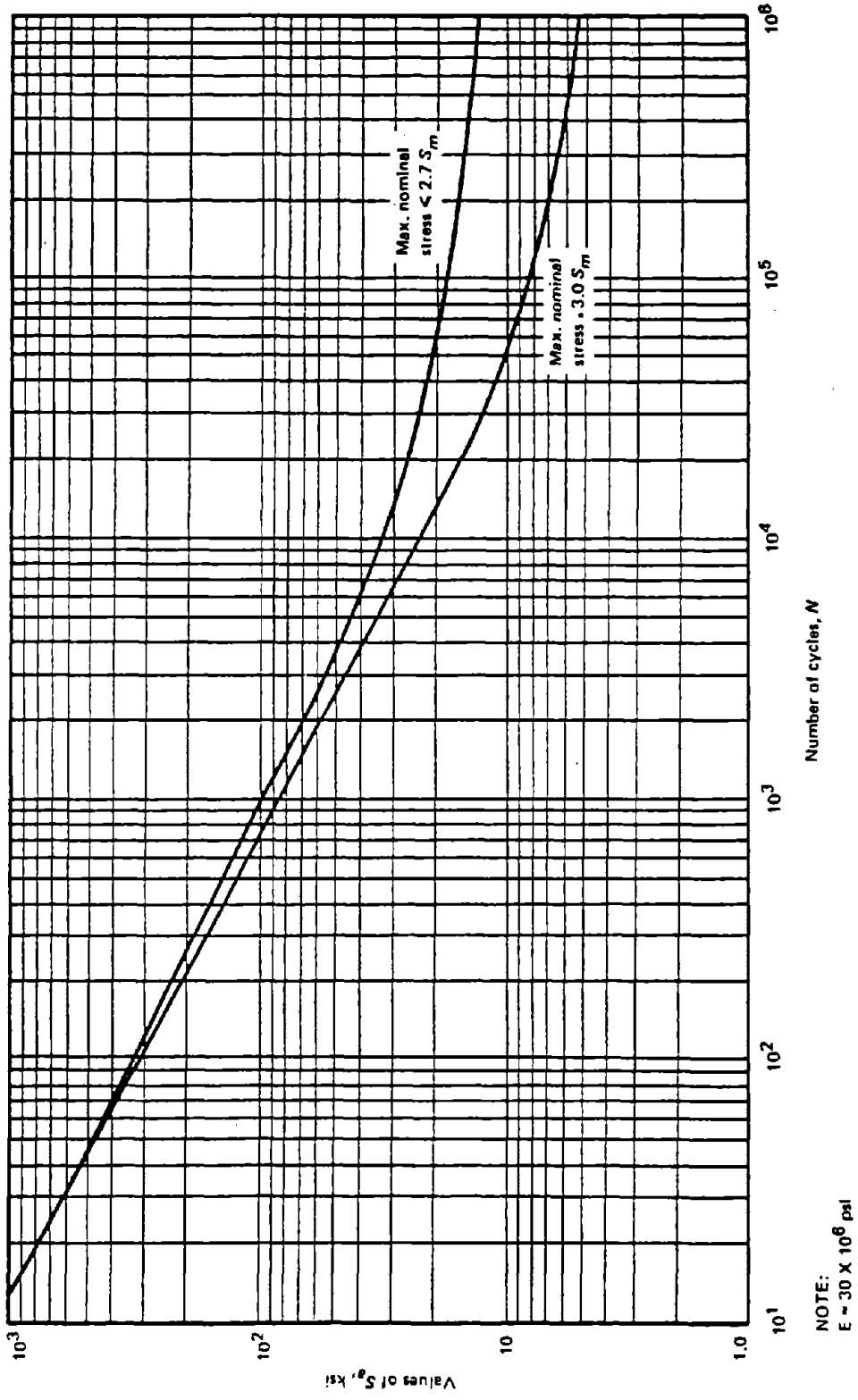

Figure 2-5. Design Fatigue Curves for High Strength Steel Bolting for Temperatures Not Exceeding 370°C [700°F] (Figure I-9.4 of Reference 2.4).

equilibrium of external and internal forces and moments. Primary stresses that exceed the yield strength by a significant amount will result in gross distortion or possibly in failure of the component. In Section III terminology, primary stresses are not self-limiting. The following are examples of primary stresses:

1. Membrane stresses in cylindrical or spherical shell structures due to internal pressure;

2. Bending stress at the center of a flat plate due to pressure acting normal to the plane of the plate.

Secondary or self-limiting stresses are defined by NB-3213 as stresses developed by the constraint of adjacent material or by self-constraint of the structure. Secondary stresses are self-limiting. Local yielding and minor distortions can satisfy the displacement compatibility conditions which cause the stress to occur. Section III classifies some types of thermal stresses as secondary stresses. Thermal stresses are developed whenever a volume of material is restrained from assuming the size and shape that it would obtain for a change in temperature assuming no restraint. NB-3213 defines two general categories of thermal stresses, which are termed general and local thermal stresses. General thermal stress is associated with the distortion of the component in which it occurs. Examples of general thermal stresses are:

1. Stresses in a cylindrical shell due to an axial distribution of temperatures along the shell with uniform temperatures through the thickness;

2. Stress produced by a temperature difference between a nozzle and vessel wall to which it is connected.

Local thermal stresses are classified as peak stresses, which will be discussed later in this section. Secondary stresses can also be caused by mechanical loadings such as internal pressure. Mechanical loadings produce secondary stresses at gross structural discontinuities, which are defined by NB-3213 as geometric or material discontinuities which affect the stress or strain distribution through the entire wall thickness of the pressure retaining member. Examples of gross structural discontinuities are:

1. Junction between a hemispherical head and cylindrical shell;

2. Junction between a shell structure and flange;

3. Nozzle to vessel wall junction;

4. Junction between cylindrical shells of different thicknesses or materials.

The concepts of ratcheting and shakedown are important to the fatigue evaluation methodology of Section III. Ratcheting is a progressive incremental plastic deformation or strain which can occur in a component that is subjected to variations of mechanical stress, thermal stress, or both. Shakedown of strains in a component occurs when, after a few cycles of load application, ratcheting ceases. Progressive incremental plastic deformation is absent from the subsequent response of the component. When the allowable stresses for the primary plus

secondary category are discussed later in this section, further reference will be made to shakedown.

NB-3213 defines peak stress as that increment of stress which is additive to the primary plus secondary stresses. Peak stresses include the effects of stress concentrations and local thermal stresses. The basic characteristic of a peak stress is that it does not cause any noticeable distortion and is objectionable only as a possible source of a fatigue crack or a brittle fracture. Local thermal stress is associated with almost complete suppression of differential expansion and produces no significant distortion of the component. Examples of local thermal stresses are:

1. The stress on the inside surface of a nozzle caused by the "thermal shock" of injecting cold water flowing into the nozzle;

2. The difference between the actual stress and the equivalent linear stress (the linear stress distribution which has the same net bending moment across the section as the actual stress distribution) resulting from a radial temperature distribution through the thickness of a cylindrical shell;

3. The thermal stress in a cladding material which has a coefficient of thermal expansion different from that of the base metal.

Peak stresses are also associated with local structural discontinuities. A local structural discontinuity is a geometric or material discontinuity which affects the stress or strain distribution through a fractional portion of the wall thickness. The stress distribution associated with a local discontinuity causes only very localized types of deformation or strain and has no significant effect on the shell type discontinuity deformations which are commonly associated with secondary stresses. Examples of local structural discontinuities are:

1. Fillet welds and partial penetration welds;

2. Small fillet radii;

3. Small attachments.

The fatigue strength reduction factor is a stress intensification factor which accounts for the presence of a local structural discontinuity on the fatigue life of a component. Experimental or theoretical stress concentration factors may be used for the fatigue strength reduction factor.

Two types of cycles are relevant to Section III fatigue evaluations; operational and stress cycles. An operational cycle is defined as the initiation and establishment of new conditions followed by a return to conditions which existed at the initiation of the cycle. An example of a typical operating cycle which occurs in a nuclear power plant is the startup/shutdown cycle. Operating cycles are defined in the Design Specification. A stress cycle occurs when the alternating stress goes from an initial value through an algebraic maximum value and an algebraic minimum value and returns to the initial value. A single operational cycle may result in one or more stress cycles. A typical stress cycle is shown in Figure 2-6.

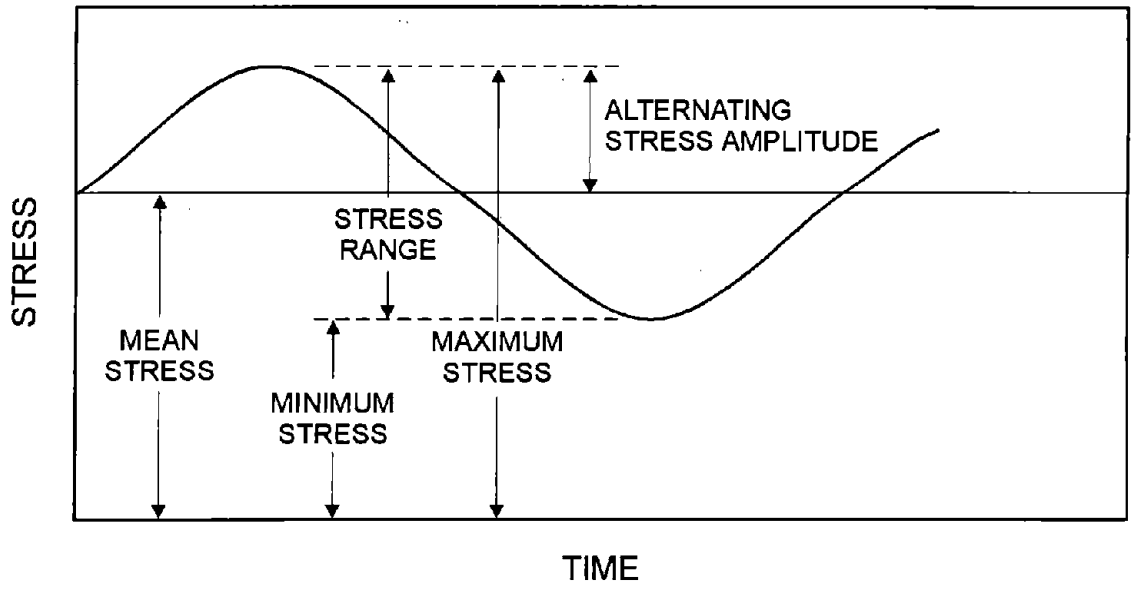

Figure 2-6. Stress Fluctuation Around a Mean Value.

As can be seen from Figures 2-1 and 2-2, the allowable stresses in NB-3200 are based on S_m, which is termed the design stress intensity. Some explanation of the term "stress intensity" is required. The use of this term stems from the fact that the methodology of NB-3200 is based on the maximum shear stress theory. This theory is used to calculate the combined effects of the biaxial or triaxial states of stress which exist in Class 1 components for comparison to the results of uniaxial tensile tests. The maximum shear stress theory states that yielding in a component occurs when the maximum shear stress reaches a value equal to the maximum shear stress at the yield point in a uniaxial tensile test. From Mohr's circle (see Figure 2-7), the maximum shear stress at a point is defined as one-half of the algebraic difference between the largest and smallest of the three principal stresses. If the principal stresses are σ_1, σ_2, and σ_3, and $\sigma_1 > \sigma_2 > \sigma_3$, the maximum shear stress is $(\sigma_1 - \sigma_3)/2$. For the uniaxial tensile test, at yield, $\sigma_1 = S_y$ (S_y is the uniaxial yield strength), $\sigma_2 = 0$ and $\sigma_3 = 0$; therefore the maximum shear stress is $S_y/2$. Based on the maximum shear stress theory, yielding in the component occurs when $(\sigma_1 - \sigma_3)/2 = S_y/2$. To avoid the unnecessary operation of dividing both the calculated and allowable stresses by two, a new term called "equivalent intensity of combined stress" or "stress intensity" is used in Section III [2.6]. The stress intensity is the largest absolute value of $\sigma_1 - \sigma_2$, $\sigma_1 - \sigma_3$, and $\sigma_2 - \sigma_3$. Based on the above and Figure 2-7, the stress intensity is then twice the maximum shear stress and is equal to the largest algebraic difference between any two of the three principal stresses. In this way, the stress intensity is made directly comparable to strength values found from uniaxial tensile tests.

Design stress intensity (S_m) values for various materials are presented in Part D of ASME Section II [2.7] as a function of temperature. Figure 2-8 shows the allowable values for primary membrane (P_m) and primary bending (P_b) stress intensities compared to a yield curve

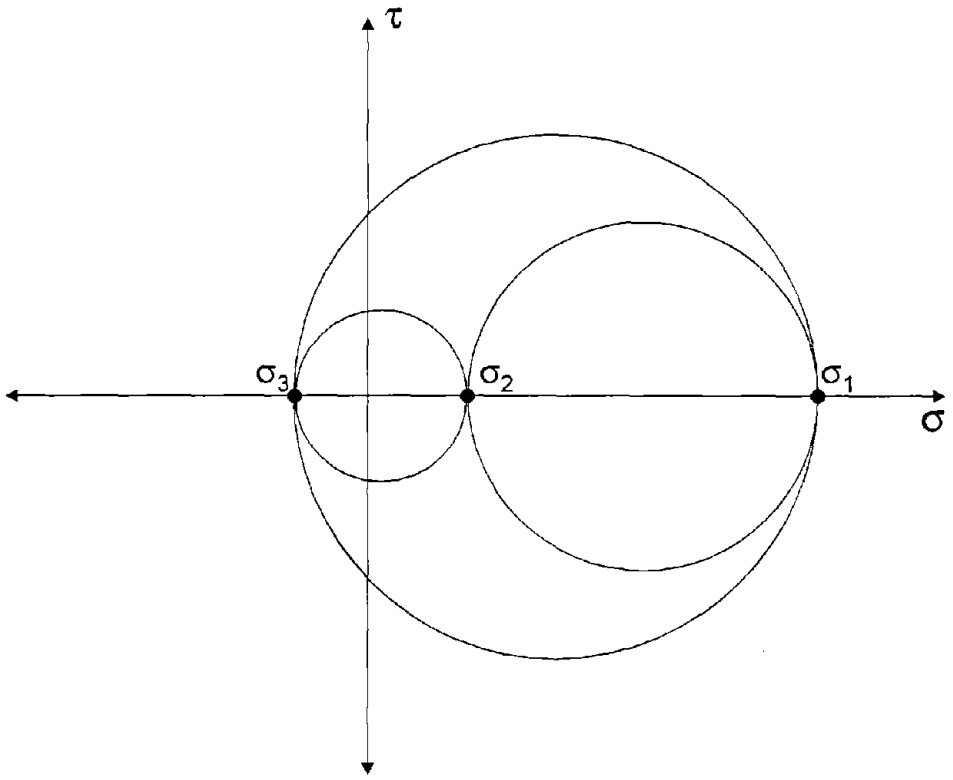

Figure 2-7. Mohr's Circle.

which was developed based on limit design theory [2.6]. Materials were assumed to be elastic - perfectly plastic, with no strain-hardening. Therefore, a load producing the yield stress in tension in a straight bar will result in failure or "collapse." If the same bar were loaded only by a bending moment, collapse will not occur until the load has been increased by a factor known as the "shape factor" of the section. At this load a plastic hinge will form at the location of maximum moment. The shape factor for a rectangular section in bending is 1.5. Figure 2-8 shows the average tensile stress (x-axis) plotted versus the extreme fiber stress (y-axis) for various combinations of tensile and bending stresses in a rectangular plate. The values on both axes are plotted as multiples of S_y. Figure 2-8 also shows the margin of safety against plastic collapse which is created by limiting P_m and $P_m + P_b$ stress intensities to (2/3) S_y and 1.0 S_y, respectively.

From the above paragraph, it might seem that S_m is strictly a function of yield strength of the material at temperature. Because materials used in Class 1 components have widely varying ductilities and strain-hardening properties, yield strength by itself is not an adequate criterion. In order to prevent failures in materials with low ductility and high yield to ultimate strength ratios, Section III considers both the yield strength and ultimate tensile strength in development of allowable stresses for various materials. Table 2-1 shows the basic stress intensity limits of NB-3200 as a function of both yield strength and ultimate tensile strength.

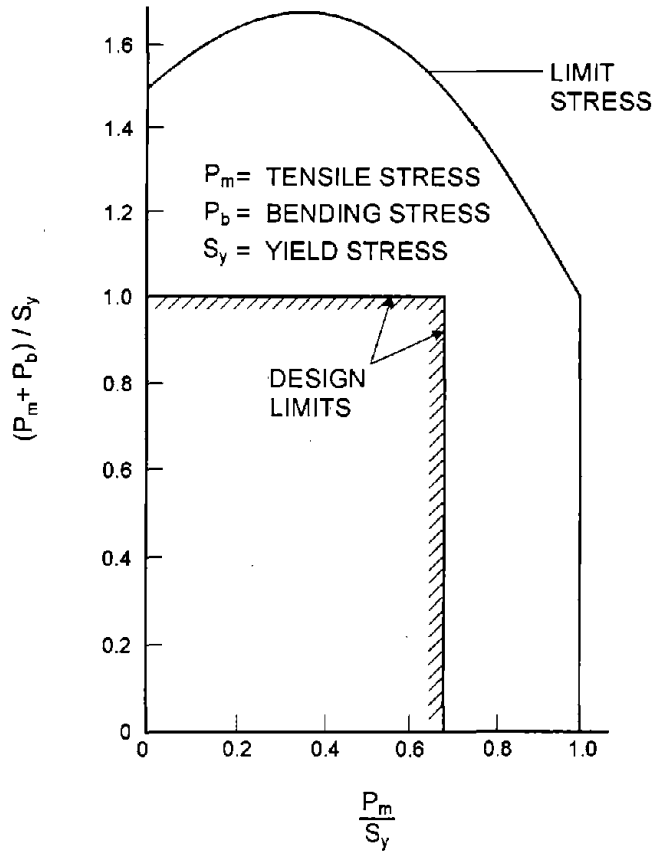

Figure 2-8. Limit Stress for Combined Tension and Bending (Rectangular Section).

Table 2-1. Basic Stress Intensity Limits

Stress Intensity	Tabulated Value	Yield Strength	Ultimate Tensile Strength
General primary membrane (P_m)	S_m	$\leq 2/3S_y$	$\leq 1/3S_u$
Local primary membrane (P_L)	$1.5S_m$	$\leq S_y$	$\leq 1/2S_u$
Primary membrane plus bending ($P_L + P_b$)	$1.5S_m$	$\leq S_y$	$\leq 1/2S_u$
Primary plus secondary ($P_L + P_b + Q$)	$3S_m$	$\leq 2S_y$	$\leq S_u$

Besides defining allowable stress intensity limits for general primary membrane (P_m), local primary membrane (P_L) and local primary membrane plus bending ($P_L + P_b$), Table 2-1 defines limits for primary plus secondary stress intensities ($P_L + P_b + Q$), where the symbol Q denotes secondary stresses. The purpose of limiting primary plus secondary stress intensities to 3.0 S_m is to ensure elastic shakedown. Figure 2-9 illustrates the basis for the limitation of 2.0 S_y on primary plus secondary stresses. This figure shows the idealized results of a displacement controlled uniaxial tensile test. A displacement controlled test means that a specific maximum displacement or strain is imposed on the specimen, as opposed to a load controlled test, where a specified maximum load or stress is imposed. The test is displacement controlled because this is consistent with the definition of secondary stresses. Let the maximum imposed strain in the test be e_1; assuming that e_1 is larger than the yield strain of e_y, a maximum "pseudo-elastic" stress of $S_1 = Ee_1$ can be calculated, with E being Young's modulus for the test material. Figure 2-9a shows the case where $S_y < S_1 < 2.0\ S_y$. For the case where $S_1 < 2.0\ S_y$, the "loading" portion of the stress-strain curve is given by OAB. Since the idealized material is assumed to be elastic-perfectly plastic, the stress in the specimen cannot exceed S_y. Point B corresponds to the maximum imposed strain of e_1. The "unloading" portion of the curve is line BC with a slope equal to E. If $S_1 < 2.0\ S_y$ ($e_1 < 2.0\ e_y$), the absolute value of the compressive residual stress at point C will be less than S_y. Assuming that S_1 continues to be less than 2.0 S_y for subsequent cycles, elastic shakedown occurs, with the stress cycling along line BC. The limit of elastic shakedown occurs when $S_1 = 2.0\ S_y$. This is shown in Figure 2-9a by path OAB′. Point B′ corresponds to a strain of 2.0 e_y. Unloading then occurs along line B′C′ at a slope of E. The absolute value of the residual compressive stress at point C′ is equal to S_y. Elastic behavior will continue to occur along line B′C′ if subsequent pseudo-stress cycles remain between zero and 2.0 e_y.

Figure 2-9b illustrates the case where S_1 is greater than 2.0 S_y. Loading occurs along line OAD, with point D corresponding to a strain of $e_1 > 2.0\ S_y$. Unloading to zero strain occurs along path DEF. Point F corresponds to a residual compressive stress of S_y. However, reloading occurs along line FG, and if the specimen continues to be strain cycled between 0 and e_1, the cycling will now follow the stable hysteresis loop FGDE. Although there is no incremental strain with each cycle, there is a plastic strain equal to GD that is associated with each cycle. Therefore, the shakedown is not purely elastic when $S_1 > 2.0\ S_y$. This is called plastic shakedown.

An additional important point is made in Figure 2-9. When considering secondary stresses, strain rather than stress is the key quantity, since secondary stresses are the result of imposed strains. In addition, Section III assumes that the secondary stresses are calculated for linear elastic material behavior, so the calculated stresses are pseudo-elastic stresses if the yield strain is exceeded.

If the stress intensity limitations shown in Figures 2-1 and 2-2 for general and local membrane, primary bending, and primary plus secondary stresses are met, the requirements for total stress ($P_L + P_b + P_e + Q + F$) can be considered. As was stated previously, when peak stresses, denoted by F, are included, the acceptance criteria is based on demonstration that the cumulative usage factor (U) is less than or equal to 1.0. NB-3222.4(e) defines the requirements for fatigue evaluation of Class 1 components and the specific steps required to calculate partial and cumulative usage factors. However, it is possible that some Class 1 components may not

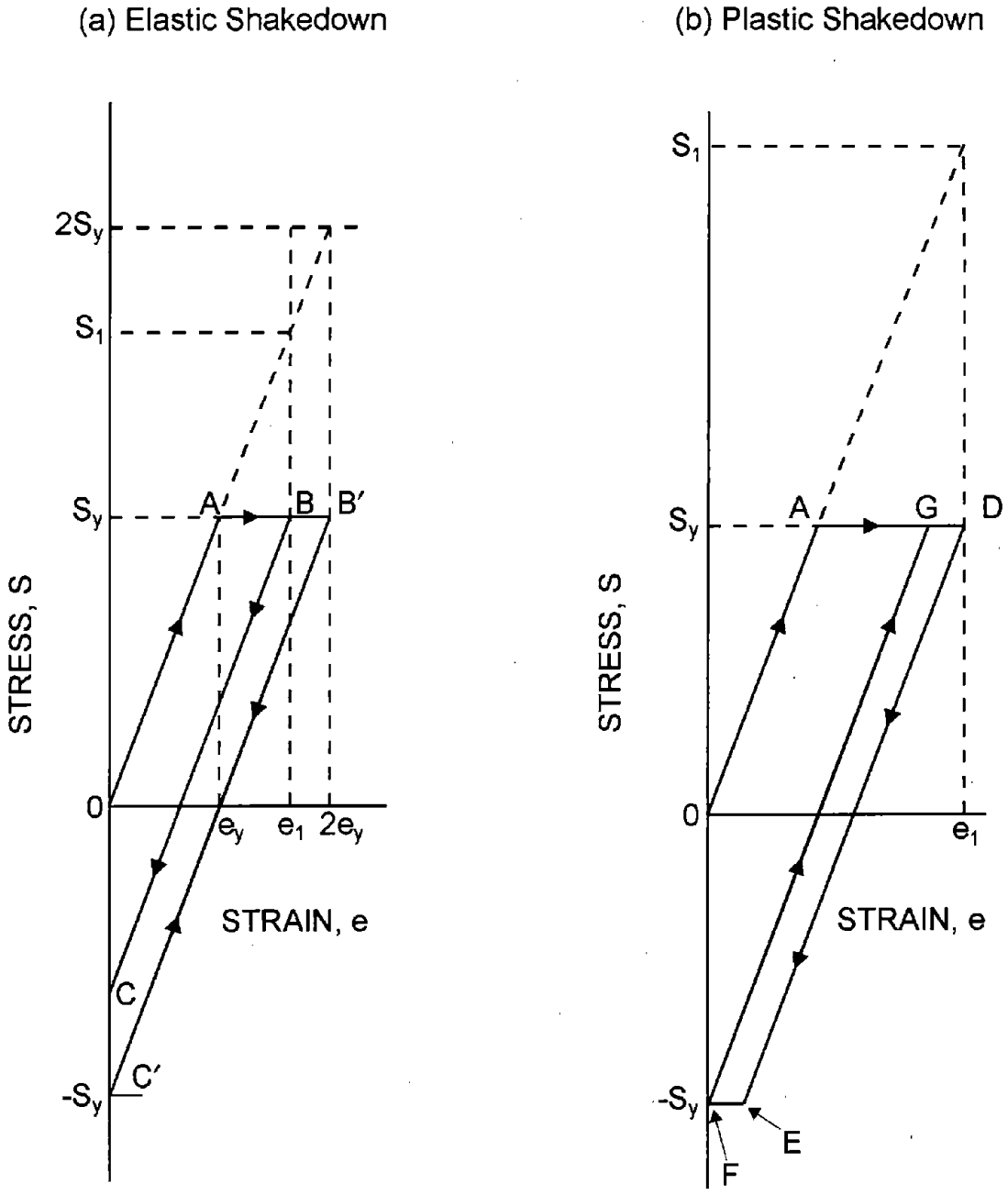

Figure 2-9. Strain History Beyond Yield.

require a detailed fatigue evaluation for cyclic loadings. NB-3222.4(d) states the conditions which must be met by the component to avoid a detailed fatigue evaluation. The rules for exemption are based on a set of assumptions which provide for an overall conservative design and have been proven in practice. These assumptions are taken directly from Reference 2.6:

1. The worst geometrical stress concentration factor (K) to be considered is 2. This assumption is unconservative since $K = 4$ is specified for some geometries.

2. The concentration factor of 2 occurs at a point where the nominal stress is $3S_m$, the highest allowable value of primary-plus-secondary stresses. This is a conservative assumption. The net result of assumptions 1 and 2 is that the peak stress due to pressure is assumed to be $6S_m$, which appears to be a safe assumption for a good design.

3. *All* significant pressure cycles and thermal cycles have the same stress range as the *most* severe cycle. This is a highly conservative assumption. (A "significant" cycle is defined as one which produces a stress amplitude higher than the endurance limit of the material.)

4. The highest stress produced by a pressure cycle does not coincide with the highest stress produced by a thermal cycle. This is unconservative and must be balanced against the conservatism of assumption 3.

5. The calculated stress produced by a temperature difference ΔT between two points does not exceed $2\ E\alpha\Delta T$, but the peak stress is raised to $4\ E\alpha\Delta T$ because of the assumption that $K = 2$ (α is the coefficient of thermal expansion). This assumption is conservative, as shown by the following examples of thermal stress:

   (a) For the case of a linear thermal gradient through the thickness of a vessel wall, if the temperature difference between the inside and the outside of the wall is ΔT, the stress is:

   $$\sigma = \frac{E\alpha\Delta T}{2(1-\nu)} = 0.715\ E\alpha\Delta T\ (for\ \nu = 0.3)$$

   (b) When a vessel wall is subjected to a sudden change of temperature, ΔT, so that the temperature change only penetrates a short distance into the wall thickness, the thermal stress is:

   $$\sigma = \frac{E\alpha\Delta T}{1-\nu} = 1.43\ E\alpha\Delta T\ (for\ \nu = 0.3)$$

   (c) When the average temperature of a nozzle is ΔT degrees different from that of the rigid wall to which it is attached, the upper limit to the magnitude of the discontinuity stress is:

   $$\sigma = 1.83\ E\alpha\Delta T\ (for\ \nu = 0.3)$$

Thus the coefficient of $E\alpha\Delta T$ is always less than the assumed value of 2.0 for these limiting cases.

When the two locations in the vessel whose temperatures differ by ΔT are separated from each other by more than $2\sqrt{Rt}$ (R and t are the vessel mean radius and thickness, respectively), there is sufficient flexibility between the two locations to produce a significant reduction in thermal stress. Therefore only temperature differences between "adjacent" points (a distance of less than $2\sqrt{Rt}$) need be considered.

In order for a component to qualify for exemption from fatigue evaluation, it must not be subjected to significant cyclic loadings. If usage factors were calculated for these components using the rules of NB-3222.4(e), a cumulative usage factor of substantially less than 1.0 would be anticipated.

Class 1 components that require a detailed fatigue evaluation are the principal subject of this report. The first step in the fatigue evaluation methodology is to calculate the stress differences and the alternating stress intensity S_{alt} in accordance with NB-3216. To take into account the possibility of rotation of the principal stresses at the point being considered during the stress cycle, the following procedure is required [2.4]:

1. Consider the values of the six total stress components (including peak stress) σ_t , σ_l , σ_r , τ_{lt} , τ_{lr} , and τ_{rt} versus time for the complete stress cycle, taking into account both the gross and local structural discontinuities and the thermal effects which vary during the cycle.

2. Choose a point in time when the conditions are at one of the extremes for the cycle (either the algebraic maximum or minimum) and identify the stress components at this time by the subscript i. In most cases it will be possible to choose at least one time during the cycle when the conditions are known to be extreme. In some cases it may be necessary to try different points in time to find the ones which results in the largest value of alternating stress intensity.

3. Subtract each of the six stress components σ_{ti} , σ_{li} , etc., from the corresponding stress components σ_t , σ_l , etc. at each point in time during cycle and call the resulting components σ'_t , σ'_l , etc.

4. At each point in time during the cycle, calculate the principal stresses σ'_1 , σ'_2 , and σ'_3 derived from the six stress components σ'_t σ'_l , etc. Note that the directions of the principal stresses may change during the cycle but each principal stress retains its identity as it rotates.

5. Determine the stress differences $S'_{12} = \sigma'_1 - \sigma'_2$, $S'_{23} = \sigma'_2 - \sigma'_3$ and $S'_{31} = \sigma'_3 - \sigma'_1$ versus time for the complete cycle and find the largest

absolute magnitude of any stress difference at any time. The alternating stress intensity S_{alt} is one-half of this magnitude.

For a typical Class 1 component, there will be a number of stress cycles of different origins which produce total stresses of different magnitudes. The number of times that each of these stress cycles can occur also varies. The cumulative effect of various stress cycles is evaluated by means of a linear damage relationship. Assume that there are n_1 cycles of S_{alt1}, n_2 cycles of S_{alt2}, . . . up to n_n cycles of S_{altn}. The applicable fatigue design curve (Figures 2-3 through 2-5) is then entered for each value of S_{alt}. Each S_{alt} is multiplied by the ratio of the modulus of elasticity given on the design curve divided by the value of the modulus of elasticity used in the analysis. The modified values of S_{alt} are used in conjunction with the fatigue design curves to determine the allowable number of cycles. For each S_{alt1} . . . S_{altn}, an allowable number of cycles N_1 . . . N_n can be found on the abscissa of the design fatigue curve. The usage factors can then be calculated as follows; $U_1 = n_1 / N_1$, $U_2 = n_2 / N_2$, . . . $U_n = n_n / N_n$. The cumulative usage factor, U, is then calculated by use of the linear damage rule; $U = U_1 + U_2 + \ldots + U_n$ (Palmgren-Miner damage rule). For fatigue requirements to be met, U must not exceed 1.0.

Paragraph NB-3227 of Section III contains special stress limits. These deviations from the basic stress limits are provided to cover special Service Loadings or configurations. Some of these deviations are more restrictive, and some are less restrictive, than the basic limits shown in Figures 2-1 and 2-2. In cases of conflicts, the special stress limits take precedence for the particular situations to which they apply.

The loadings and configurations addressed by the special limits include:

- Provisions for modifying the stress limits for bearing loads relative to the distance of the point of load application to a free edge (NB-3227.1).
- Special stress limits for cross sections loaded in pure shear (NB-3227.2).
- Requirements to prevent progressive distortion of non-integral connections (NB-3227.3).
- A limit on the sum of the principal stresses (NB-3227.4).
- Special rules to be applied at the transition between a vessel nozzle and the attached piping (NB-3227.5).
- A modified Poisson's ratio value to be used when computing local thermal stresses (NB-3227.6).
- Special rules to be applied to welded seals such as omega and canopy seals (NB-3227.7).

The special stress requirements which are most relevant to fatigue evaluations of Class 1 components are defined in NB-3227.5 (Nozzle Piping Transition) and NB-3227.6 (Applications

of Elastic Analysis for Stresses Beyond the Yield Strength). The purpose of NB-3227.5 is to ensure that no yielding can be produced in the RPV wall by piping reaction loads. This is done by conservatively including the stresses (other than gross structural discontinuity stresses) caused by all piping reactions, including those attributable to restrained free end displacements of attached piping, in the P_m classification. Normally stresses due to restraint of free end displacements of piping are classified as secondary or Q stresses, since they are defined as general thermal stresses.

NB-3227.6 recognizes that the limitation of $3S_m$ on primary plus secondary stresses ensures elastic shakedown except in regions containing significant local structural discontinuities or local thermal stresses. Therefore, in evaluating local thermal stresses for fatigue evaluation, the use of a modified Poisson's ratio is required to account for the increased total strain due to plastic behavior. Elastic equations are to be used to calculate the local thermal stress, except that the numerical value for Poisson's ratio is determined from the expression:

$$\nu = 0.5 - 0.2(S_y / S_a), \text{ but not less than } 0.3$$

where:

S_y = yield strength of the material at the temperature of the cycle

S_a = value obtained from the applicable fatigue design curve for the specified number of cycles for the condition being considered. (S_a and S_{alt} are the same.)

The maximum value for Poisson's ratio would then be 0.5, which is Poisson's ratio for plastic flow, since the volume of a material does not change for large plastic deformations. The maximum value can be achieved when S_y / S_a approaches 0, or when the S_a is substantially larger than the yield stress. This occurs when there are only a few cycles under consideration.

NB-3200 allows the $3S_m$ limitation on primary plus secondary stresses to be exceeded provided that other criteria are met. These criteria for exceeding $3S_m$ are defined in NB-3228.5 (simplified elastic-plastic analysis), NB-3222.5 (Thermal Stress Ratchet), and are discussed in Section 2.4.

2.4 Discussion of Simplified Elastic-Plastic Analysis and Thermal Ratcheting

From NB-3228.5, the $3S_m$ limit on the range of primary plus secondary stress intensity may be exceeded provided that the requirements of (a) through (f) below are met:

(a) The range of primary plus secondary membrane plus bending stress intensity, excluding thermal bending stresses, shall be $\leq 3S_m$.

(b) The value of S_a used for entering the design fatigue curve is multiplied by the factor K_e, where:

K_e is the elastic-plastic penalty factor.

S_n, range of primary plus secondary stress intensity, psi	K_e
$S_n \leq 3S_m$	1.0
$3S_m < S_n < 3mS_m$	$1.0+[(1-n)/n(m-1)](S_n/3S_m-1)$
$S_n \geq 3mS_m$	1/n

m, n are material parameters provided in Table NB-3228.5(b)-1, see Table 2-2 below.

The values of the material parameters m and n for the various classes of permitted materials are as given in Table NB-3228.5(b)-1 of Reference 2.4, which is duplicated in Table 2-2.

(c) The rest of the fatigue evaluation stays the same as required in NB-3222.4, except that the procedure of NB-3227.6 need not be used.

(d) The component meets the thermal ratcheting requirements of NB-3222.5.

(e) The temperature does not exceed those listed in Table 2-2 for the various classes of materials.

(f) The material shall have a specified minimum yield strength to specified minimum tensile strength ratio of less than 0.80.

Table 2-2.* Values of m, n, and T_{max} for Various Classes of Permitted Materials

Materials	m	n	T_{max} ,°C [°F]
Carbon steel	3.0	0.2	370 [700]
Low alloy steel	2.0	0.2	370 [700]
Martensitic stainless steel	2.0	0.2	370 [700]
Austenitic stainless steel	1.7	0.3	425 [800]
Nickel-chromium-iron	1.7	0.3	425 [800]
Nickel-copper	1.7	0.3	425 [800]

* This is Table NB-3228.5(b)-1 of ASME Section III [2.4].

The factor K_e has been called the "elastic-plastic penalty factor" since it must be used to factor the alternating stress intensity amplitudes (S_{alt}) when using the fatigue design curves. Because the fatigue curves are logarithmic, a relatively small K_e, 1.5 for example, can significantly affect the fatigue usage factor.

The factor K_e is, in effect, a peak strain concentration factor which takes into account the effects of localized plastic strain. It can be thought of as a correction factor applied to the elastic stress concentration factor. During elastic behavior, i.e., when $S_n < 3S_m$, $K_e = 1.0$. As the local

strains are increased, the strains predicted by the elastic stress concentration factor are low relative to the actual strains which include the effects of plastic behavior. Therefore, when $S_n > 3S_m$, $K_e > 1.0$. In Reference 2.1 it is estimated that the maximum value of K_e is approximately $1/n$, where n is the strain hardening exponent of the material. The strain hardening exponent, n, is the slope of the uniaxial stress-strain curve for the material plotted on log-log coordinates. Figure 2-10 shows K_e plotted versus $S_n/3S_m$. For elastic behavior, or $S_n/3S_m < 1.0$, $K_e = 1.0$. For $1 < S_n/3S_m < m$, K_e increases above 1.0 with a slope of $((1/n) - 1)/(m-1)$. The quantity "m" was introduced to provide the slope for K_e that was observed in fatigue tests.

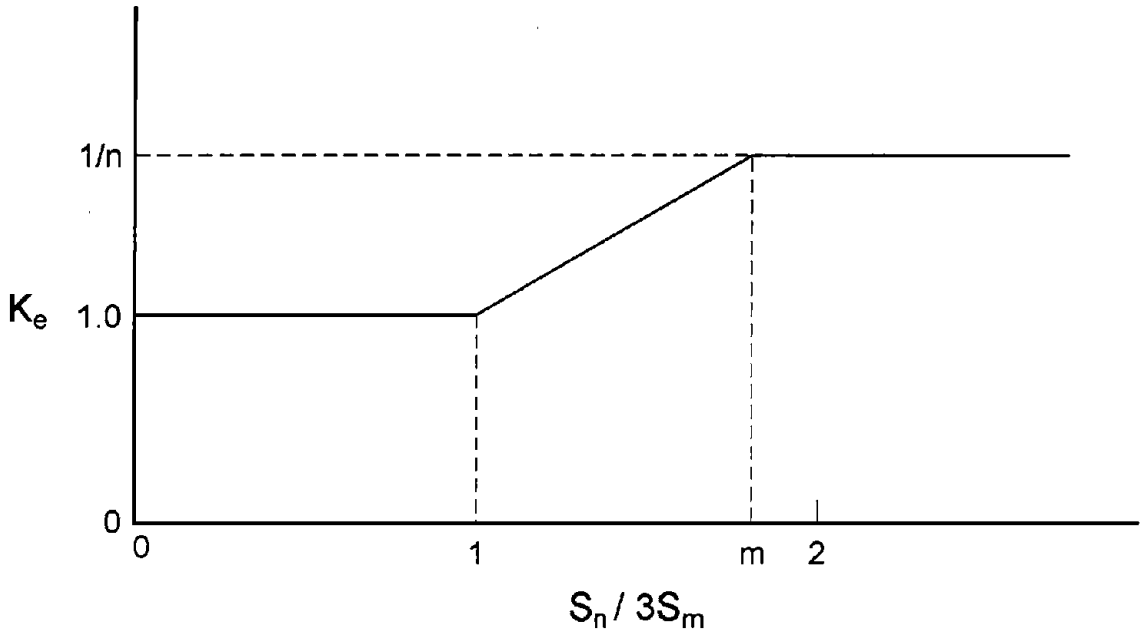

Figure 2-10. Strain Concentration (Elastic-Plastic Penalty) Factor for Fatigue.

It is important to note that the component is also required to meet the thermal ratcheting requirements of NB-3222.5. Thermal ratcheting occurs when large thermal cyclic strains are superimposed on the membrane stresses, which are due to steady state primary loads such as pressure. The increment of plastic strain is nearly constant for each thermal cycle, and the component may be cycled to failure. NB-3222.5 defines the following requirements to ensure that failure due to thermal ratcheting will not occur when the $3S_m$ limitation is exceeded. The following paragraph is taken directly from subparagraph NB-3222.5(a) [2.4].

> The limiting value of the maximum cyclic thermal stress permitted in a portion of an axisymmetric shell loaded by steady state internal pressure in order to prevent cyclic growth in diameter is as follows. Let
>
> y' = maximum allowable range of thermal stress computed on an elastic basis divided by the yield strength S_y

x = maximum general membrane stress due to pressure divided by the yield strength S_y

Case 1: Linear variation of temperature through the wall: for $0 < x < 0.5$, $y' = 1/x$ and, for $0.5 < x < 1.0$, $y' = 4\ (1\text{-}x)$.

Case 2: Parabolic constantly increasing or constantly decreasing variation of temperature through the wall: for $0.615 < x < 1.0$, $y' = 5.2(1 - x)$ and, approximately for $x < 0.615$, $y' = 4.65$, 3.55, and 2.70 for $x = 0.3$, 0.4, and 0.5, respectively.

The basis of the Section III thermal ratcheting rules for a linear variation of temperature through the wall thickness is taken from Reference 2.8. The elastic regime is characterized by no plastic action. In the shakedown regime, plastic flow occurs during the initial loading cycles, with elastic behavior governing during the following cycles. In the plastic cycling regime, plastic flow occurs for each cycle, but the increment of plastic strain reduces with increasing cycles until it reaches zero. At this point a "plastic shakedown" is achieved. The goal of the above rules is to keep the material in the shakedown or elastic regimes for the case of linear or parabolic temperature distribution.

2.5 NB-3650 Rules for Evaluation of Class 1 Piping

The ASME Section III rules for evaluation of Class 1 piping components have many similarities to the "design by analysis" rules of NB-3200. NB-3650 is based on the maximum shear stress theory, and primary, secondary and peak stress categories are evaluated. The allowable stress limits for the different stress categories are the same as for NB-3200, and if the limitations on primary plus secondary stresses are exceeded, simplified elastic-plastic analysis with consideration of thermal stress ratcheting is allowed. The major difference between NB-3200 and NB-3650 is that the latter takes a "design by formula" approach, with the design being considered acceptable if it passes a series of equations for the various loadings to which the component is exposed. The introduction to Reference 2.3 includes a discussion of the Class 1 piping design criteria and philosophy. The following paragraphs provide a description and discussion of these equations.

A primary stress limit is provided to show that the design is acceptable for load-controlled (primary) loadings and is similar to Equation 11 of ANSI B31.1. The primary stress intensity limit is satisfied if the requirements of Equation 9 (of Section III) are met:

$$B_1 \frac{PD_o}{2t} + B_2 \frac{D_o}{2I} M_i \leq 1.5 S_m \qquad \text{(Section III, Cl.1, Eq. 9)}$$

where:

B_1 , B_2 = primary stress indices for the specific product under investigation (defined in Table NB-3681(a)-1 of Reference 2.4).

P = Design Pressure, psi.

D_o = outside diameter of pipe, in.

t = nominal wall thickness of product, in.

I = moment of inertia, in^4.

M_i = resultant moment due to a combination of Design Mechanical Loads, in-lb.

S_m = basic allowable design stress intensity value, psi.

For loading conditions classified as Service Level B (in the Design Specification), the above equation must also be met, except that the allowable stress may be increased from 1.5 S_m to 1.8 S_m. The magnitude of allowable increase is consistent with the 20% allowable increase in Equation 12 of ANSI B31.1.

The remainder of the equations for Service Levels A and B are provided to ensure satisfactory cyclic (fatigue) behavior. To satisfy the range of primary plus secondary stresses, Equation 10 (see below) must be satisfied. Calculation of the stress range is based on the effect of changes that occur in mechanical or thermal loadings which take place as the system goes from one load set (e.g., pressure, temperature, moment, and force loading) to any other load set which could also exist. Equation 10 must be satisfied for all pairs of load sets:

$$S_n = C_1\frac{P_oD_o}{2t} + C_2\frac{D_o}{2I}M_i$$

$$+C_3E_{ab}|\alpha_aT_a - \alpha_bT_b| \le 3S_m \qquad \text{(Section III, Cl. 1, Eq. 10)}$$

where:

C_1, C_2, C_3 = secondary stress indices for the specific component under investigation (defined in Table NB-3681(a)-1 of Reference 2.4).

D_o, t, I, S_m = as defined for Equation 9.

P_o = range of service pressure, psi.

M_i = resultant range of moment which occurs when the system goes from one service load set to another, in-lb.

E_{ab} = average modulus of elasticity of the two sides of a material or structural discontinuity at room temperature, psi.

α_a, α_b = coefficient of thermal expansion on side a and side b of a structural or material discontinuity, in/in-°F.

T_a, T_b = range of average temperature on side a and side b of a structural discontinuity, when the system goes from one service load to another, °F.

The fatigue resistance of each piping component is assessed by evaluating the range of peak stress. For every pair of load sets, S_p values are calculated using Equation 11:

$$S_p = K_1C_1\frac{P_oD_o}{2t} + K_2C_2\frac{D_o}{2I}M_i + K_3C_3E_{ab}|\alpha_aT_a - \alpha_bT_b|$$

$$+ \frac{1}{2(1-\nu)} K_3 E\alpha |\Delta T_1| + \frac{1}{1-\nu} E\alpha |\Delta T_2| \,, \qquad \text{(Section III, Cl. 1, Eq. 11)}$$

where:

K_1 , K_2 , K_3 = local stress indices for the specific component under investigation (defined in Table NB-3681(a)-1 of Reference 2.4).

$E\alpha$ = modulus of elasticity (E) times the mean coefficient of thermal expansion (α), both at room temperature, psi/°F.

ΔT_1 = range of the temperature difference for each load set pair between the temperature of the outside surface T_o and the temperature of the inside surface T_i of the piping product assuming a moment generating equivalent linear temperature distribution, °F.

ΔT_2 = range for that portion of the nonlinear thermal gradient through the wall thickness not included in ΔT_1, °F.

A load set pair is defined as two loading sets or cases which are used to compute a stress range.

As can be seen from Equations 10 and 11 of NB-3650, the C_1 , C_2 , C_3 , K_1 , K_2, and K_3 stress indices are very important in the fatigue evaluation of Class 1 piping components. The foreword to ANSI/USAS B31.7 [2.3] states that these stress indices are based on a "condensation of results given in many papers on both technical and experimental work on piping components. In some cases these factors can be supported quite well on both theoretical and experimental grounds. In other cases, they are based on engineering judgement which is conservative."

If Equation 10 cannot be satisfied for all load set pairs, the alternative analysis described below may still permit qualifying the component. Only those load set pairs which do not satisfy Equation 10 need to be considered.

(a) Equation 12 shall be met:

$$S_e = C_2 \frac{D_o}{2I} M_i^* \le 3S_m \qquad \text{(Section III, Cl. 1, Eq. 12)}$$

where:

S_e = nominal value of expansion stress, psi

M_i^* = same as M_i in Equation 10, except that it includes only moments due to thermal expansion and thermal anchor movements, in-lb.

(b) When the limits of Equation 10 are exceeded and before the rules of Equation 13 which follows can be utilized, the value of the range of ΔT_1 cannot exceed that calculated per NB-3653.7 as follows:

$$\Delta T_1 \ range \leq \frac{y' S_y}{0.7 E\alpha} C_4$$

where:

y' = 3.33, 2.00, 1.20, and 0.80 for x = 0.3, 0.5, 0.7, and 0.8, respectively

x = $(PD_o/2t)\ (1/S_y)$

P = maximum pressure for the set of conditions under consideration, psi

C_4 = 1.1 for ferritic material

= 1.3 for austenitic material

$E\alpha$ = as defined in Equation 11, psi/°F

S_y = material yield strength value, psi, taken at average fluid temperature of the transient under consideration.

It should be noted that the limitations on the ΔT_1 *range* are to ensure that thermal ratcheting does not occur.

(c) The primary plus secondary membrane plus bending stress intensity, excluding thermal bending and thermal expansion stresses, shall be $<3S_m$. This requirement is satisfied by meeting Equation 13:

$$C_1 \frac{P_o D_o}{2t} + C_2 \frac{D_o M_i}{2I} + C'_3 E_{ab} |\alpha_a T_a - \alpha_b T_b| \leq 3S_m \quad \text{(Section III, Cl. 1, Eq. 13)}$$

where:

M_i = moment as defined for Equation 9, in-lb, and all other terms as previously described,

C'_3 = stress index (values defined in Table NB-3681 (a)-1 of Reference 2.4).

(d) If these conditions are met, the value of S_{alt} shall be calculated by Equation 14:

$$S_{alt} = K_e \frac{S_p}{2} \quad \text{(Section III, Cl. 1, Eq. 14)}$$

where:

S_{alt} = alternating stress intensity, psi.

S_p = peak stress intensity value calculated by Equation 11, psi.

K_e = the elastic-plastic penalty factor.

S_n, range of primary plus secondary stress intensity, psi	K_e
$S_n \leq 3S_m$	1.0
$3S_m < S_n < 3mS_m$	$1.0+[(1-n)/n(m-1)](S_n/3S_m-1)$
$S_n \geq 3mS_m$	1/n

m, n are material parameters provided in Table NB-3228.5(b)-1, see Table 2-2.

The alternating stress for all load set pairs is then computed as one-half of the peak stress ranges calculated from Equation 11, or by the alternate approach of Equation 14 if Equation 10 is not met. The fatigue analysis is then performed using the applicable Code fatigue curve and the number of design cycles for each load case from the Design Specification.

For ASME Section III Code editions prior to the Summer 1979 Addenda, Equation 10 contained an additional term. In these earlier Code editions, the ΔT_1 term of the peak stress in Equation 11 was also included in the secondary stress Equation 10:

$$S_n = C_1\frac{P_o D_o}{2t} + \frac{C_2 D_o}{2I} M_i + C_3 E_{ab}|\alpha_a T_a - \alpha_b T_b| + \frac{E\alpha|\Delta T_1|}{2(1-\nu)} \leq 3S_m \qquad \text{(Section III, Cl. 1, Eq. 10)}$$

Addition of this term frequently increased the stress S_n above $3S_m$. When this occurred, Equations 12 and 13 had to be met, and the fatigue analysis was conducted using a relatively high K_e factor, increasing the alternating stresses used in the fatigue analysis. The ASME Section III Committee on Piping Design decided that this was overly conservative and modified the equation accordingly, starting with the Summer 1979 Addenda. However, most current Section III plants were designed to the earlier version of the Section III Code.

2.6 ASME Section III Design Fatigue Curves

The number of significant stress cycles that a Class 1 nuclear power plant component will be subjected to is typically much less than 10,000. This is in contrast to rotating machine design, where millions of cycles can be expected and must be considered in the design. As a result the endurance limit is used as the maximum cyclic stress. In the case of Class 1 components, the most likely location for a fatigue failure is at a local discontinuity such as a fillet weld or at an

area of high localized thermal stresses. Use of the endurance limit as the maximum stress at these local areas for relatively few cycles would be inappropriate and unnecessarily conservative.

In order to perform a reasonable evaluation of low cycle fatigue, the effects of localized plastic strains must be considered, since fatigue cracks can only be produced by strains well beyond yield for a limited number of cycles. Since fatigue damage in the plastic region is a function of strain and not stress, the Code design fatigue curves were developed from uniaxial tests where imposed displacements (strains) rather than forces were applied. The stress values shown on the ordinates of Figures 2-3 through 2-5 are actually the imposed test strains multiplied by the value for Young's modulus shown in the figures, so these stresses are fictitious for values significantly greater than the yield stress of the material.

The design fatigue curves have been adjusted for mean stress. The combination of mean stress and alternating stress amplitude is shown in Figure 2-6. It is possible that the presence of a mean stress may have a deleterious effect on the fatigue life of a component. The Section III design fatigue curves have been corrected for the effects of mean stress by use of a modified Goodman diagram (see Figure 2-11). Based on the discussion in Reference 2.6, the following equation was used:

$$S'_N = S_N[(S_u - S_y)/(S_u - S_N] \text{ for } S_N < S_y$$

where:

S_N = the stress amplitude required for failure in N cycles with zero mean stress.
S_u = the ultimate strength of the material.
S_y = the yield strength of the material.
S'_N = the stress amplitude required for failure in N cycles with the effects of mean stress considered.

If $S_N \geq S_y$, no adjustment to the stress amplitude in the design fatigue curves was required. In the development of the design fatigue curves for Section III, it was felt that the calculation of certain mean stresses, such as those due to weld residual stresses, would be quite difficult, and would have a large degree of uncertainty. The above equation therefore assumes the largest possible adjustment due to mean stress in the calculation for S'_N. The design fatigue curves for carbon and low alloy steel are reduced by mean stress effects for $N > 50{,}000$ cycles. For stainless steels, S_N is always greater than S_y over the full range of cycles so no mean stress adjustment to the curves was required. The above equation for S'_N was found to be too conservative when adjusting the design fatigue strength curve for high strength bolts, so the Peterson cubic equation [2.6, 2.9] was used in development of the design fatigue curves for high strength bolts.

There is a fair amount of controversy in the nuclear industry regarding the factor of safety or degree of conservatism that is built into the design fatigue curves. Reference 2.6 states that the design fatigue curves were based on a least squares curve fit to the results of strain controlled fatigue tests performed on small polished specimens. The stress amplitude values shown on the ordinates of the design fatigue curves were then obtained from the best fit curves by "applying a factor of two on stress or a factor of twenty on cycles, whichever was more conservative at each point." At lower numbers of cycles, the factor of twenty governed. At higher cycles, the

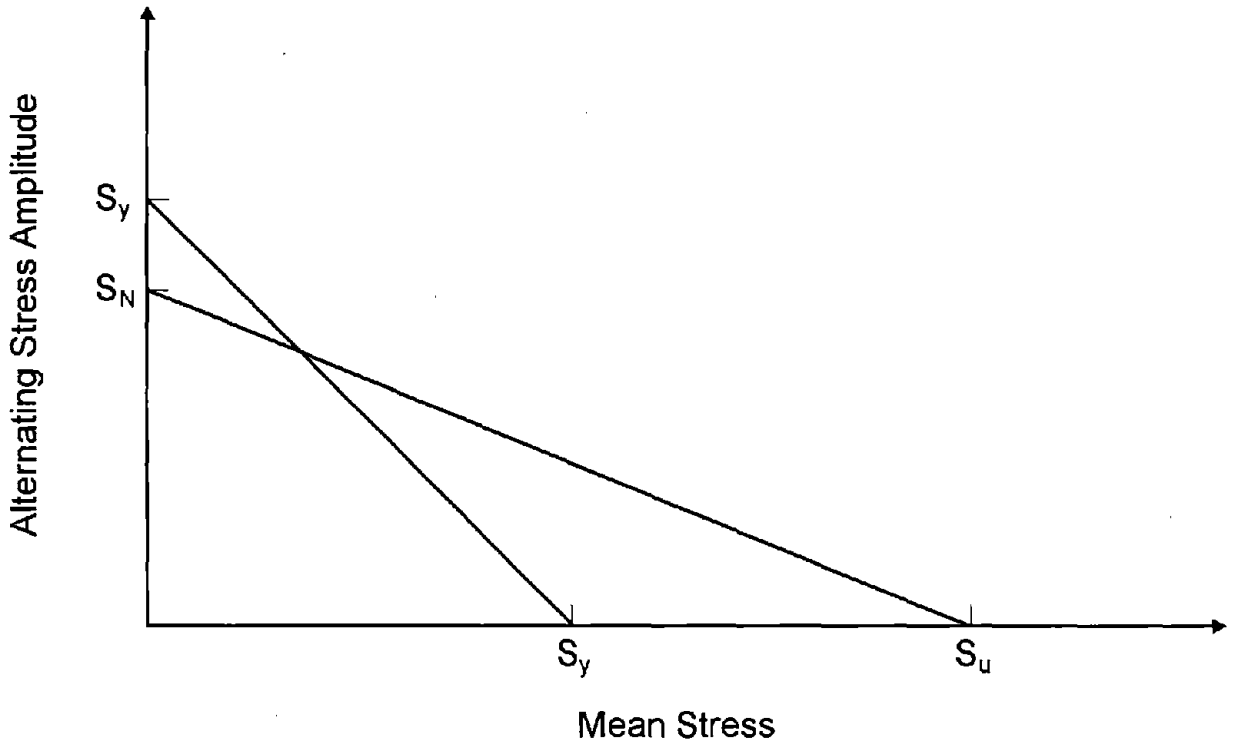

Figure 2-11. Modified Goodman Diagram.

fatigue curve flattens, and a factor on cycles has little effect, so a factor of two on stress was used. The point at which the design fatigue curves go from being governed by cycles to being governed by stress occurs at approximately 50,000 cycles. See Figure 6-10 and the discussion in Section 6.3.5 for more details on this subject. The factors of two and twenty were intended to cover scatter of data, size effect, surface finish, and atmosphere. From References 2.2 and 2.10, the factor of twenty was divided into the following subfactors:

Scatter of data (minimum to mean)	2.0
Size effect	2.5
Surface finish, atmosphere, etc.	4.0

The controversy arises over whether the factor of 4.0 includes the effects of Light Water Reactor (LWR) water environments. Reference 2.2 states that "Atmosphere was intended to reflect the effects of an industrial atmosphere in comparison with an air-conditioned lab, not the effects of a specific coolant." This would mean that environmental effects such as strain rate, oxygen level and temperature were not originally intended to be included in the factor of 20. As was stated previously, one of the main intents of this report is to investigate the effect of environment on Section III fatigue evaluations.

Figure 2-12 shows the results of the PVRC fatigue tests conducted at Southwest Research Institute [2.6]. The tests were performed on 36" diameter vessels. The beginning of each horizontal line indicates the presence of a visible crack that was about 3/16" long. It can be seen

that crack initiation, particularly at high stress amplitudes, can occur very close to the ASME design curve. Through thickness failures, designated by Xs at the end of horizontal lines, occur at no less than 3 times the allowable number of cycles. But Figure 2-12 clearly demonstrates that the design fatigue curves do not necessarily guarantee a factor of safety of 20 against fatigue failure of an actual Class 1 component in service. Therefore, even though the Code requirements are met, one still should not assume the component will operate safely for 20 times its original design life.

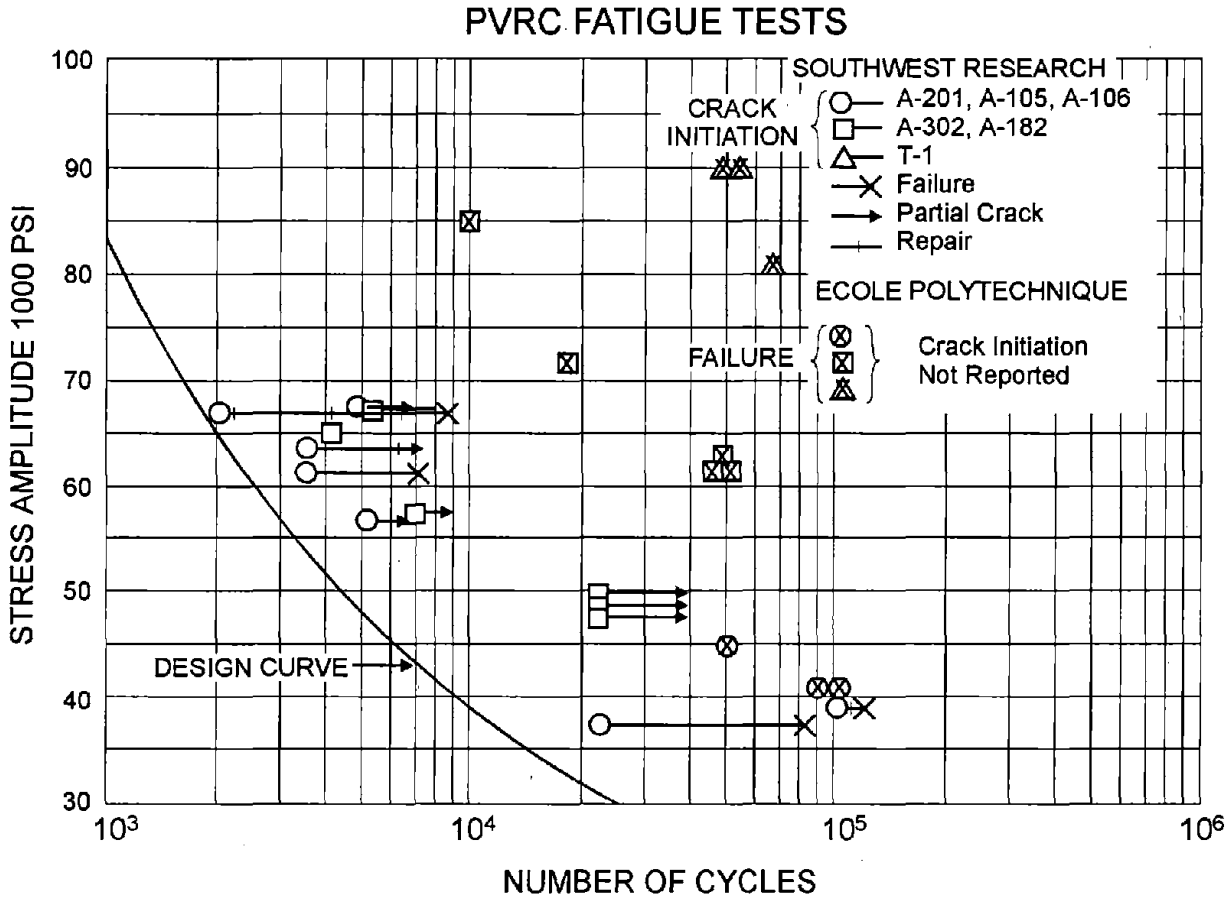

Figure 2-12. Fatigue Data for Low Alloy Steels.

In addition to the PVRC tests conducted on vessels, numerous fatigue tests have been performed on piping welds and components as summarized in Reference 2.11. The margins on cycles to failure for these tests, which were conducted in air, are shown in Table 2-3. For each weld or component, the ratio of the number of cycles to failure during the test to the Code allowable number of cycles is presented. Failure during the test occurred when a leak in the weld or component was detected. The Code allowable number of cycles was taken from Figure 2-3 or Figure 2-4(a) (Figures I-9.1 and I-9.2.1 of the Code). In effect, the values in Table 2-3 can be considered the design margin to leakage. In general, Table 2-3 indicates that for carbon steel piping components, the margins to failure are significantly greater than the factor of 20 on cycles used in the development of Figures 2-3 and 2-4(a). One exception may be the girth butt welds where margins were the lowest in comparison with other fittings. The margins for elbows and tees, the most commonly used fittings, were well in excess of 20. It is also noted that the margins were consistently higher for carbon steel than for stainless steel.

Table 2-3. Margins to Failure of Piping Welds and Components.

Component/Weld	Carbon Steel	Stainless Steel
Girth Butt Welds	14 - 128	6 - 76
Elbows	118 - 2500	47 - 170
Forged Welding Tees	55 - 2100	104 - 660
Fabricated Tees	123 - 1700	25 - 322

2.7 References

2.1 B.F. Langer, "Design-Stress Basis for Pressure Vessels," Experimental Mechanics, January 1971.

2.2 W.E. Cooper, "The Initial Scope and Intent of the Section III Fatigue Design Procedures," Paper Presented at PVRC Workshop on Cyclic Life and Environmental Effects in Nuclear Applications, January 1992.

2.3 "Nuclear Power Piping," ANSI/USAS B31.7-1969, Published by American Society of Mechanical Engineers.

2.4 "Rules for Construction of Nuclear Power Plant Components," Section III, Division 1, 1992 ASME Boiler and Pressure Vessel Code, American Society of Mechanical Engineers. (Figures 2-1 through 2-5 used with permission.)

2.5 O.C. Zienkiewicz, "The Finite Element Method in Engineering Science," McGraw-Hill Company, 1977.

2.6 "Criteria of the ASME Boiler and Pressure Vessel Code for Design by Analysis" in Sections III and VIII, Division 2, American Society of Mechanical Engineers, 1969.

2.7 "Materials Part D-Properties," Section II, 1992 ASME Boiler and Pressure Vessel Code, American Society of Mechanical Engineers.

2.8 D.R. Miller, "Thermal-Stress Ratchet Mechanism in Pressure Vessels," *ASME Transactions*, Vol. 81, Sec. D, No. 2, 1959.

2.9 A.L. Snow and B.F. Langer, "Low-Cycle Fatigue of Large Diameter Bolts," *Journal of Engineering for Industry*, Vol. 89, Sec. B, No. 1, February 1967, p. 53.

2.10 "Tentative Structural Design Basis for Reactor Pressure Vessels and Directly Associated Components," PB 151987, U.S. Department of Commerce, Office of Technical Services, December 1958.

2.11 M.E. Mayfield, E.D. Rodabaugh, and R.J. Eiber, "A Comparison of Fatigue Test Data on Piping with the ASME Fatigue Evaluation Procedure," ASME Paper No. 79-PVP-92.

This page intentionally left blank.

3. GENERIC EVALUATION OF CONSERVATISMS

The purpose of this section is to describe several conservatisms that may exist when calculating ASME Section III fatigue usage factors. These conservatisms may reside in the Class 1 component Design Specification, the analytical methods, the application of the ASME Code to fatigue evaluations, and in the ASME Code version itself.

3.1 Definition of Design Transients

As described in Section 2, design transients for each Class 1 component are defined in the component Design Specification. Typically, information is given on the pressure, temperature and flow rate conditions associated with various modes of plant operation. Transients are presented in the form of idealized time histories, with the idealization being in the form of linear ramps and step changes. Of particular importance to fatigue evaluations are the temperature transients, and the main source of conservatism in the temperature transients are the step changes (see Figure 3-1). The worst condition that can occur is a step-down followed later in time by a step-up in temperature. This leads to large secondary and peak stress ranges, which in turn can lead to large fatigue usage factors. "Real" transients seldom exhibit step changes, though they may approach them for transients where cold water is injected into a hot nozzle and later turned off. In addition, the ramps defined in a Design Specification may occur over too short a period of time, and the maximum pressures and temperatures may be conservatively high. The number of cycles of each transient should have been defined such that they would bound the expected number during the plant lifetime. In some cases, the number of transients that have occurred in actual plant operation exceeds the number defined in the Design Specifications.

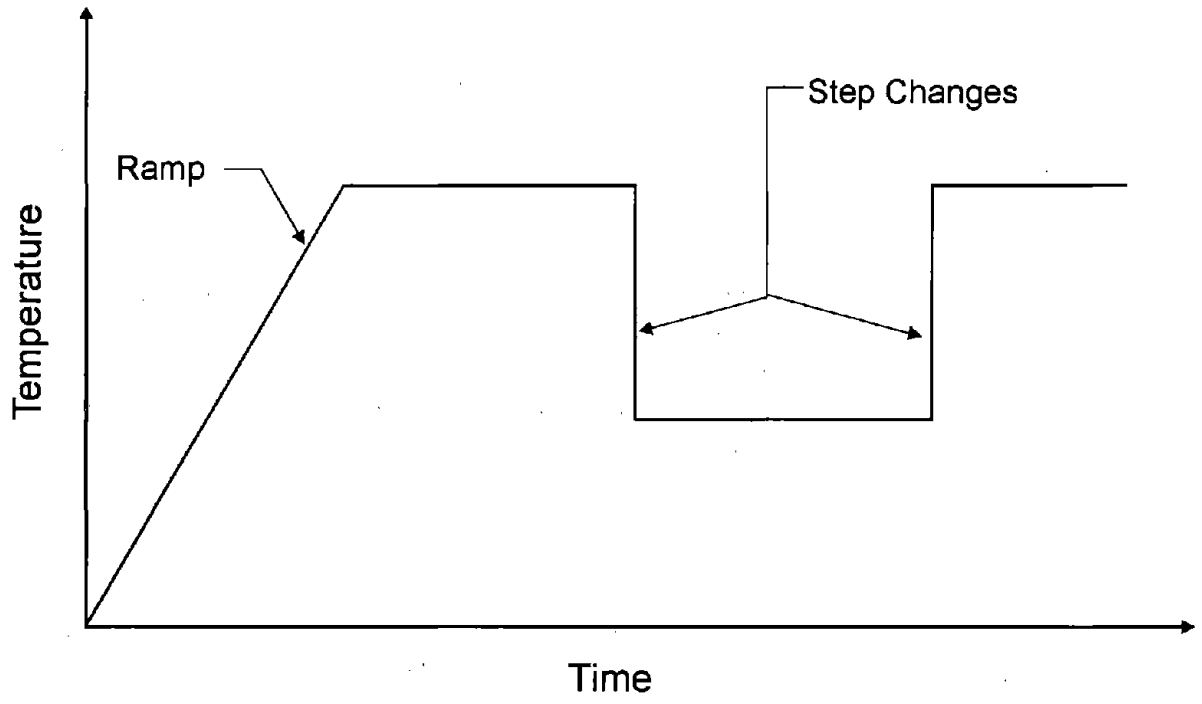

Figure 3-1. Illustration of Ramp and Step Changes.

3.2 Analytical Methods

Analytical methods used in the evaluation of Class 1 components can be classified into the following categories:

1. Formulas
2. Interaction Methods
3. Finite Difference Solutions
4. Finite Element Analysis

The two basic types of analyses performed are heat transfer and stress analyses. The purpose of the heat transfer analysis is to calculate the temperature distribution throughout the component at critical times during the operating transients. For an analysis of a Class 1 component using the rules of NB-3200, the heat transfer evaluation may be done by formula, finite difference or finite element analysis methods. For evaluation of Class 1 piping to NB-3650 criteria, the heat transfer evaluation is normally accomplished by use of standard formulas, although finite difference or finite element techniques are sometimes used to qualify certain "problem areas" which have high usage factors predicted by NB-3650 rules. In these cases, the piping component may also be qualified by the NB-3200 criteria.

The most conservative of the heat transfer methods is heat transfer analysis by formula. The formulas assume one-dimensional heat transfer, and depending upon the component in question, this could be quite conservative. A typical example of this conservatism occurs at junctions of components with different thicknesses, such as pipe to valve body welds. The one-dimensional heat transfer formulas assume heat flow in the radial (through the pipe or valve body wall thickness) direction, but not in the axial direction. For transients with increasing temperature, this leads to higher average temperatures in the thinner walled (pipe) component, and the $|\alpha_a T_a - \alpha_b T_b|$ term in Equation 10 of NB-3650 (Section 2.5) may cause high computed stresses. A two-dimensional finite difference or finite element analysis can eliminate some of these average temperature differentials by incorporating axial heat flow between the different components.

Another potential area of significant conservatism occurs in the choice of boundary conditions for the heat transfer analysis. The boundary conditions are heat transfer coefficients and temperatures which are imposed on surfaces of the component. The boundary temperatures and sometimes the heat transfer coefficients are defined in the Design Specification. Typically, the heat transfer analyses are performed using constant heat transfer coefficients throughout the analysis. Since the heat transfer coefficients are functions of the metal and fluid temperature and the flow rate, among other variables, the "real" heat transfer coefficient will be a function of time. The heat transfer coefficients used in Class 1 component evaluations are chosen with conservatively high values to bound the actual heat transfer coefficients which will occur. This can be another source of significant conservatism in Class 1 heat transfer analyses.

Stress analysis of Class 1 components evaluated using NB-3200 rules have been performed based on handbook formulas for stress, "interaction methods" and finite element models. Interaction methods [3.1] are closed formed analytical solutions for thick shell components. Continuity of displacements and rotations between different components, such as nozzles and vessel walls, are enforced by application of axial and shear forces and bending moments. The interaction models are axisymmetric, and can be used to calculate stresses due to pressure and axially varying temperatures. The interaction models can only analyze for averaged through-wall temperatures. Stresses due to linear and nonlinear through-wall (radial) temperature variations must be calculated by other means, usually by formula. Since the formulas assume complete suppression of thermal expansion, they yield conservatively high stresses.

Many recent evaluations of nozzles (late 1970s onward) have used finite element analyses to calculate stresses. Linear elastic behavior is assumed. However, as is discussed in Section 2, linear elastic models overpredict stresses when the yield strain is exceeded. Although the ASME Code Section III takes this into account when setting allowables for primary plus secondary stresses in the fatigue evaluation, the least amount of conservatism occurs with the use of finite element methods that model plastic behavior.

Class 1 piping is analyzed to the stress criteria of NB-3650 by use of three dimensional beam-type models. These models are "exact" solutions, within the limitations that material properties, nozzle and support stiffnesses, loadings and other input parameters are known, and may also add conservatisms into fatigue usage calculations.

3.3 Application of ASME Code

The purpose of the original Class 1 component stress reports was not to calculate the lowest possible cumulative fatigue usage factor based on a detailed analysis, but to demonstrate that the component had a cumulative fatigue usage factor of ≤ 1.0. This sometimes led to conservative "groupings" of design transients which led in turn to conservatively high usage factor calculations. As an example, assume that the total number of all operating cycles in the plant due to thermal and mechanical loadings is 1,000. Also assume that the largest peak stress range is due to a single transient with 10 cycles defined in the Design Specification. The design fatigue curve is then entered at this single peak stress (S_{alt}) value, and an allowable number of cycles, N, is found. If the cumulative usage factor is calculated as $1{,}000/N$ and this value is less than unity, then no further analysis is required. Although extreme, this is an example of conservative grouping of design transients.

Other conservatisms are associated with the calculation of K_e ("elastic-plastic penalty factor"). As is discussed in Section 2, K_e is inversely proportional to $3S_m$. Since S_m is a function of temperature, particularly for austenitic stainless steels, choosing S_m at the maximum operating temperature can lead to a higher than necessary value for K_e. The fatigue evaluation can be very sensitive to increased values of K_e, since this "penalty factor" is applied directly to the peak stress intensity range before entering the design fatigue curve. As is shown in the notes to Figure 2-2, NB-3200 allows S_m to be the average of the tabulated S_m values at the highest and lowest metal temperatures during the transient, as long as all of the primary plus secondary stresses associated with the transient pair are due to thermal, not mechanical, stresses. In some

cases, $3S_m$ is taken at the maximum operating temperature, and a lower than necessary value of $3S_m$ is used causing K_e to be higher than required.

K_e is also a function of the calculated primary plus secondary stress intensity range. The peak and secondary stresses due to a thermal transient vary with time. Typically, the maximum peak stress occurs earlier in a transient than the maximum secondary stress. This means that the K_e factor could be calculated for each point in time and applied to the peak stress. However, the normal practice is to calculate K_e based on the maximum primary plus secondary stress intensity range and then apply it to the maximum peak stress intensity range. Extra conservatism results from this practice.

Similar time phasing arguments for primary plus secondary and peak stresses could be made in the NB-3650 rules for piping. The calculation of peak stress (S_p) is done based on Equation 11 (Section 2.5). Contributions from three thermal components, $|\alpha_a T_a - \alpha_b T_b|$, $|\Delta T_1|$, and $|\Delta T_2|$ are summed along with contributions from mechanical loads to obtain the peak stress. However, these three components reach their maximums at different times in the thermal transient, as can be seen in Figure 3-2. This figure shows typical temperature and stress transients obtained for a ramped temperature transient at a thickness change between components a and b. The maximums for ΔT_1, ΔT_2, and $T_a - T_b$ occur at different times, but these maximums are summed together as if there was no time phasing. A less conservative method of combining these contributions in Equations 10 and 11 would be to find the time of maximum secondary (S_n) or peak (S_p) thermal stress, and then take the ΔT_1, ΔT_2, and $T_a - T_b$ associated with these time points and substitute these quantities back into Equations 10 and 11. In this manner, some credit could be taken for time phasing and the conservatism would be reduced. However, a finite element model of the piping component would be required, which would increase the cost of the analysis.

3.4 Conservatisms Within ASME Section III Code

All codes have conservatism built into them. The question is always whether the conservatism is excessive or not. Three areas of rather obvious conservatism in Section III of the ASME Code that are important to fatigue evaluations are:

- Analysis by Formula in NB-3650
- Inclusion of ΔT_1 in Equation 10 of NB-3650
- K_e

The first two of these areas of conservatism are closely related. Equations 10 and 11 of NB-3650 (see Section 2.5) calculate the thermal stresses due to ΔT_1, ΔT_2, and $T_a - T_b$ based on conservative formulas. The more sophisticated analyses such as allowed by NB-3200 would predict lower primary plus secondary and peak thermal stresses than the conservative formulas. The purpose of adding these equations into the Code was to provide a set of relatively simple rules for the evaluation of Class 1 piping. However, with the simplicity comes a significant amount of conservatism. Besides the use of the conservative formulas for thermal stresses, the maximum primary plus secondary and peak stresses due to pressure, bending moment and ΔT_1, ΔT_2 and $T_a - T_b$ thermal loads (using absolute values), are all assumed to be absolutely additive

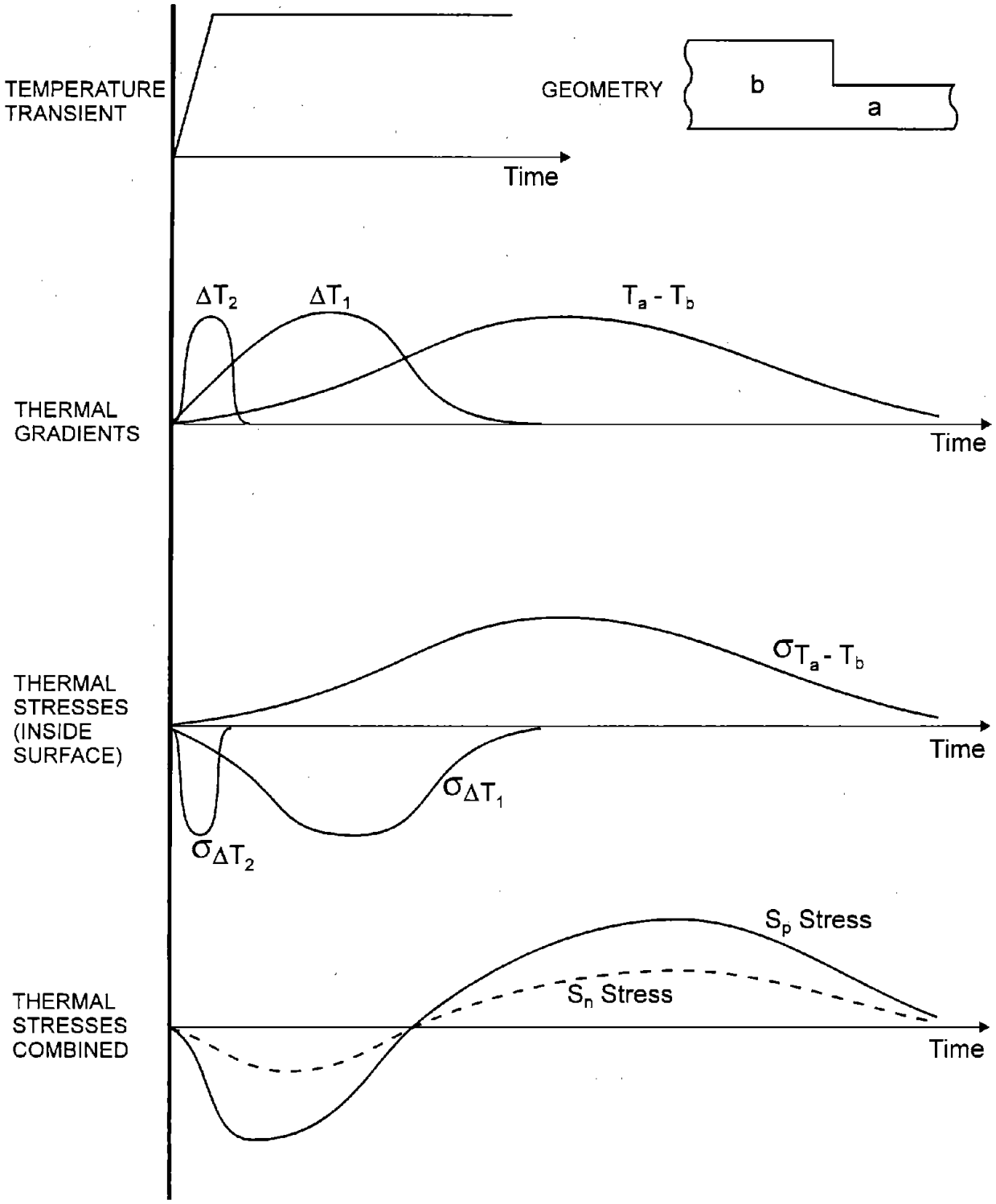

Figure 3-2. Thermal Stress-Time History for Typical Temperature Increase Transient.

and occur at the same location in the component. This conservatism can be eliminated by using the rules of NB-3200 for piping components, but this is not normally done unless the cumulative fatigue usage factor for the component is predicted to be greater than 1.0 using the formulas.

As stated in Section 2.5, the ΔT_1 term was included in Equation 10 for editions of ASME Section III prior to 1980. This is a conservatism for components designed to these earlier Code editions, and most of the currently operating nuclear power plants were designed to the earlier Code editions.

K_e is a significant area of conservatism in the Section III fatigue evaluation process. If any Class 1 component has a high fatigue usage factor (i.e., close to 1.0), it is generally found that K_e was calculated to be greater than 1.0 for at least one load set pair. As described in Section 2.4, K_e is equivalent to the actual peak strain divided by the peak strain calculated for completely elastic behavior. In Reference 3.2, K_e was calculated for two basic configurations; a tapered flat bar in tension and a cantilever beam (see Figures 3-3 and 3-4). For each configuration the maximum strain due to a given imposed displacement was calculated by two different methods. In the first method, the actual peak strain was calculated for an imposed displacement based on material behavior described by the following relationship:

$$\sigma = A\varepsilon^n$$

where:

σ = stress at any cross-section
ε = true strain at any cross-section
A = strength coefficient
n = strain-hardening exponent

Typical behavior modeled by this equation is shown in Figure 3-5. The maximum elastic peak strain is then calculated for the same imposed displacement. K_e is then the ratio between the peak strain calculated based on actual (elastic-plastic) behavior and the peak strain calculated assuming elastic behavior. For the tapered flat bar, Reference 3.2 demonstrates that:

$$K_e = \frac{(\frac{1}{n} - 1)}{1 - \rho^{(1-1/n)}} \log_e \rho$$

where:

$\rho = \frac{b_1}{b_o}$ = taper ratio.

Similarly, for the cantilever beam:

$$K_e = \frac{1 + 2n}{3n}$$

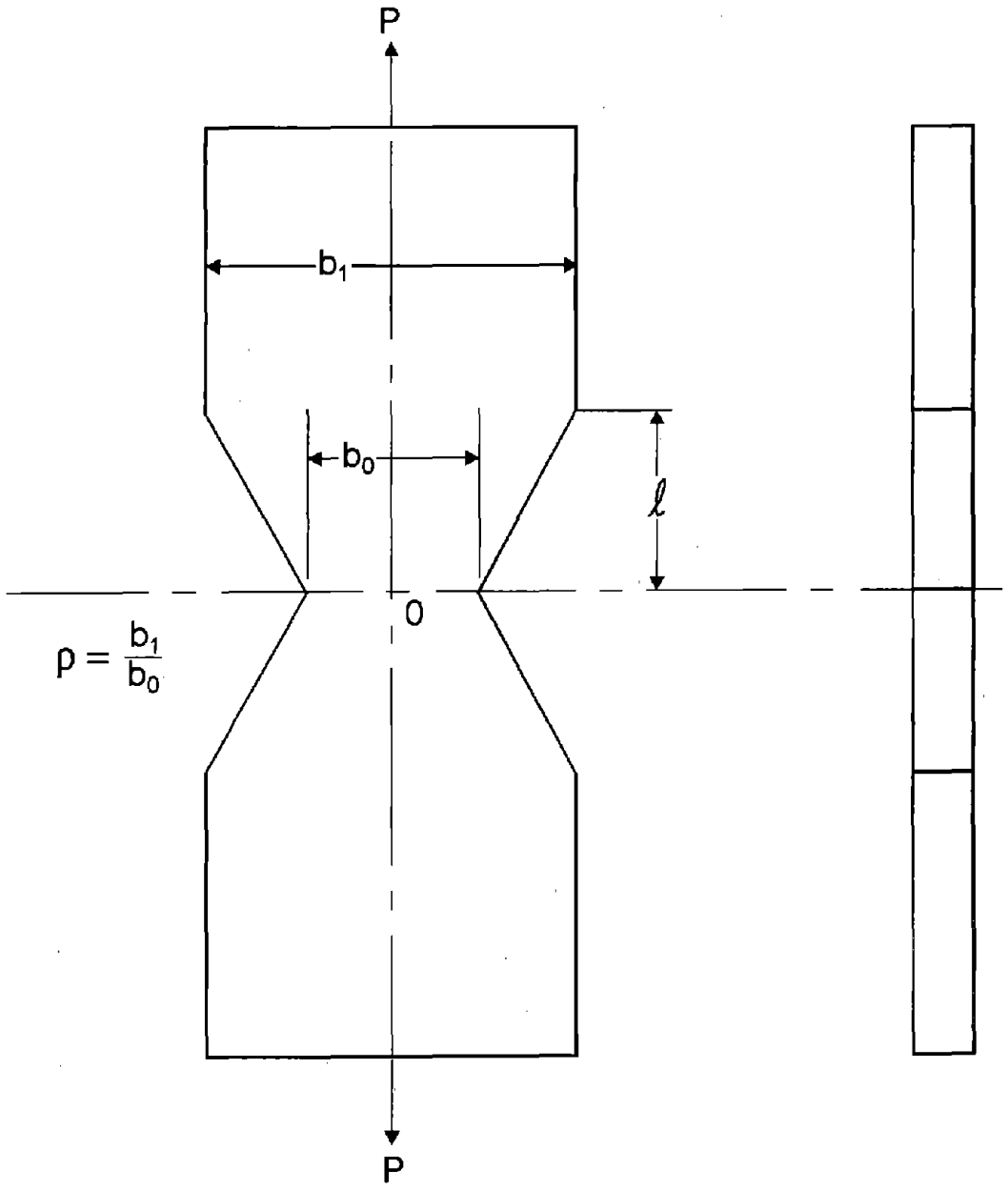

Figure 3-3. Tapered Flat Bar in Tension.

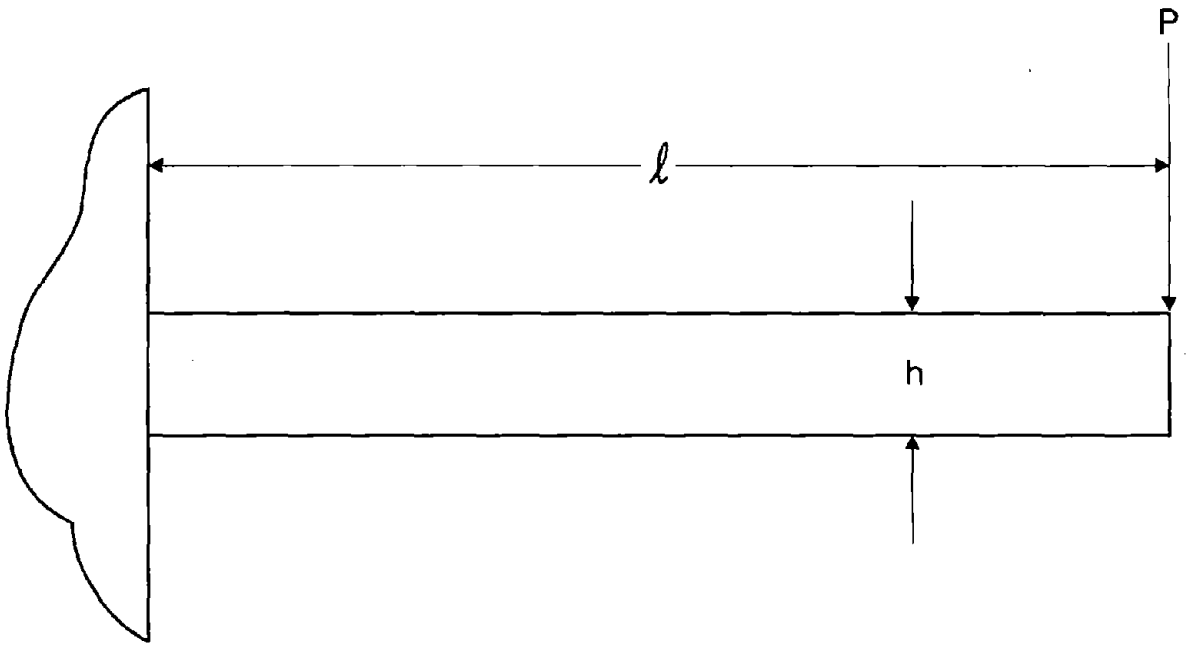

Figure 3-4. Cantilever Beam.

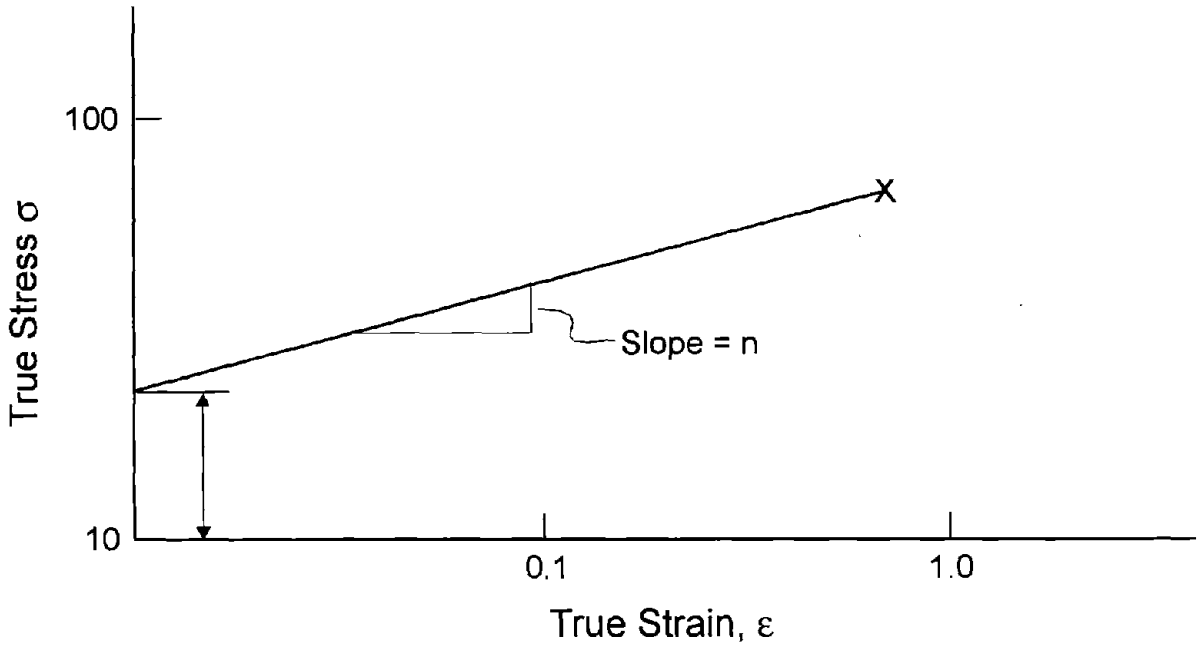

Figure 3-5. True Stress-Strain Curve Plotted on Log-Log Coordinates.

K_e is plotted as a function of n in Figure 3-6 for the tapered flat bar in tension (ρ = 2, 3, and 10) and for the cantilever beam. In addition, the equation $K_e = 1/n$ is plotted. As stated in Section 2.4, the maximum value of K_e in Section III is $1/n$. Since a linear interpolation is performed between K_e = 1.0 and $K_e = 1/n$, this maximum value affects all K_e calculations. For carbon steel (n = 0.2) and austenitic stainless steel (n = 0.3), $1/n$ equals 5.0 and 3.33, respectively. For the cantilever beam, K_e = 2.33 for carbon steel (n = 0.2) and 1.78 for stainless steel (n = 0.3). In the case of the tapered flat bar in tension, K_e = 2.96 for n = 0.2 and 2.02 for n = 0.3 assuming ρ = 2, which is a reasonable assumption for the tapered transitions normally seen in fatigue sensitive components such as nozzle safe-ends. It can be seen that the reduction of the maximum value of K_e can be drastic when the value of the K_e for the actual configuration is used instead of the Code value of $1/n$. For a stainless steel tapered transition with ρ = 2, the reduction is from 3.33 to 2.02, or 39%. This could have a large effect on the calculation of the fatigue usage factor, and represents a conservatism inherent in the Code.

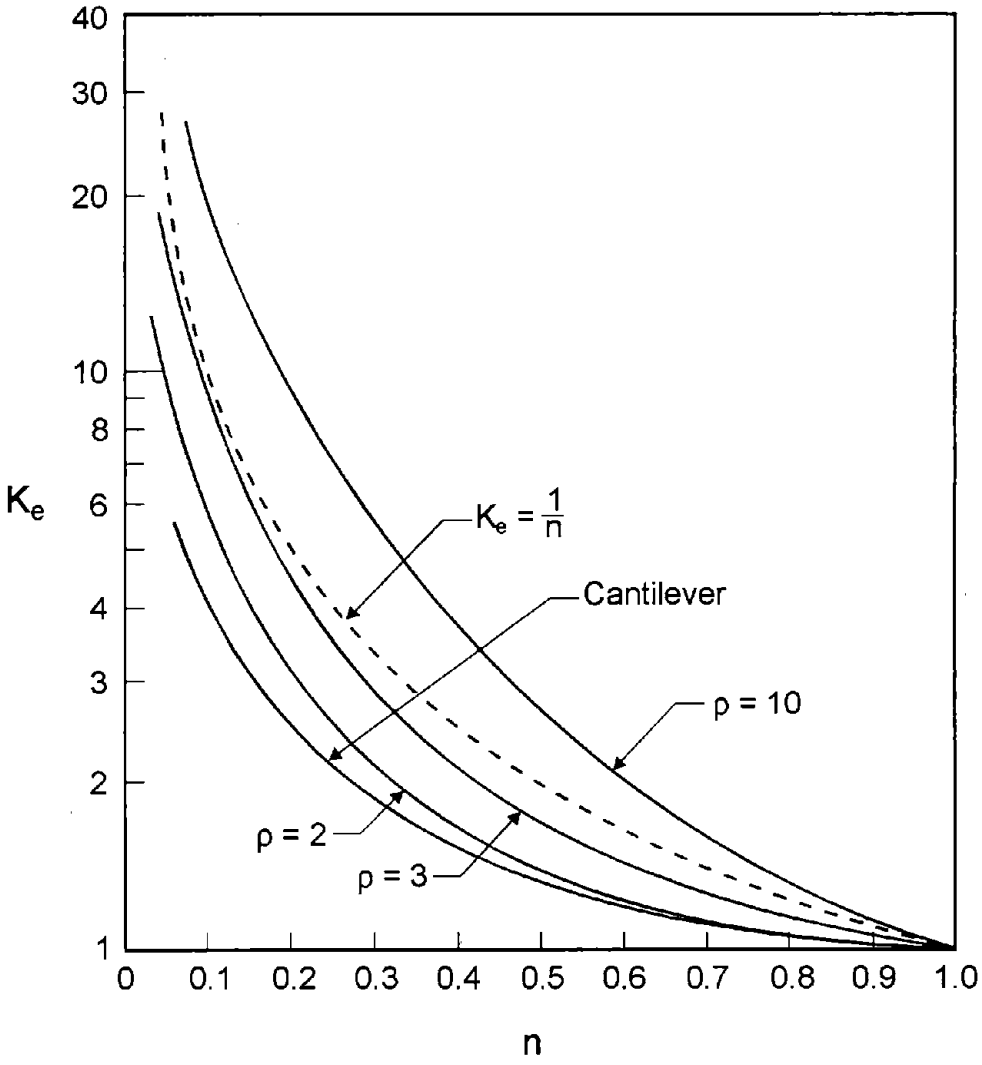

Figure 3-6. Strain Concentration Factors for Tapered Bar and Cantilever.

Another aspect of conservatism in the Code which is related to K_e concerns the two cases of loading, a tapered flat bar in tension and a cantilever beam, which were considered in the development of K_e. When considering components such as nozzles or piping, these two cases correspond to loadings due to pressure and piping reactions. However, the most significant contributions to the peak stresses are due to temperatures which vary in a linear and nonlinear manner through the component thickness. The peak stress which occurs in the nozzle safe-end when a step change in temperature occurs is highly nonlinear through the wall thickness. Clearly, this type of stress distribution was not considered in the development of K_e for Section III, and it would seem possible that application of the Code formulas for K_e to these nonlinear stress distributions would result in additional conservatism.

3.5 References

3.1 C.M. Freidrich, "Seal-Shell-2-A Computer Program for the Stress Analysis of a Thick Shell of Revolution with Axisymmetric Pressures, Temperatures and Distributed Loads," WAPD-TM-398, AEC Research and Development Report, December 1963.

3.2 B.F. Langer, "Design - Stress Basis for Pressure Vessels," *Experimental Mechanics*, January 1971.

4. PLANT SPECIFIC EVALUATION OF CONSERVATISMS

In order to quantify the conservatisms discussed in Section 3, ASME Section III Class 1 stress evaluations for a number of nuclear components were reviewed. The components were selected from four nuclear plants designed by the major domestic NSSS (Nuclear Steam Supply System) suppliers: General Electric (GE), Combustion Engineering (CE), Babcock & Wilcox (B&W), and Westinghouse. The selections were made based on consideration of a wide variety of components. In addition, components with high usage factors were chosen. Specific evaluations follow.

4.1 Results of GE Boiling Water Reactor (BWR) Review

The Class 1 components with the highest reported cumulative usage factors at this BWR plant were as follows:

- Feedwater Containment Penetration Flued Head: $U = 0.93$
- RPV Internal Steam Dryer Support Bracket: $U = 0.91$
- RPV Head Flange: $U = 0.89$
- Main Steam Drain Piping: $U = 0.95$
- RPV Head Bolts: $U = 0.74$
- RPV Support Skirt: $U = 0.66$
- Feedwater Nozzle Safe End: $U = 0.81$

For the feedwater containment penetration flued head, two fatigue evaluations were performed. The first evaluation, which was performed for the "standard" flued head design, was a reasonably detailed evaluation which lumped the thermal transients into 10 groups. A cumulative usage factor of 0.0923 was calculated. The second fatigue evaluation was performed for a "special case" flued head design. The only difference between the standard and special case designs was the length of the head. The width and shape remained the same. Since most of the peak stress was due to thermal transients, it would not be expected that there would be much difference in the cumulative usage factors. However, a large amount of grouping was used in the fatigue evaluation of the special case design, with all transients being lumped into only two groups. Because of this very conservative grouping, a cumulative usage factor of 0.93 was calculated for the special case design. One would expect that a more detailed fatigue evaluation would yield a cumulative usage factor much closer to 0.0923 than the reported maximum value of 0.93 (see assessment for RPV support skirt).

Stress analysis of the RPV internal steam dryer support bracket was performed with a detailed finite element model. Grouping of transients was not a significant contributor to the cumulative usage factor of 0.91. Most of this usage factor was due to the load set pair of startup/ shutdown, for which there were 111 cycles defined. Because the primary plus secondary stress

intensity was calculated to be 550 MPa [79.7 ksi] compared to a $3S_m$ of 414 MPa [60 ksi], a K_e = 2.094 was calculated for this load set pair. The design fatigue curve then yielded an allowable number of cycles, N = 150. The usage factor for this load set pair (not cumulative usage factor) was then 111/150 = 0.74. The only conservatism in this usage factor appears to be the use of K_e from the simplified-elastic plastic analysis. If plastic analysis was used instead, the K_e penalty would not have to be taken and it is expected that the usage factor could be reduced substantially.

A cumulative usage factor of 0.89 was calculated for the RPV head flange. This factor was very conservatively estimated by lumping cycles together. As an example, 360 cycles of leak checks were lumped with 40 cycles of hydrotest. The RPV pressures for hydrotest and leak check are 8,618 kPa [1250 psig] and 2,758 kPa [400 psig], respectively. The RPV temperature is 37.8°C [100°F]. In addition, bolt preload, shutdown and scrams were grouped together. These two groups were combined with the zero load case to obtain a stress range, which is also conservative, since the flange stress will only go to zero when the flange bolts are unbolted. Although sufficient stress information was not available to recalculate the cumulative usage factor in a less conservative manner, the load grouping adds substantial conservatism to the cumulative usage factor calculation.

The cumulative usage factor of 0.74 for the RPV head bolts is almost completely due to the bolt-unbolt operations. The first area of conservatism is the assumption that a single bolt experiences the maximum and minimum stress conditions during each bolting/unbolting pass even though the maximum might be for one bolt while the minimum is for another. The bolts are tensioned eight at a time so there are nine separate operations per tensioner for each bolt-up or unbolt pass. There are also three complete passes required for full bolt-up and two for unbolt. Each bolt then sees a different stress level than the bolt next to it due to the difference in times between when they are tensioned. To make one fatigue analysis apply to all bolts, one bolt is assumed to see the maximum stress ranges which occur for any of the 72 bolts during each phase of the bolt-up or unbolt process. This will not occur in practice, and is a source of conservatism.

The other source of conservatism in the fatigue evaluation of the RPV head bolts is the assumption of 120 vessel startups, or in effect 120 bolt-up and unbolt operations. Stress cycles due to these operations accounted for more than 70% of the cumulative usage factor, but it appears unlikely that 120 bolt-up/unbolt cycles would occur over a 40 year plant life (3 per year).

A significant amount of load grouping was a factor in the calculation of a cumulative usage factor of 0.66 for the RPV support skirt. Table 4-1 shows that this usage factor was calculated by taking the total of the cycles for all design transients, and dividing this by the allowable number of cycles for the highest peak stress range. However, the highest stress range included SRV blowdowns, for which only 8 cycles were expected. Elimination of this conservative transient grouping showed that the cumulative usage factor could be reduced to 0.15.

Table 4-1. Assessment of Conservatisms for RPV Support Skirt

Design Transient	# Cycles
Hydrotests	40
Startup/Shutdown	120[(1)]
Turbine Trip	10
Feedwater Bypass	70
Scrams	180
Loss of Feedwater Pumps	30
Design Seismic	10
Leak Checks	360
Total number of cycles	820

[(1)] Includes 8 SRV blowdowns (all shutdowns assumed to be SRV blowdowns)

- Highest peak stress: load pair of startup and SRV blowdown
- Allowable number of cycles for highest peak stress range was 1250

  $\therefore$ Reported usage factor (U) = $\frac{820}{1250} = 0.66$

- Detailed analysis showed that less conservative grouping of transients could reduce usage factor to 0.15

For the main steam drain piping, the cumulative usage factor of 0.95 at a socket-welded nozzle was due primarily to SRV discharge dynamic response loadings. Equation 10 of NB-3650 contained the $|\alpha_a T_a - \alpha_b T_b|$ term for the Code of Record (1974 edition), but this term was not a large contributor to the primary plus secondary stresses for the load set pairs which contributed substantially to the cumulative usage factor. The amount of transient grouping that was done did not appear to be overly conservative. The ΔT_1s and ΔT_2s were also found to be quite small, so thermal stresses were not large contributors to the cumulative usage factor.

One way of reducing the cumulative fatigue usage for the main steam line drain piping would be incorporation of the results of the in-plant SRV testing which was performed subsequent to the Class 1 stress evaluation. Typically, the building response obtained from the SRV tests was significantly lower than the analytically predicted results, so calibration factors could be developed from the test results which could reduce the SRV piping stresses that were used in the fatigue evaluation. This would then lead to a reduction in the cumulative usage factor.

The cumulative usage factor for the feedwater nozzle safe end was calculated to be 0.81. These results were obtained from finite element models for both thermal and stress evaluations. Although some grouping of design transients was done, these groupings do not appear to add a significant amount of conservatism to the fatigue analysis. Based on a review of the available documentation, it was decided that there were two possible sources of conservatism; conservative calculation of K_e and the use of conservatively high values for heat transfer coefficients used in the thermal analysis.

The K_e calculation may have been conservative based on the reasons given in Section 3.3; the K_e for each load set pair stress range was calculated based on the maximum primary plus secondary stress intensity range, and did not take time phasing into account. The heat transfer values are typically taken from Design Specifications and are conservatively high, which would tend to produce conservatively high stresses in the component. Since the heat transfer coefficient is a function not only of flow rate and fluid temperature but also metal surface temperature, it would be reasonable to vary the heat transfer coefficient as these parameters change during the operating transient. The introduction of a time varying heat transfer coefficient into the thermal and stress evaluations, although difficult, should reduce some of the conservatism in the thermal stresses.

In order to quantify these conservatisms for the case of a carbon steel pipe with stainless steel cladding, a simplified thermal stress evaluation was performed for two cases; one with a constant heat transfer coefficient and another with a heat transfer coefficient dependent on flow rate and fluid and metal surface temperature that varied with time. The pipe geometry, modeled as a one-dimensional bimetallic cylinder, is shown in Figure 4-1. Design transients which were analyzed are shown in Figure 4-2. These are typical BWR feedwater nozzle transients.

Table 4-2 shows a summary of the results for the simplified analysis. The usage factors for the constant and varying heat transfer coefficient cases were calculated using two different methods. The first method does not take time phasing into account in the K_e calculation, and is conservative. The second method does take time phasing into account, and yields less conservative results. As can be seen from Table 4-2, there are significant gains in reducing the usage factor by varying the heat transfer coefficient according to the fluid and metal surface temperature and flow rate. When time phasing between the secondary and peak stresses is taken into account, a reduction of the usage factor by 8% occurred for the transients shown in Figure 4-2. When only the varying heat transfer coefficient is incorporated in the analysis (no time phasing), an 82% reduction in usage factor was obtained. When both varying heat transfer coefficient and time phasing were included, a reduction of 84% was obtained for the usage factor. Since it is not clear from the available documentation how these effects were analyzed for the BWR feedwater nozzle safe end, it cannot be said that these results show that the usage factor of 0.81 can be reduced by any amount, if at all. It does indicate, however, that calculation of the heat transfer coefficient and K_e (with regard to time phasing of secondary and peak stresses) can have a significant effect on the usage factor. Based on this single example, incorporation of a varying heat transfer coefficient has a more significant effect on the usage factor than incorporation of time phasing between secondary and peak stresses when calculating K_e.

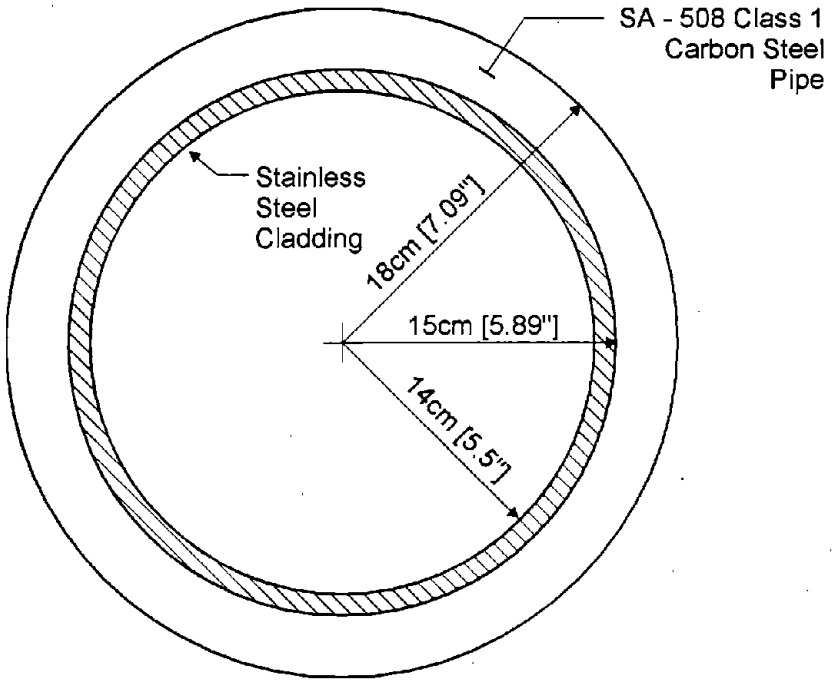

Figure 4-1. Carbon Steel Pipe With Cladding.

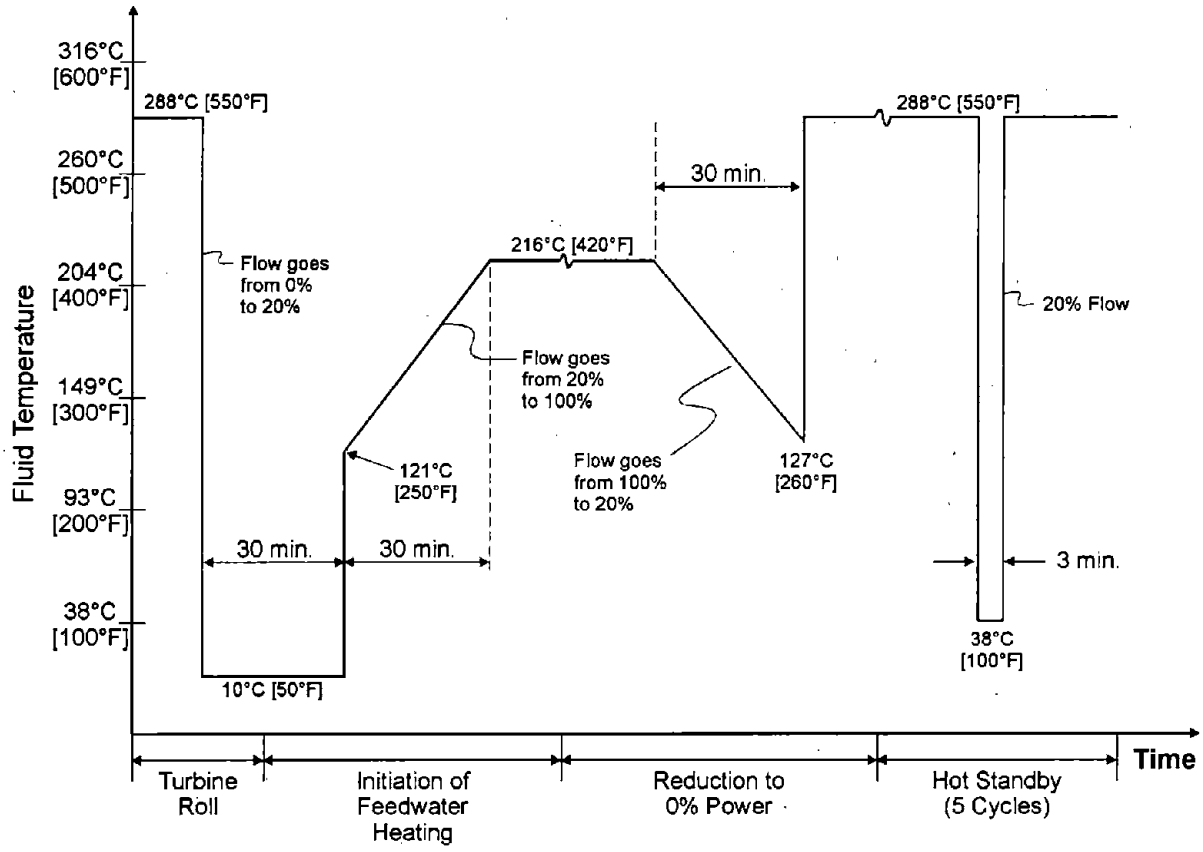

Figure 4-2. Typical BWR Feedwater Nozzle Transients.

Table 4-2. Effects of Time Phasing and Heat Transfer Coefficient on Usage Factors (Normalized)

Heat Transfer Coefficient	Time Phasing	
	No	Yes
Constant	1.00	0.92
Varying	0.18	0.16

4.2 Results of CE Pressurized Water Reactor (PWR) Review

The Class 1 components of the CE PWR plant that were evaluated in this study are as follows:

- LPI/Core Flooding Line: U = 3.31
- Charging Inlet Nozzle: U = 0.73
- RTD Surge Line Nozzle: U = 0.73
- Safety Injection Nozzle: U = 2.275 (simplified elastic-plastic analysis)
  U = 0.278 (plastic analysis)

The fatigue evaluation for the LPI/core flooding line was originally performed based on the requirements of ANSI B31.7-1969 (up to and including the 1971 Addenda), which are essentially the same as those of NB-3650 of ASME Section III. The original analysis showed that the component would have to be replaced early in plant life. This evaluation predicted a cumulative usage factor of 3.31 for a reducing tee in the low pressure injection/core flooding piping. The main source of conservatism is the choice of S_m at the maximum operating temperature of 318°C [605°F] for all transients. The maximum operating temperature varies as defined in the Design Specification for each transient. As was stated in Section 3, for load set pairs which include only thermal effects in the secondary stress, S_m values may be taken as the average of the tabulated S_m values at the highest and lowest temperatures of the metal during the transient. When part or all of the secondary stress is due to mechanical load, the value of S_m must be based on the highest temperature during the transient. The pipe material was stainless steel, with S_m varying from 138 MPa [20.0 ksi] at 149°C [300°F] to 118 MPa [17.06 ksi] at 318°C [605°F]. The equation for K_e for stainless steel is as follows (Section 2.4).

$$K_e = 1.0 + (3.33)\left(\frac{S_n}{3S_m} - 1\right) \leq 3.33$$

In the fatigue analysis which predicted a cumulative usage factor of 3.31, S_m was evaluated at 318°C [605°F]. However, the maximum temperature for any of the operating transients which produced significant fatigue usage at the reducing tee location was 138°C

[280°F]. The analysis conservatively used $3S_m$ = 3(118) = 354 MPa [51.18 ksi]. For an S_n = 535 MPa [77.6 ksi], K_e = 2.72. However, if $3S_m$ is taken as 3(138) = 414 MPa [60 ksi], which the Code allows, K_e for S_n = 535 MPa [77.6 ksi] would be reduced to 1.98, or a reduction of 27% from what was used in the stress report. The peak stress (S_p) associated with S_n = 535 MPa [77.6 ksi] was 959 MPa [139.1 ksi]. For K_e = 2.72, the ANSI B31.7 design fatigue curve for stainless steel yields N = 180 for S_{alt} = 0.5 (2.72)(959) = 1,304 MPa [189.2 ksi]. For K_e = 1.98, N = 500 for S_{alt} = 0.5 (1.98) 959 = 949 Mpa [137.7] ksi. Therefore, a 27% reduction in K_e results in a reduction in the usage factor for this load set pair from 3.31 to 1.19 or a reduction of 64%.

S_m values could be further increased for all load set pairs which included only thermal stresses and were associated with transients with operating temperatures of less than 138°C [280°F]. However, S_m for the stainless steel material used in the reducing tee has a constant value of 138 Mpa [20 ksi] for all temperatures under 149°C [300°F], so no further advantage of higher values of S_m could be taken.

In addition to the K_e effect, the fatigue curve presented in B31.7-1969 is based on a material with a modulus of elasticity of 179 x 10^3 MPa [26 x 10^3 ksi]. A Young's modulus of 195 x 10^3 MPa [28.3 x 10^3 ksi] was used in the analysis. No modification based on these differing modulii was made before entering the design fatigue curve in the original analysis. However, according to NB-3222.4(e) of ASME Section III, S_{alt} should be multiplied by the ratio of the modulus of elasticity given on the design fatigue curve to the value of the modulus of elasticity used in the analysis. This would result in an additional reduction in all S_{alt} values by a factor of (179/195) = 0.92, which would lead in turn to a reduction in usage factors.

When the effects of removing the conservatisms from the S_m values and the reduction due to the ratio of the elastic moduli are taken into account, the cumulative usage factor for the reducing tee was reduced from 3.31 to 0.92. In effect, this indicates that the component is adequate for the 40 year life of the plant, as opposed to only 40/3.31 = 12.1 years.

The equation to calculate S_n (primary plus secondary) stresses in ANSI B31.7-1969 includes the ΔT_1 term as discussed in Section 2.5. The current edition of ASME Section III does not include this term, and if it is eliminated, the cumulative usage factor is reduced further from 0.92 to 0.09. In summary, a less conservative analysis reduced the cumulative usage factor of the LPI/core flooding line from 3.31 to 0.09.

The charging inlet nozzle to the reactor coolant system (RCS) was evaluated for internal pressure loadings and longitudinal gradient thermal stresses by use of an "interaction model" that was based on axisymmetric shell theory [4.1]. The longitudinal thermal gradient was based on average through wall temperatures calculated at critical points for the temperature transients defined in the Design Specification. For the linear portion of the radial thermal gradient, the formula shown below was used to calculate the associated stress σ_{ts}:

$$\sigma_{ts} = \pm \frac{E\alpha\Delta T_1}{2(1 - \nu)}$$

where:

E = Young's modulus
α = coefficient of thermal expansion
ΔT_1 = linear portion of temperature gradient through the nozzle wall (see Section 2.5)
ν = Poisson's ratio.

For the remaining nonlinear portion of the radial through wall temperature gradient, the local thermal stress σ_{tp} was calculated using the following formula:

$$\sigma_{tp} = \frac{E\alpha\Delta T_2}{(1 - \nu)}$$

where:

ΔT_2 = nonlinear portion of the radial through wall temperature gradient.

σ_{ts} is classified by NB-3200 of Section III as a secondary stress and σ_{tp} as a peak stress. The temperature distributions for the operating transients were calculated by the use of a two-dimensional finite difference model. Mean temperatures, ΔT_1 and ΔT_2 were calculated for a number of through wall sections. The maximum values of these quantities were calculated for each of the transients.

The piping reaction loads due to dead weight, thermal expansion, and seismic events were evaluated using "classical" methods treating the nozzle as a beam. Discontinuity stresses in the junction between the nozzle and RCS piping wall were calculated based on the methods of Welding Research Council (WRC) Bulletin 107 [4.2]. In order to calculate the primary plus secondary stresses, the pressures and axial thermal stresses taken from the interaction model were added to the stresses due to pipe reactions and the ΔT_1 radial thermal gradient at each through wall section. The highest primary plus secondary stress location occurred in the stainless steel safe end near the weld to the low alloy nozzle. The "ΔT_1" stress at this location was calculated to be 442 MPa [64.2 ksi] for the loss of charging flow transient. The total primary plus secondary stress intensity range at this location was 653 Mpa [94.7 ksi], so the ΔT_1 stress contribution accounted for nearly 70% of the total. Since $3S_m$ was taken as 343 MPa [49.8 ksi] for the 316 stainless steel safe end, $K_e = 1/n = 1/0.3 = 3.33$. When this K_e was applied to the peak stress range resulting from the loss of charging flow/unloading load set pair, an S_{alt} of 1,605 MPa [232.8 ksi] resulted. The allowable number of cycles from the stainless steel design fatigue curve was 105 cycles. When compared to the 200 cycles defined for this load set pair in the Design Specification, a usage factor of 200/105 = 1.9 > 1.0 was calculated. The ASME Section III fatigue requirements were not met using the simplified elastic-plastic method.

Since the primary plus secondary stress in the safe end was primarily due to the ΔT_1 thermal stress, an axisymmetric linear elastic finite element model was developed to more accurately estimate the secondary stresses calculated by the simple formula for σ_{ts}. The temperature distribution from the finite difference thermal model for the loss of charging flow transient was directly input to the finite element stress model. Using the results of the finite

element model, the primary plus secondary stress intensity for the loss of charging flow/unloading transient load set pair was reduced from 653 MPa [94.7 ksi] to 507 MPa [73.5 ksi]. Although it was still necessary to use a K_e greater than 1.0, the usage factor for this load set was reduced to 0.57, and the cumulative usage factor was calculated to be 0.73 (rather than 1.9), so the Section III fatigue requirements were met.

This example illustrates the limitations associated with the use of interaction models for analysis of Class 1 nozzles. Since the interaction model did not have the capability to calculate the thermal stresses due to the radial temperature gradient, conservative formulas were used, resulting in an artificially high usage factor. This also illustrates the "non-linear" effect on the allowable number of cycles that occurs when S_{alt} is reduced. In this case, a 34% reduction in S_{alt} resulted in a 233% increase in the allowable number of cycles for the critical load set pair.

The resistance temperature device (RTD) nozzle on the surge line piping is connected to the run pipe by means of a partial penetration weld. The RTD nozzle and surge line piping are treated as two separate bodies in the thermal analysis of the operating transients. The nozzle was analyzed as a one-dimensional body, and mean temperatures were calculated by use of closed form solutions. Only heat flow through the thickness of the nozzle was considered. This method is conservative when considering temperature differences between adjacent bodies since a two-dimensional model that contained both the nozzle and pipe would produce a lower temperature difference between the pipe and nozzle.

The stresses in the RTD nozzle were then calculated by means of an axisymmetric finite element model. The main area of interest for the fatigue evaluation was the partial penetration weld, so stresses due to temperature and pressure were calculated based on the thermal displacement "mismatch" between the nozzle and pipe wall. This mismatch was applied to the free end of the finite element model. Stresses due to mechanical and thermal loadings in the surge line piping were also included. The maximum primary plus secondary stress intensity calculated for the partial penetration weld area was 312 MPa [45.2 ksi], which was less than the $3S_m$ value of 343 MPa [49.8 ksi], so K_e was not calculated.

For the fatigue evaluation, a fatigue strength reduction factor of 4 was used at the partial penetration weld. A cumulative usage factor of 0.73 was calculated, with 0.55 due to the plant unloading/loss of load set pair, of which there were 29,910 cycles.

The main area of conservatism in the RTD nozzle fatigue evaluation was the one-dimensional thermal analysis. The large "mismatch" in displacements, which was produced at the partial penetration weld, created thermal stresses in this weld which would be reduced if a two-dimensional finite difference or finite element heat transfer model of the nozzle and pipe wall had been employed. Reduced thermal stresses would be expected to substantially reduce the cumulative usage factor.

The safety injection nozzle to the RCS was analyzed by use of an interaction model. The analysis procedure was similar to that employed in the evaluation of the charging inlet nozzle. In the calculation of primary plus secondary stress intensity ranges, all of the stresses due to pipe reactions were assumed to be fully reversible in sign, which increased the range. The three loadings which contributed to the pipe stresses were dead weight, thermal expansion, and seismic

events. Of the three, only seismic is reversible. Not enough detail was available in the stress report to quantify the conservatism involved.

The cooldown transient resulted in the largest primary and secondary stresses and usage factors. The primary plus secondary stress intensity exceeded $3S_m$ for the cooldown load set pair (cooldown at 1.956 hours/cooldown at 2.205 hours), and a K_e of 2.7 was used. The high stress range is due to a step decrease in temperature from 177°C [350°F] to 4°C [40°F] followed by a step increase to 163°C [325°F]. Similar to that for the charging inlet nozzle, the thermal stresses due to radial thermal gradient were calculated by formula, but the stress due to ΔT_1 was not separated out in the calculation. The nozzle safe-end usage factor for the cooldown load set pair was 2.273, and the cumulative usage factor was calculated as 2.275. Therefore, Code requirements for fatigue were not met by the safety injection nozzle when simplified elastic-plastic analysis was used.

In order to demonstrate compliance with the ASME Section III fatigue requirements, the provisions for Shakedown Analysis in paragraph NB-3228.4 of the Code were used. A finite element model of the safe end was developed, and a plastic analysis was performed to demonstrate shakedown. The total strain range after shakedown due to the cooldown load set pair was then multiplied by one-half of Young's modulus. This value was then used to enter the design fatigue curve, which gave N = 1800 cycles, as compared to the value of 500 cycles in the Design Specification. Since virtually all of the fatigue usage was due to the cooldown load set pair, fatigue requirements for the Safety Injection Nozzle were satisfied.

This example serves to demonstrate the conservatism of the simplified elastic-plastic method as compared to a plastic analysis. The usage factor for the critical load set pair was reduced from 2.273 to 500/1800 = 0.278, or by a factor of approximately 8, by the application of a plastic analysis.

4.3 Results of Babcock & Wilcox PWR Review

The Class 1 components with the highest reported cumulative usage factors at the B&W PWRs included in this study were:

- Steam Generator Support Skirt: U = 1.0
- RPV Core Flooding Nozzle: U = 0.80
- RPV Instrument Tube Nozzle: U = 0.57
- RPV Primary Inlet/Outlet Nozzle: U = 0.52

For the steam generator support skirt, the usage factor of 1.0 was due primarily to the thermal stresses created by heat-up/cooldown transients. A total of 240 cycles of these transients were assumed. Based on the information available in the stress report, a significant amount of load grouping was not done. The primary plus secondary stress range for this transient was 838 MPa [121.5 ksi], which was larger than $3S_m$ = 552 MPa [80 ksi]. This steam generator was designed based on the 1968 Edition of Section III, which did not contain rules for simplified

elastic-plastic analysis. K_e was then calculated based on the 1969 Edition of ANSI B31.7, which contained the K_e concept, although the method of calculating K_e was different from what is now contained in Section III. The major reason for the high usage factor appears to be use of an interaction model to calculate the stresses in the skirt to shell junction. The thermal stresses due to the radial temperature distribution were calculated by the formula for σ_{tp} (see Section 4.2), so it should be expected that substantial conservatism would result.

Interaction models were also used to perform the stress analysis of the RPV core flooding nozzle, instrument tube and primary inlet/outlet nozzles. As has been previously stated, these models overestimate the thermal peak stresses as compared to a two-dimensional finite element model. In addition, a K_e of 1.7 was used with the critical load set pair in the fatigue evaluation of the core flooding nozzle. It is believed that a plastic analysis of this component, which would eliminate the use of K_e, would yield a significantly lower usage factor.

For the RPV instrument tube nozzle, a stress analysis was performed which was quite similar to that described for the RTD surge line nozzle in Section 4.2. The conservatisms in this analysis could be reduced by the use of two-dimensional heat transfer/stress analysis finite element models instead of the one-dimensional heat transfer analysis and interaction method stress analysis.

The calculated cumulative usage factor for the RPV primary inlet/outlet nozzle was 0.52. The primary contributor to this was a partial usage factor of 0.40 due to the plant loading/unloading load set pair grouped with the 0 to 15% full power heatup transient. The plant loading/unloading load set pair consisted of 48,000 cycles of a heatup/cooldown of 25.9°C [54°F] temperature increase which was postulated to take place within 20 minutes. Transient grouping was performed to create 49,440 cycles of a heatup/cooldown of 41.9°C [75.5°F] that ramped up and then down within 28.8 minutes. Since the 41.9°C [75.5°F] temperature increase/decrease was a 62% increase over the plant loading/unloading transient defined in the Design Specification, this was a significant source of conservatism in the fatigue evaluation.

4.4 Results of Westinghouse PWR Review

Stress analyses for a Westinghouse Reactor Pressure Vessel, Pressurizer, and Class 1 piping components were reviewed. Results are summarized in the following paragraphs.

Compared to a BWR, there are very few locations in a PWR RPV that are susceptible to severe thermal transients. There are relatively few vessel nozzles since the ECCS and instrumentation systems are connected to the RCS piping. The subject plant is of a relatively late vintage, and the vessel stress analysis was conducted to the 1971 ASME Code with Summer 1973 Addenda. The methods of analysis did not include current state of the art finite element methods for stress analysis, but instead included interaction analysis using thick shell equations which were performed manually. A finite difference thermal analysis was conducted.

The locations of maximum usage were:

- Vessel Closure Studs: $U = 0.478$

- Maximum Vessel Wall Thickness Transition: $U = 0.012$
- Vessel Reactor Coolant Nozzle: $U = 0.101$
- Control Rod Drive Mechanism (CRDM) Housing-to-Vessel Weld: $U = 0.109$
- Bottom Instrument Nozzle-to-Vessel Weld: $U = 0.318$
- Core Support Lug: $U = 0.061$

Some key conservatisms found in the analyses of these components included:

- For the refueling transient, it was assumed that the vessel was instantaneously filled with 0°C [32°F] water when the vessel was at 60°C [140°F] (i.e., step change in temperature). All other heating and cooling transients did not exceed 38°C/hr [100°F/hr].
- For the CRDM and bottom instrument penetration analyses, the junction between the vessel and the attached components were separately analyzed for thermal effects. The forces and moments to ensure compatibility between the two parts were determined and converted to a stress at the fillet weld. A fatigue strength reduction factor of 4.0 was then applied.
- For the vessel nozzles, the interaction analysis could not determine peak stresses. Therefore, an additional stress was determined using the equation for σ_{tp} discussed in Section 4.2. Poisson's ratio was taken based on NB-3227.6 (see Section 2.3).

The Pressurizer was also analyzed to the 1971 ASME Code with 1973 Addenda. The level of detail provided in the component stress report made it quite difficult to determine exactly how the reported usages were derived.

Areas of high reported usage include:

- Upper head and adjacent shell (cladding): $U = 0.90$
- Spray Nozzle: $U = 0.821$
- Relief Valve Support Bracket: $U = 0.618$
- Shell at Seismic Lug: $U = 0.97$
- Heater Penetration: $U = 0.13$
- Surge Nozzle (at shell): $U = 0.998$
- Surge Nozzle (at nozzle end): $U = 0.599$
- Instrument Nozzle (at shell): $U = 0.16$

- Pressurizer Support (at shell): $U = 0.99$
- Pressurizer Support (at "support foot"): $U = 0.70$

The highest usages were generally in the cladding, where the computed stresses were increased to account for Poisson's ratio effects (NB-3227.6). It was apparent that the analysis was conducted to the level of detail necessary to show that usage factors were less than unity.

There was a significant amount of grouping of the transients in the Pressurizer evaluation. For example, the most critical transient was the inadvertent auxiliary spray transient, of which 10 were postulated. This was grouped with 510 other transients which included Loss of Load, Inadvertent Safety Injection, Large Step Increase of Load, etc. The stress magnitudes of these other transients were less.

The Class 1 piping analysis was conducted to the 1971 ASME Code with Summer 1973 Addenda. Table 4-3 summarizes the results. The piping analysis was conducted in several steps, depending on the results. If the usage was greater than unity based on analysis, then a more detailed evaluation was made of the piping heat transfer analysis and the affected locations were re-evaluated. For the simplified analysis, a bounding value of heat transfer was assumed and ΔT_1 and ΔT_2 were determined for some bounding pipe sizes. For the $\alpha_a T_a$ - $\alpha_b T_b$ term, the difference was based on two unconnected one-dimensional thermal analyses. If problems still existed, then NB-3200 finite element thermal and stress analyses were conducted. In general, plastic stress analyses were conducted to qualify nozzles affected by sudden injection transients.

Table 4-3. Summary of Piping Stress Analysis for Westinghouse Plant

System	Total Locations	Usage (CUF)				
		CUF > 0.9	CUF > 0.8	CUF > 0.7	CUF > 0.4	CUF > 0.1
Reactor Coolant Loops A+C	58	1	4	4	6	12
Reactor Coolant Loop B+D	91	0	0	1	4	42
Pressurizer Safety & Relief	45	0	0	0	0	2
Pressurizer Spray	126	0	1	2	4	4
Reactor Coolant Bypass	22	0	0	0	0	0
High Head Safety Injection	166	0	7	11	22	38
Low Head Safety Injection	181	5	20	20	34	44
Loop Fill & Drain	192	5	14	33	83	89
Charging & Letdown	139	0	0	0	7	38
Seal Water	37	0	0	0	0	0
Residual Heat Removal	230	0	3	7	15	15
TOTAL	1287	11(0.8%)	49(3.8%)	78(6.1%)	175(13.6%)	284(22.1%)

The overriding conservatism in all of the analyses is that ΔT_1 was included in Equation 10 (pre-1979 ASME Code edition). Table 4-4 shows the number of locations where S_n from Equation 10 exceeded $3S_m$ ~ 414 MPa [~ 60 ksi]. In all cases, it was these locations where predicted usage was high. Exclusion of the ΔT_1 term, as permitted by the post-1979 Section III Code, would result in much lower usage. In addition, there was significant grouping of the multitude of transients that were defined for the reactor coolant piping in order to limit the number of individual load sets that needed to be analyzed.

Table 4-4. Summary of High Secondary Stress Regions

System	Number of Locations			
	690 MPa [100 ksi] No. >	620 MPa [90 ksi] No. >	552 MPa [80 ksi] No. >	414 MPa [60 ksi] No. >
Reactor Coolant Loop A+C	1	2	6	26
Reactor Coolant Loop B+D	3	4	7	60
Pressurizer Safety & Relief	0	1	2	7
Pressurizer Spray	0	2	6	8
Reactor Coolant Bypass	0	0	0	1
High Head Safety Injection	4	15	34	95
Low Head Safety Injection	21	25	28	126
Loop Fill & Drain	13	35	90	102
Charging & Letdown	3	9	24	70
Seal Water	0	0	0	4
Residual Heat Removal	1	4	14	135
TOTAL	46	97	211	634

4.5 References

4.1 WAPD-TM-398, AEC Research and Development Report, "Seal-Shell-2-A Computer Program for the Stress Analysis of a Thick Shell of Revolution with Axisymmetric Pressures, Temperatures and Distributed Loads," C.M. Freidrich, December 1963.

4.2 WRC Bulletin 107, "Local Stresses in Spherical and Cylindrical Shells Due to External Loadings," Wichman, Hopper & Mershon, Welding Research Council, August 1965.

5. FATIGUE MONITORING EXPERIENCE

Fatigue monitoring is the process whereby actual plant operational data are assessed to determine the severity of accumulated fatigue damage as compared to that considered in the design process. Although the technical approaches may vary, the end result is to compute the fatigue usage that occurs as a result of actual plant transient cycles. In the following, the methodology employed in this study will be described. In addition, the results of monitoring at a BWR plant feedwater nozzle for a series of 11 startups and shutdowns will be discussed.

5.1 Technical Approaches

5.1.1 Partial Cycle Evaluation

In the original plant design analysis, there are typically a few thermal transients that contribute most of the fatigue usage. In the design evaluation, the most adverse rates of change and range of temperatures are included in the Design Specification for the component or system. With partial cycle evaluation, additional analysis is conducted to show the sensitivity of the key design cycle temperature magnitudes and/or rates of change as they might affect the stresses in a component. From this analysis, the ratio of the usage from the design event to that of the actual plant event can be determined. References 5.1 and 5.2 describe such an approach in more detail.

5.1.2 Fatigue Transient Evaluation

Using fatigue monitoring, actual plant data are evaluated to determine the stress time history at monitored locations. The process is illustrated in Figure 5-1.

- Plant process data are evaluated. This results in a continuous history of plant transient data that may be used to determine the pressure, temperature and flow rate at fatigue-sensitive areas.

- Plant process data are evaluated to determine transient stresses at monitored locations. The analytical approach relies on transfer functions and Green's Functions to predict stresses from pressure, temperature, etc., time histories (e.g., as described in References 5.3, 5.4, and 5.5).

- The history of actual plant stresses is evaluated using an approach such as Rainflow or Ordered Overall Range (OOR) cycle counting, taking into account the actual cycle sequence of the event history [5.6]. This results in a stress range spectrum of "Number of Stress Ranges" versus "Stress Range Magnitude."

- The stress range spectrum is evaluated using the ASME Code methodology and fatigue design curves. Appropriate methodology must be included to perform simplified elastic-plastic analysis if the primary plus secondary stress range is predicted to exceed $3S_m$.

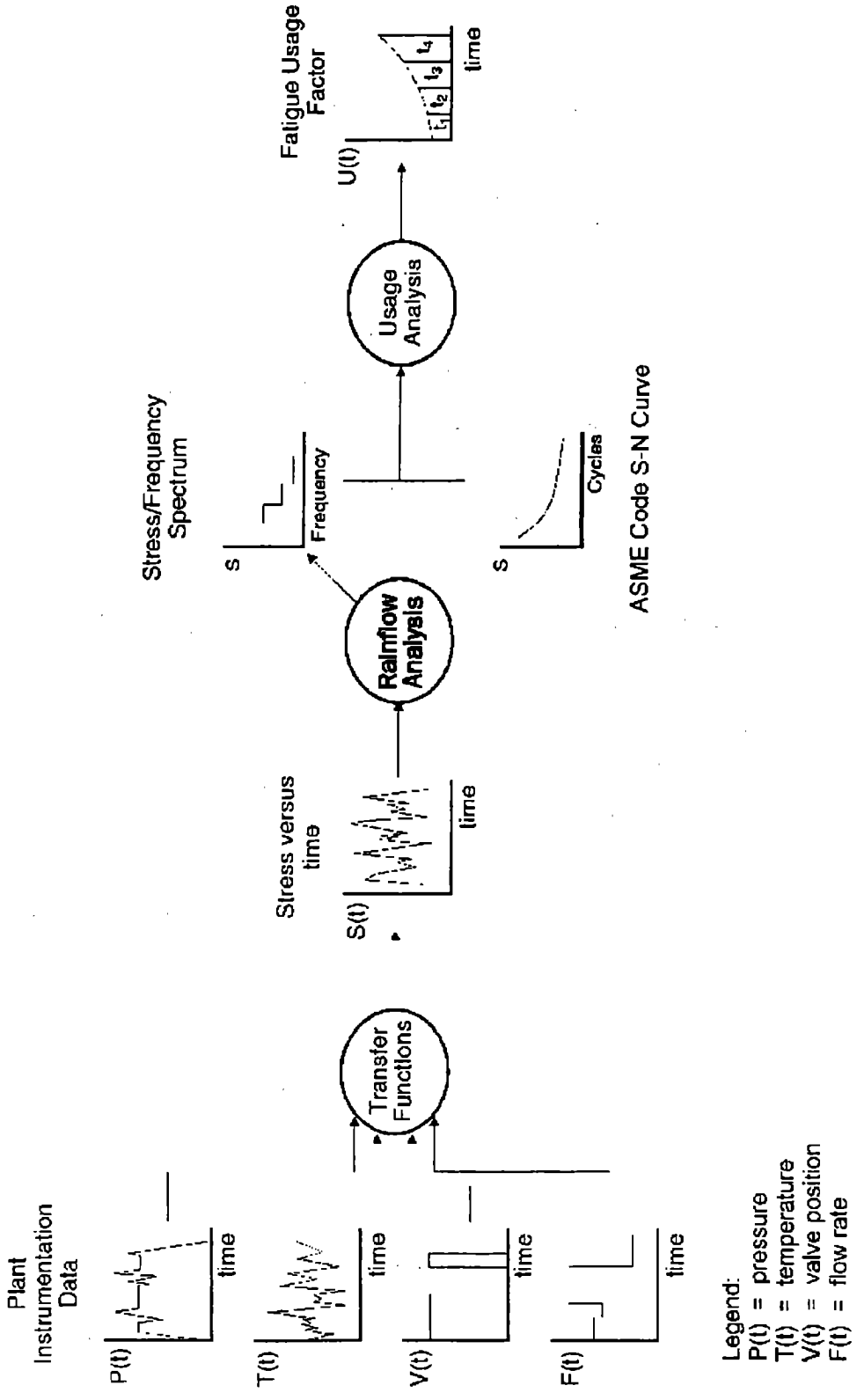

Figure 5-1. Schematic of Fatigue Usage Monitoring Methodology.

This method is inherently successful in evaluating the effects of actual plant transients as compared to those considered in the design process. The time history of local temperature change is determined based upon actual plant data history. No bounding assumptions are necessary regarding rates of change or magnitudes of step changes for temperatures at monitored locations. This results in a predicted stress history for the actual transients that are encountered in operation. Because of the shape of the ASME Code fatigue design curves (see Figures 2-3 through 2-5), small decreases in stress amplitude result in a significant increase in the number of allowable cycles. Thus, if actual stresses are lower, fatigue usage is generally much less than determined for equivalent types of cycles in the design process.

5.2 Results from Monitoring at a BWR Plant

Fatigue monitoring systems have been installed and utilized at a number of operating commercial nuclear power plants. At one BWR, the primary location of interest was the feedwater nozzle safe-ends where usage was relatively high based on the design stress analysis [5.7]. The plant had also experienced a large number of heatups, cooldowns and scrams, causing some concern that plant life might become limited due to these transients. A data acquisition system had been installed at the plant for a number of years. Therefore, actual plant data were available for assessing operating history prior to installing the monitoring system.

For the initial evaluation of plant data, a period from November 1987 through June 1989 was evaluated. During this period, the plant experienced 12 startups and 11 shutdowns, with 8 of the shutdowns occurring because of unplanned scrams. This sequence of events represents a significant data base, not just isolated events, and should provide a good indication of fatigue usage for the component.

Based on the feedwater nozzle safe-end stress report, the critical load set pair in the fatigue analysis is the combination of the turbine roll transient (initiation of feedwater flow at each startup) combined with the hot standby feedwater flow termination (stopping feedwater flow with cold feedwater in the nozzle, which might occur several times following each shutdown). For this transient pair, 646 cycles are allowed. Table 5-1 shows the fatigue analysis, including cycle pairing, for the critical location on the safe-end.

In the fatigue monitoring system, the methodology for computing stresses and fatigue usage was conservative and predicted values were higher than those reported in the feedwater nozzle safe-end stress report. The predicted number of allowable cycles (using the monitoring system) for the same controlling design transient cycle pair (with the associated step temperature changes) was approximately 45, or a usage of 0.022 per load set pair (1.0/45), versus the 646 allowable or 0.0015 per load set pair (1.0/646) in the design analysis (shown in Table 5-1).

The predicted usage from the monitoring systems for the actual 12 startups and 11 shutdowns was only 0.00115, which included several of the shutdowns with multiple feedwater injections during hot standby conditions. The 12 startups and 11 shutdowns included both of the first two load set pairs described in Table 5-1. Ratioing the design analysis cumulative usage factor of 0.4646 for the first two load set pairs by 11/135 would indicate a design usage of approximately 0.038 for the same transients, greater by a factor of about 30 than that obtained

Table 5-1. Usage Summary at BWR Feedwater Nozzle Critical Location

Load Set Pair	S_{alt}, MPa [ksi]	Allowable Cycles	Design Cycles	Usage
Turbine Roll (Dn)[(a)] Hot Standby (Up)	681.1 [124.9]	646	135	0.2090
Hot Standby (Dn) Hot Standby (Up)	568.8 [82.5]	2,610	667	0.2556
Feedwater Heater Bypass (Up) Hot Standby (Dn)	498.5 [72.3]	4,400	19	0.0043
Feedwater Heater Bypass (Dn) Feedwater Heater Bypass (Up)	226.8 [32.9]	211,000	282	0.0013
Turbine Roll (Up) Feedwater Heater Bypass (Dn)	197.9 [28.7]	500,000	121	0.0003
Turbine Roll (Up) Scram (Dn)	179.3 [26.0]	993,000	9	~0
			TOTAL	0.4705

[(a)] (Up) - (Dn) refers to increasing or decreasing temperature in the feedwater nozzle

by the monitoring system (the ratio 11/135 applies to both of the load set pairs because they occur in a fixed ratio). The peak stress range observed during actual plant operation was only 71% of that predicted for the design transients. This occurred because of a number of reasons.

- The temperature transients were not step changes as used in the design analysis,
- The actual temperature ranges were considerably less than those included in the design analysis,
- The design analysis did not include the effects of reactor water clean-up flow that tends to keep the temperature of the water flowing to the nozzles much higher than ambient.

To illustrate this further, the actual and design conditions for startup and shutdown transients are shown and described in detail (Figures 5-2 to 5-5). It is assumed that the reactor is heated with no flow to the feedwater nozzle. At the time of feedwater initiation, the nozzle is assumed to be instantaneously flooded with feedwater at 10°C [50°F]. This is followed 30 minutes later by a step change rise in feedwater temperature to 121°C [250°F], followed by a ramp up to 215.5°C [420°F] (see Figure 5-4). The "final feedwater temperature" occurs after mixing with the reactor water cleanup flow (see Figure 5-4). This is contrasted (in the same figures) with data from a typical startup. For the actual transient, there is flow from the reactor water cleanup system to the nozzle and the temperature of the feedwater at the reactor nozzle is significantly greater than 10°C [50°F]. Also, for the actual transients, temperature and pressure changes occur at slower rates.

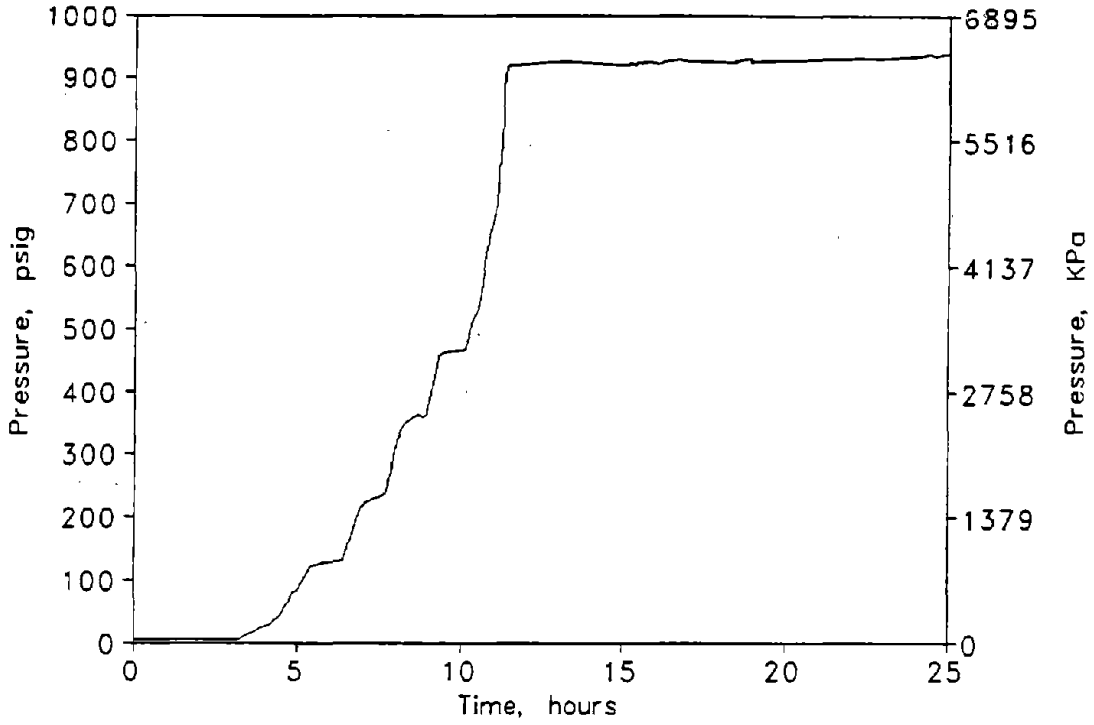

a) Typical Startup Data

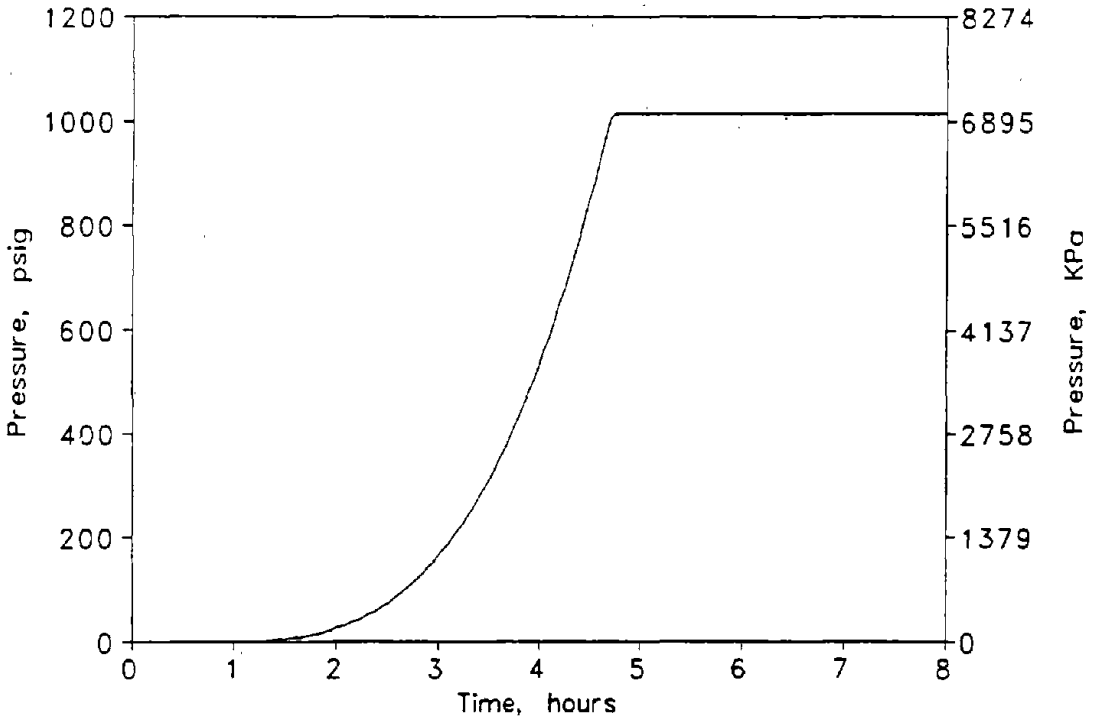

b) Design Startup Transient

Figure 5-2. Comparison of Actual Versus Design Startup Data - Reactor Pressure.

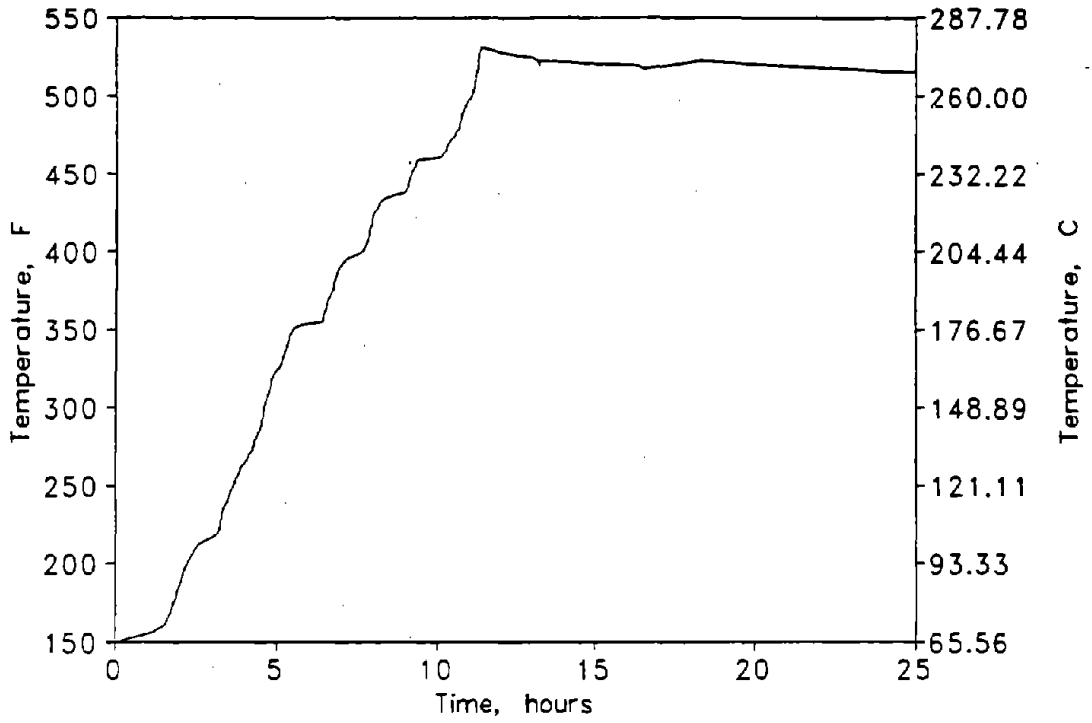

a) Typical Startup Data

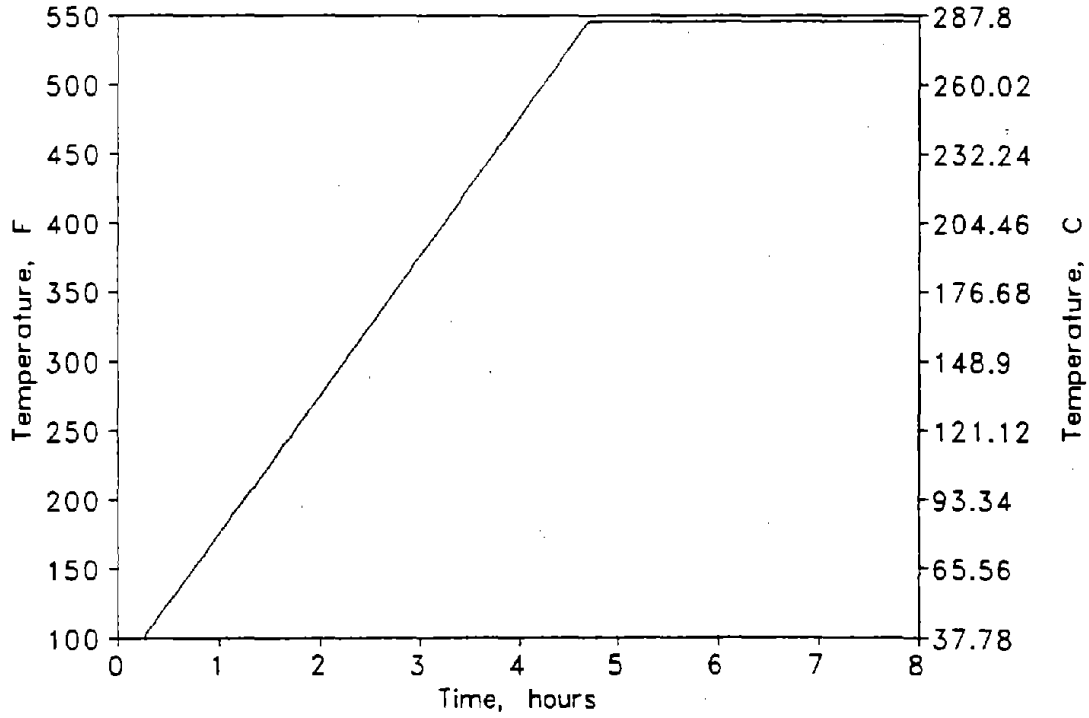

b) Design Startup Transient

Figure 5-3. Comparison of Actual Versus Design Startup Data - Reactor Temperature.

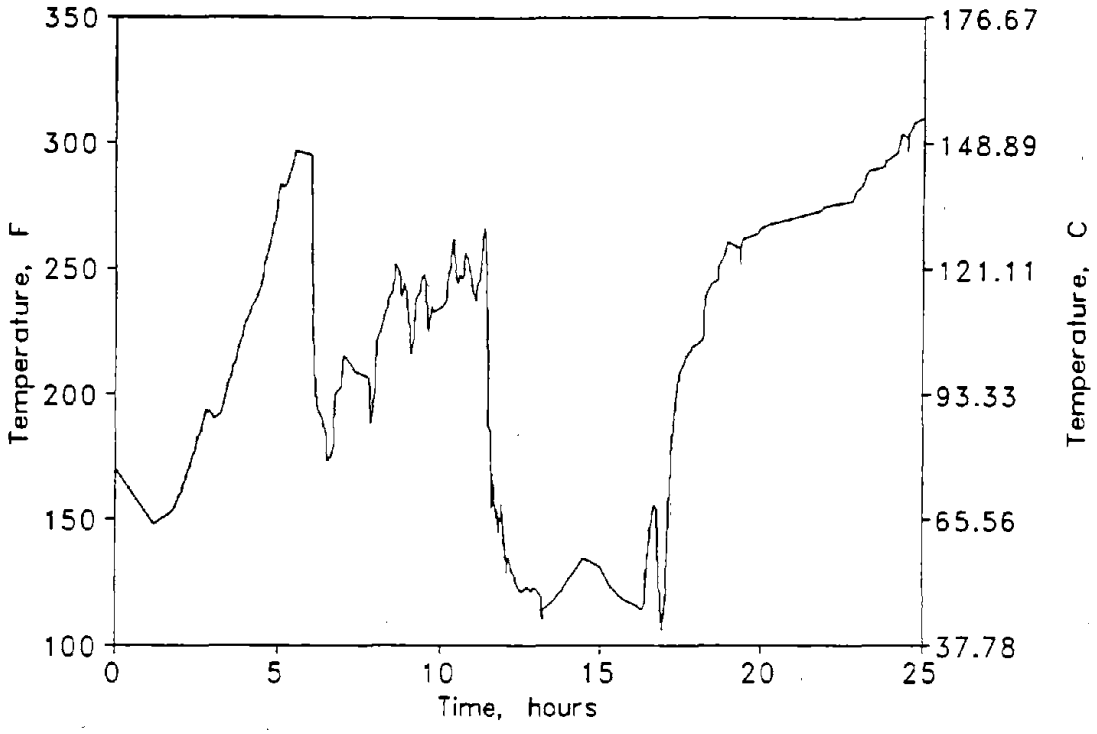

a) Typical Startup Data

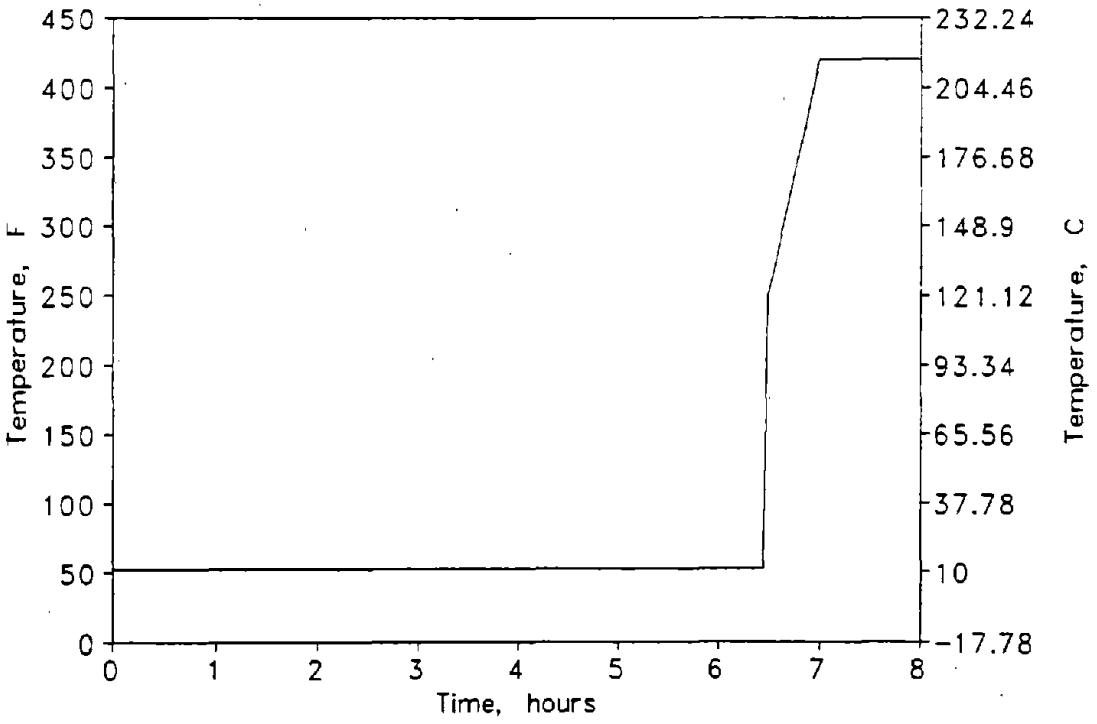

b) Design Startup Transient

Figure 5-4. Comparison of Actual Versus Design Startup Data - Final Feedwater Temperature.

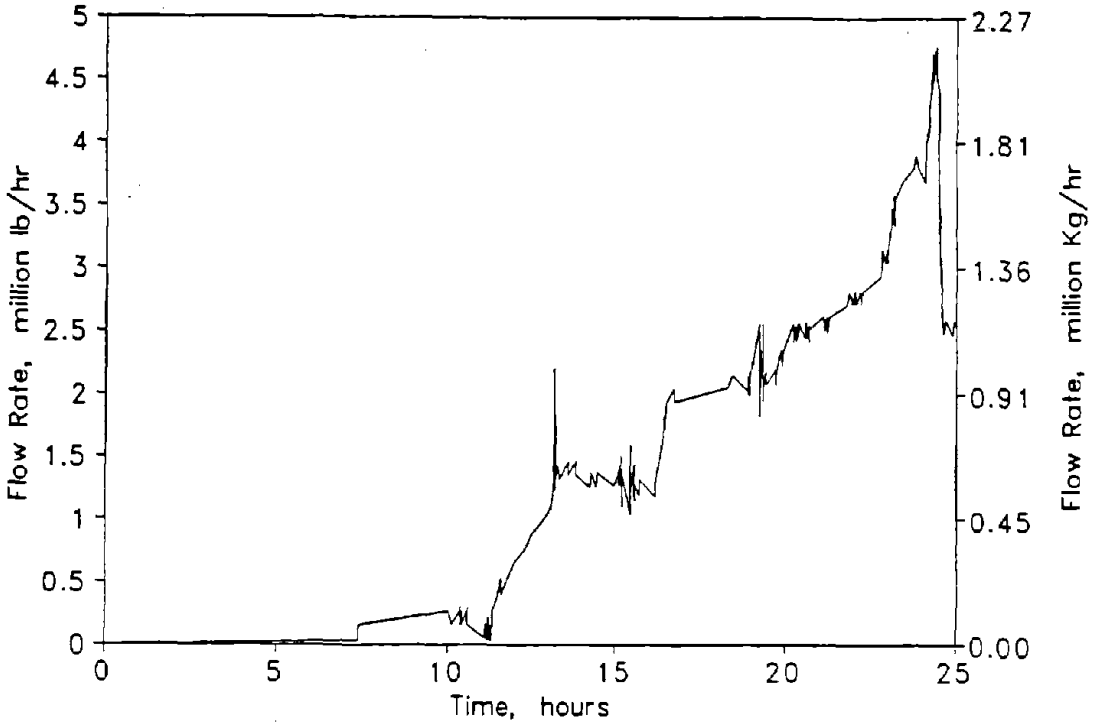

a) Typical Startup Data

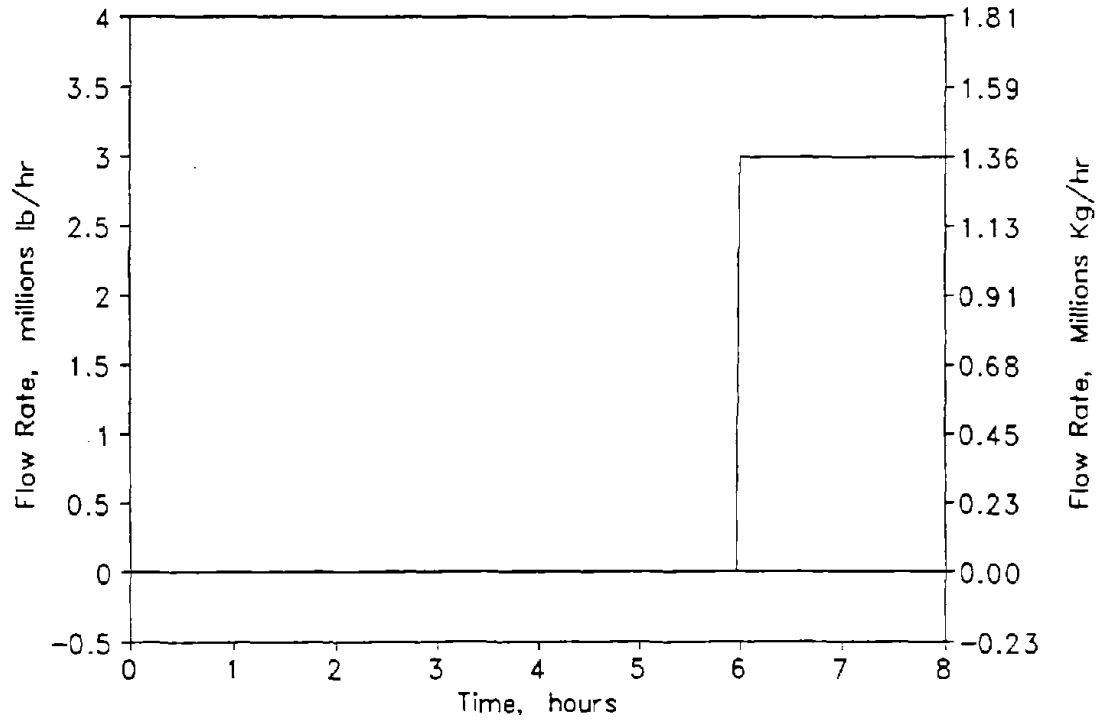

b) Design Startup Transient

Figure 5-5. Comparison of Actual Versus Design Startup Data - Feedwater Flow.

The stress response comparison between the design and actual transients (as predicted by the fatigue monitoring system) is shown in Figure 5-6. For the design transient, the major stress transient is caused by the feedwater initiation (where the nozzle is cold shocked) and the following step increase in temperature (where the nozzle is hot-shocked). The ramp-up in temperature has a relatively small effect. For the actual transient, the major stress deviation results from stratification which was conservatively included in the monitoring model. As the feedwater flow increases, the stratification disappears producing only a small transient thermal stress. Because of the reactor water cleanup flow, there was no significant thermal stress transient due to suddenly filling the nozzle with relatively cold flow. The resulting stress range was less than 20 percent of that predicted for the design transient.

Similar results are observed for the reactor shutdown. Figures 5-7 to 5-10 show the design and a typical shutdown transient. For the design transient, the feedwater is suddenly shut off while the feedwater temperature is relatively high. There are then one or more feedwater injections that later occur at 20 percent rated feedwater flow with feedwater at 37.8°C [100°F]. Five feedwater injections following feedwater termination are assumed for the design transient analysis.

Actual plant data are shown in the same figures. Upon termination of feedwater flow, the temperature of the water going to the feedwater nozzles actually increases due to the reactor water cleanup system flow. Even though there are a few feedwater injections to assist with reactor water level control, the temperature never approaches ambient conditions. In addition, actual transients occur at slower rates than for design transients.

The stress response between design and actual data is compared in Figure 5-11. Whereas the assumed injections of cold water for the design hot standby conditions produce a significant stress response for each injection, the stress response is much less for the actual plant data. Because the feedwater temperature is relatively warm (from the reactor water cleanup system), the thermal shock stresses are much lower. For the event, the actual stress range is about 75 percent of that considered for the design transients.

It is worthwhile to note that from 18 months of data analysis, there was no fatigue usage attributable to events not associated with startup and shutdown transients. There was one partial feedwater heater bypass transient, but it did not cause a stress excursion significant enough to cause any fatigue damage.

From the overall assessment of the actual plant data, it was observed that there were many more "small" cyclic temperature changes. However, the ranges of temperature and rates of temperature change were never high enough to cause any significant stress excursions.

Although this evaluation has been for a specific location, it supports the general conclusion that much of the supposedly high fatigue usage in stress reports is due to the specification of operating transients in Design Specifications that are significantly more severe than those that actually occur in operating power plants.

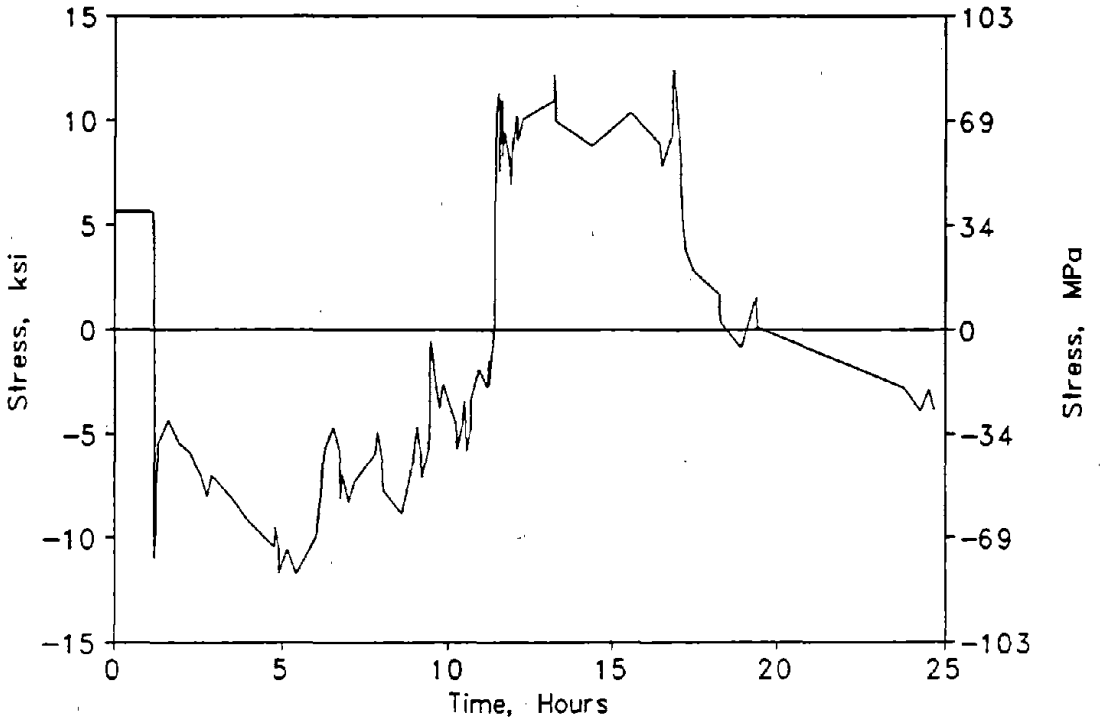

a) Typical Startup Data

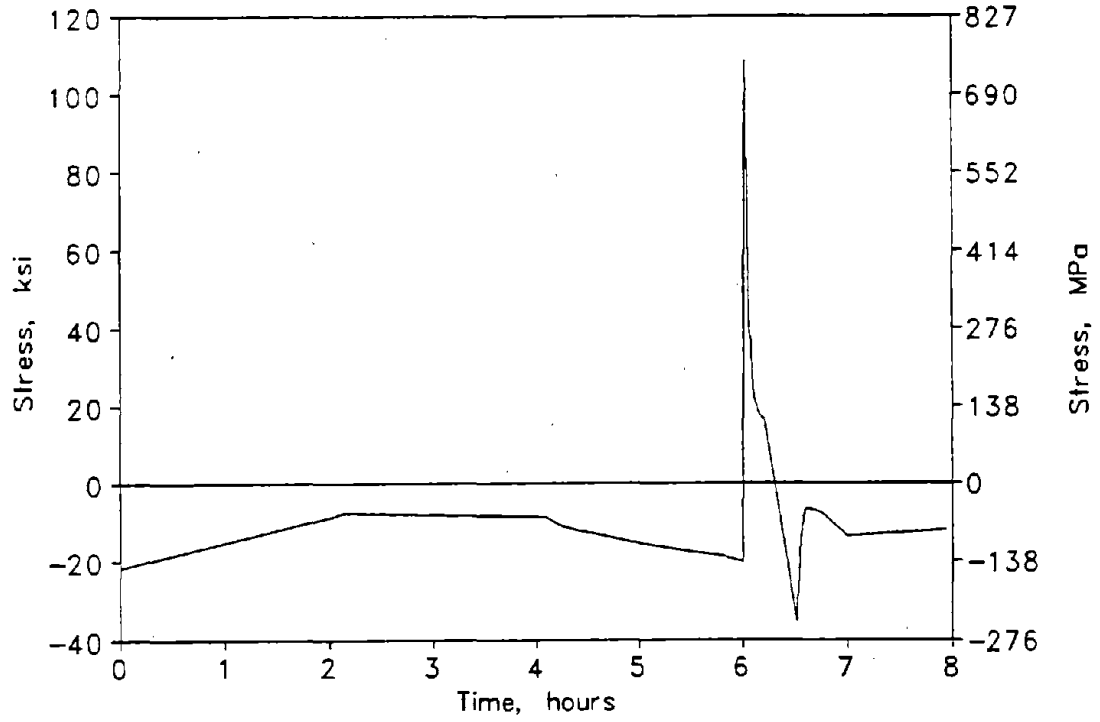

b) Design Startup Transient

Figure 5-6. Comparison of Predicted Feedwater Nozzle Safe-End Stresses During Startup for Actual Versus Design Data.

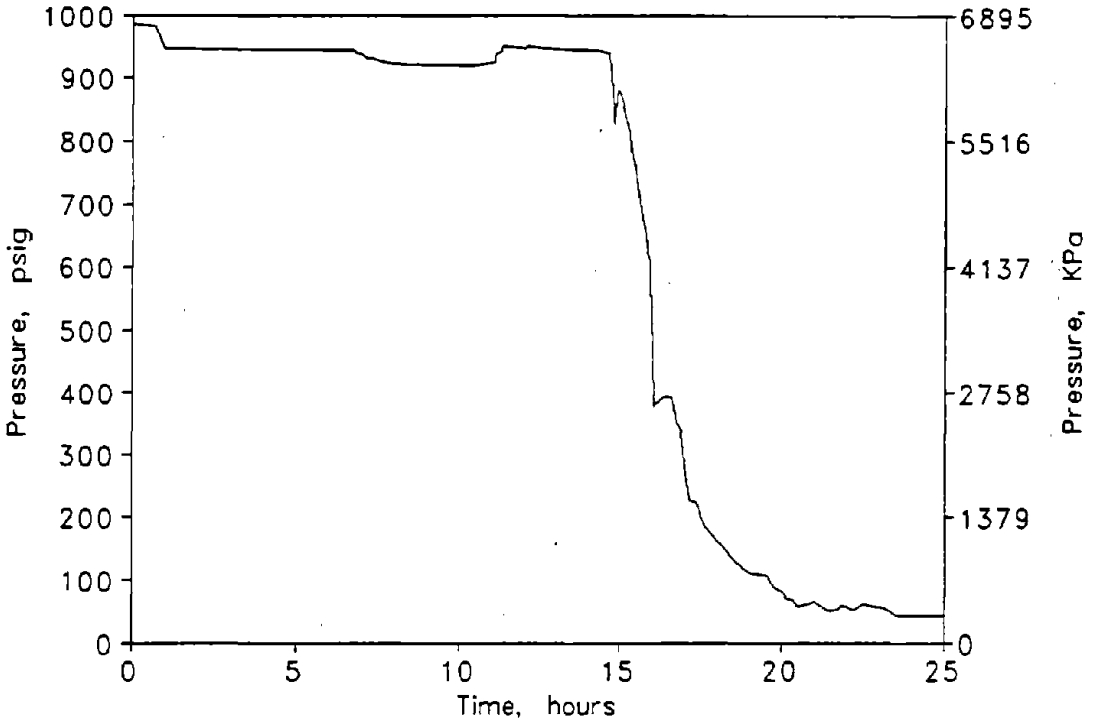

a) Typical Shutdown Data

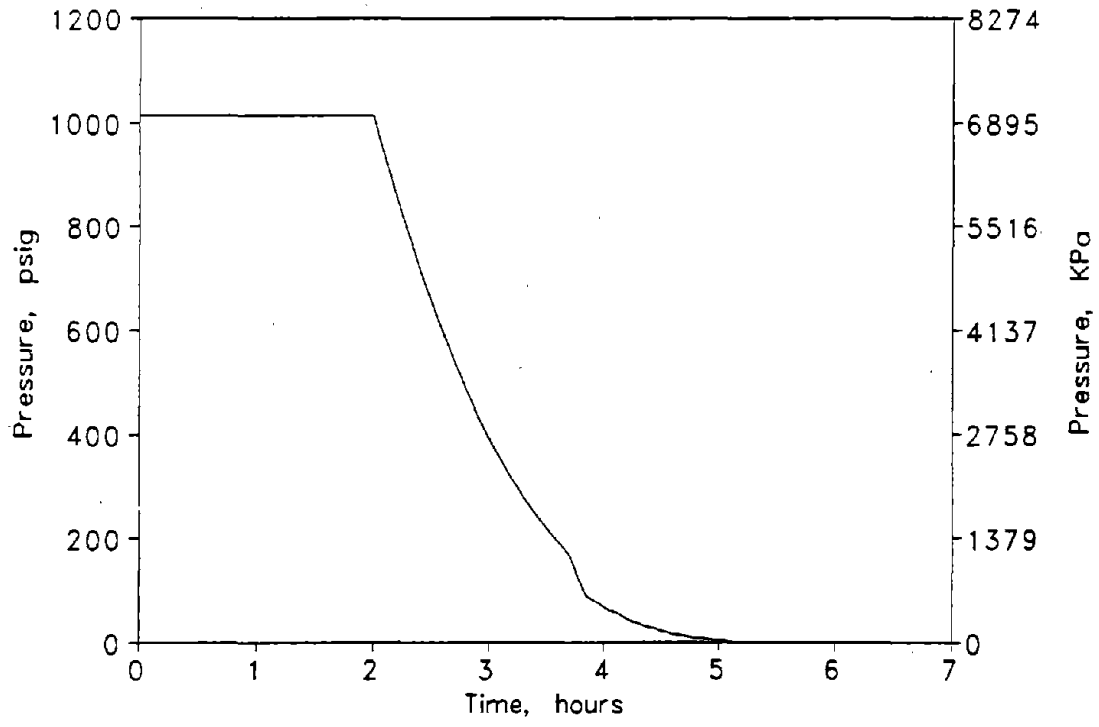

b) Design Shutdown Transient

Figure 5-7. Comparison of Actual Versus Design Shutdown Data - Reactor Pressure.

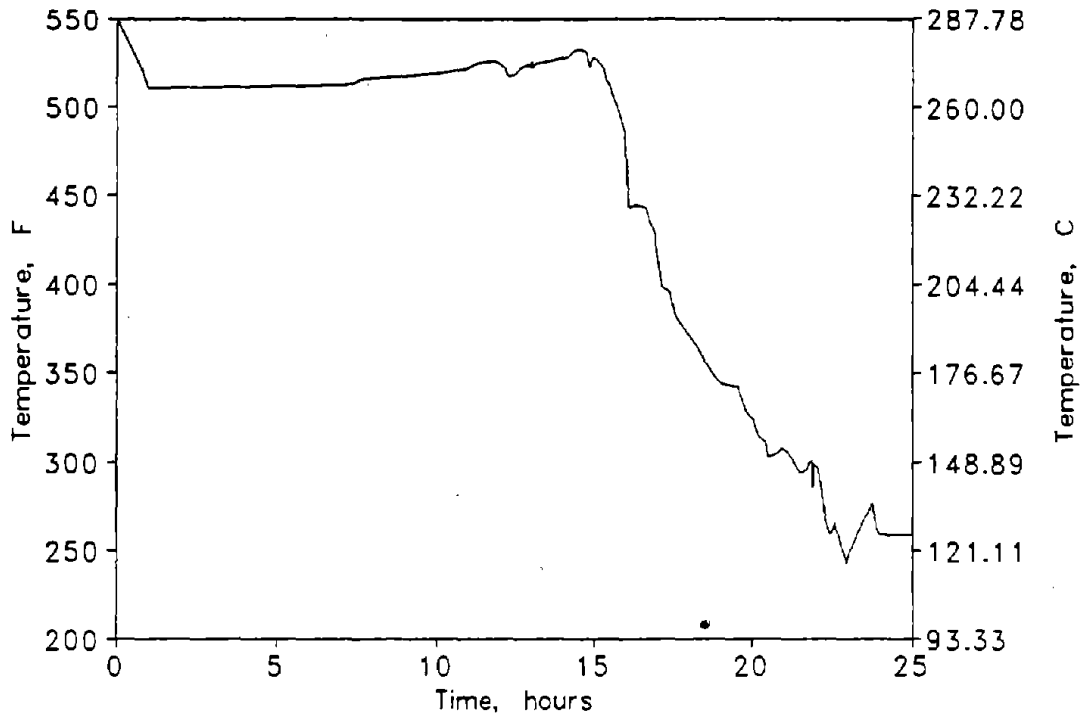

a) Typical Shutdown Data

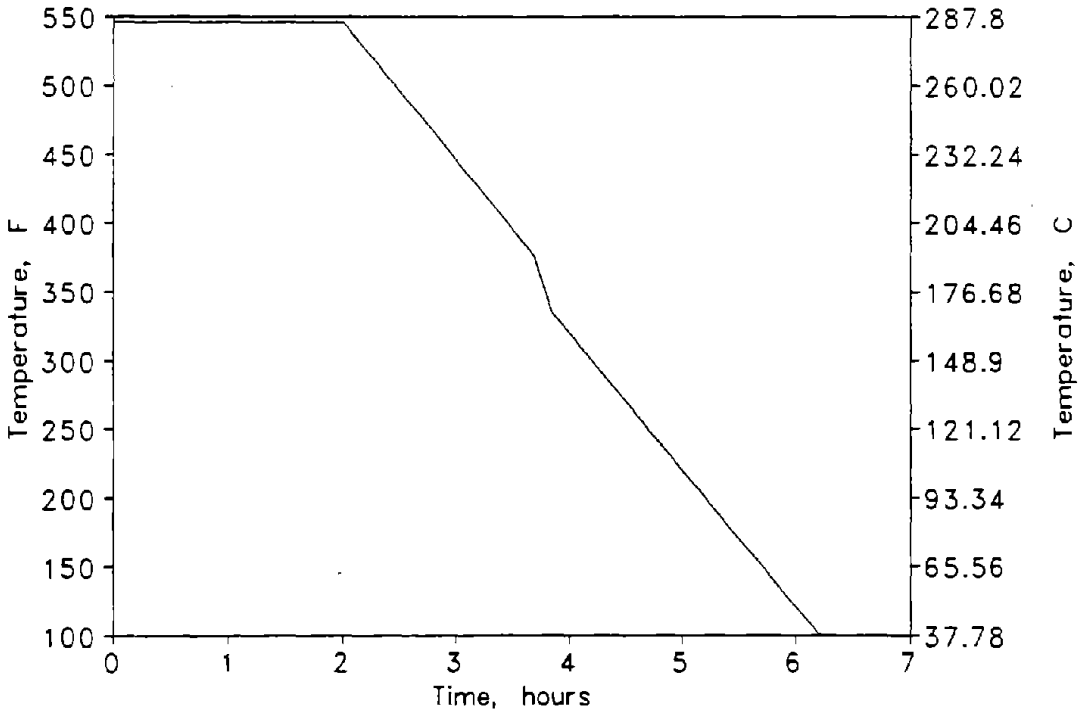

b) Design Shutdown Transient

Figure 5-8. Comparison of Actual Versus Design Shutdown Data - Reactor Temperature.

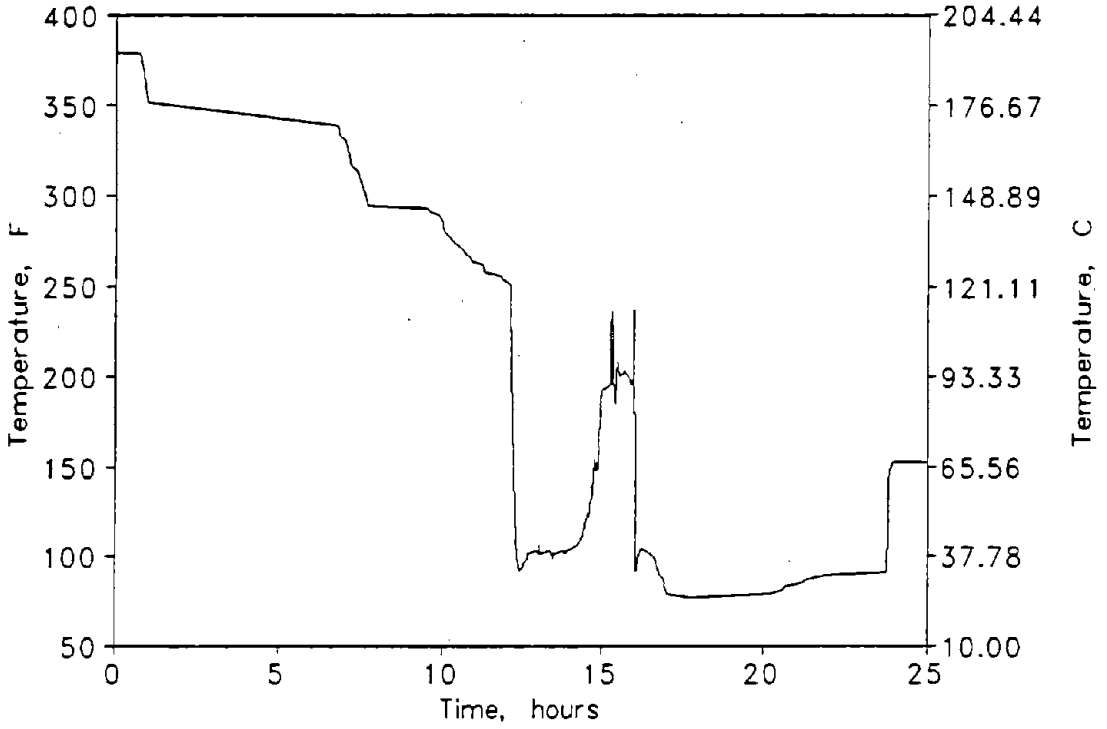

a) Typical Shutdown Data

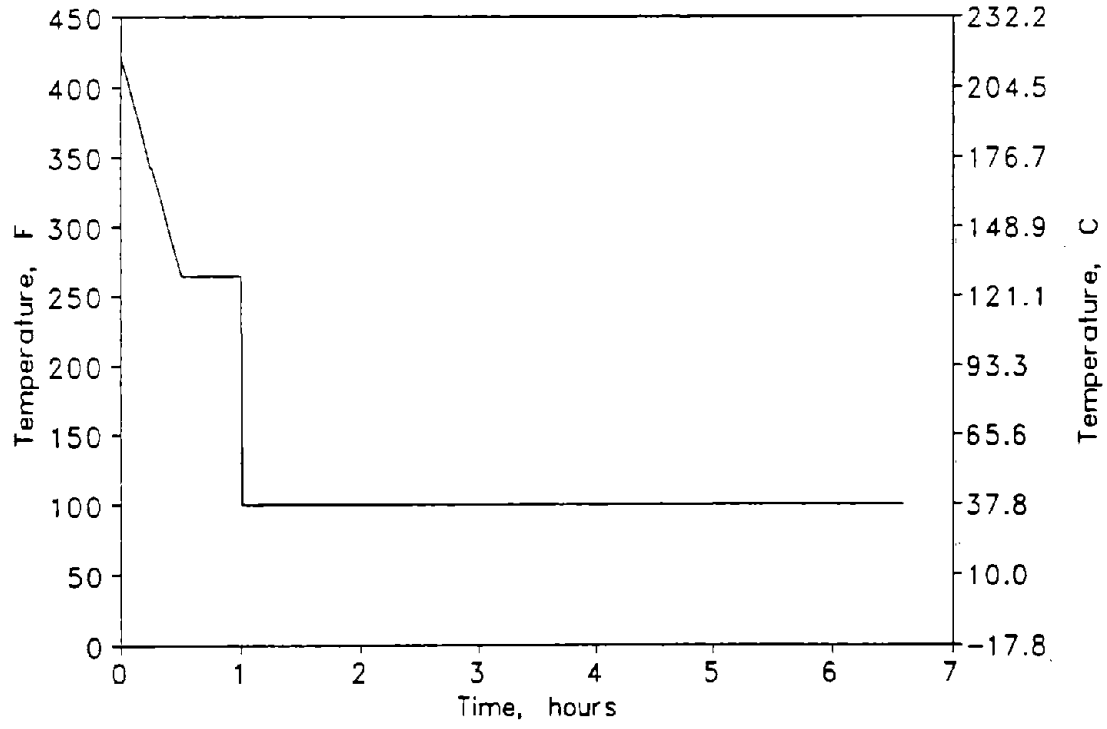

b) Design Shutdown Transient

Figure 5-9. Comparison of Actual Versus Design Shutdown Data - Final Feedwater Temperature.

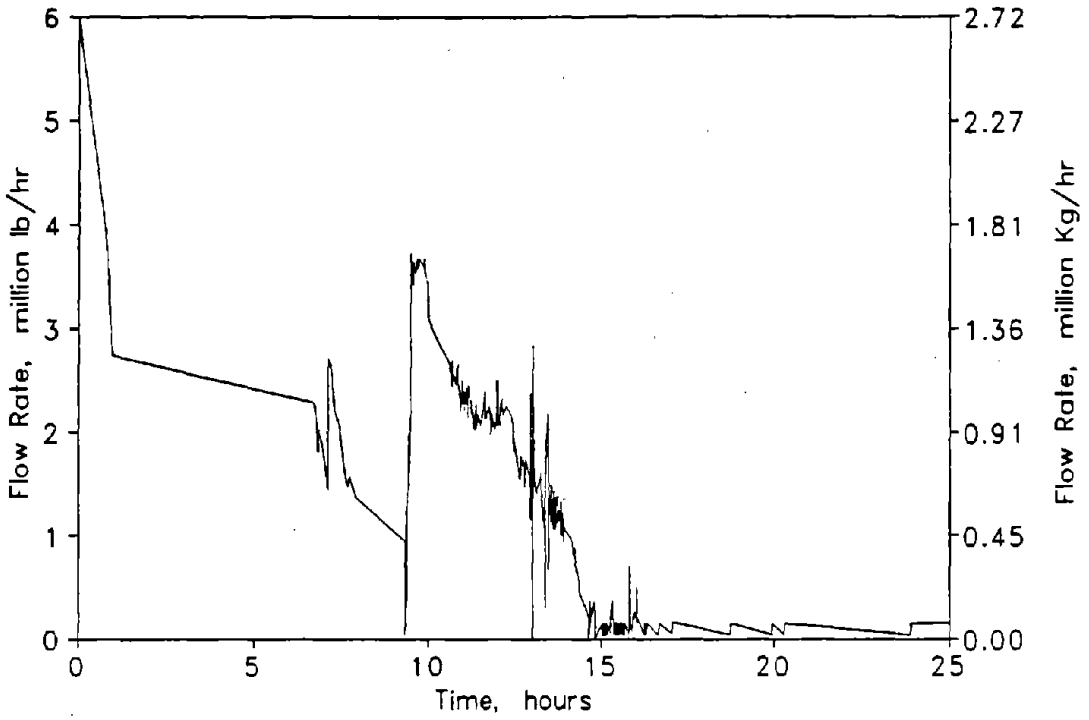

a) Typical Shutdown Data

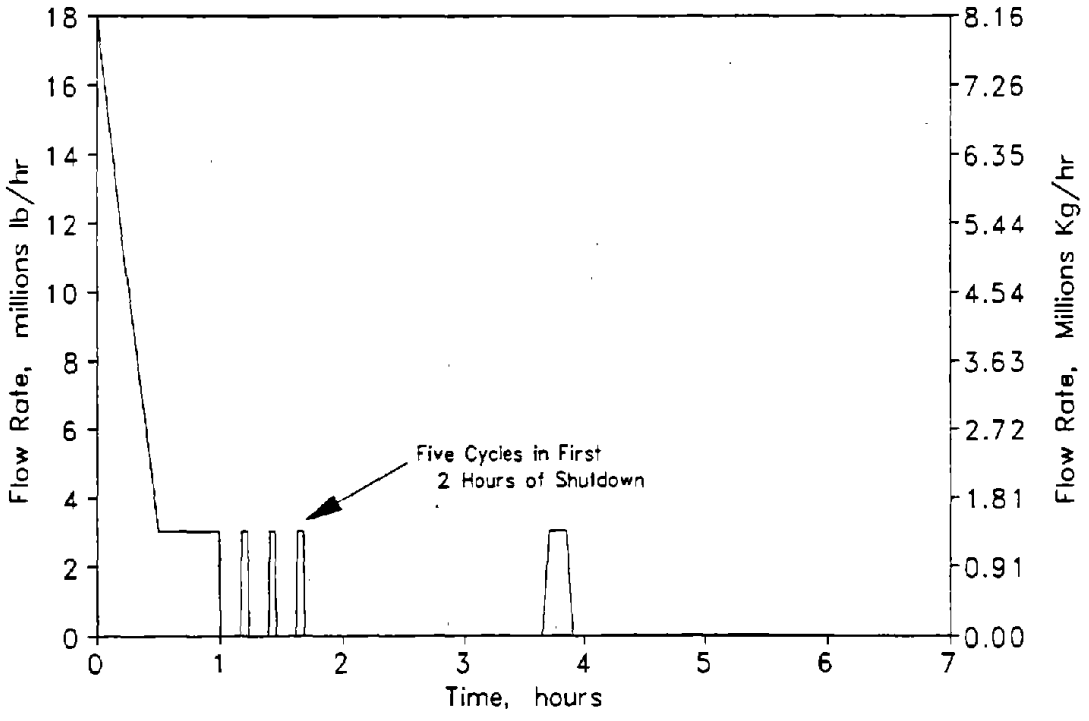

b) Design Shutdown Transient

Figure 5-10. Comparison of Actual Versus Design Shutdown Data - Feedwater Flow Rate.

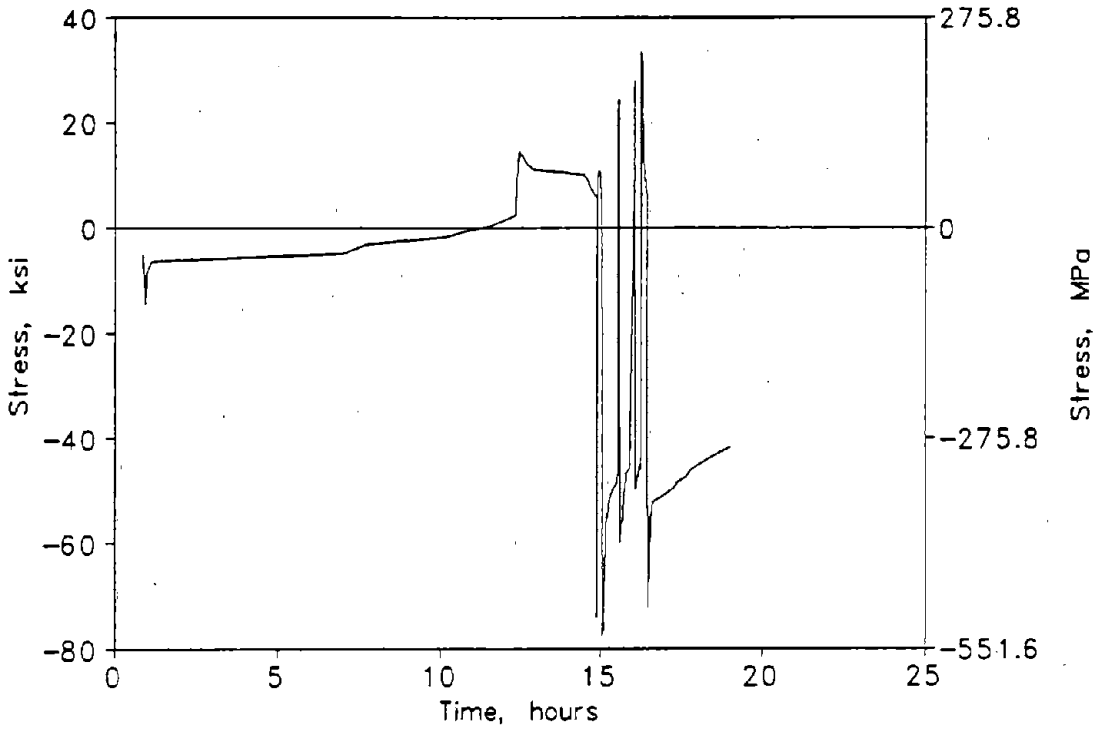

a) Typical Shutdown Data

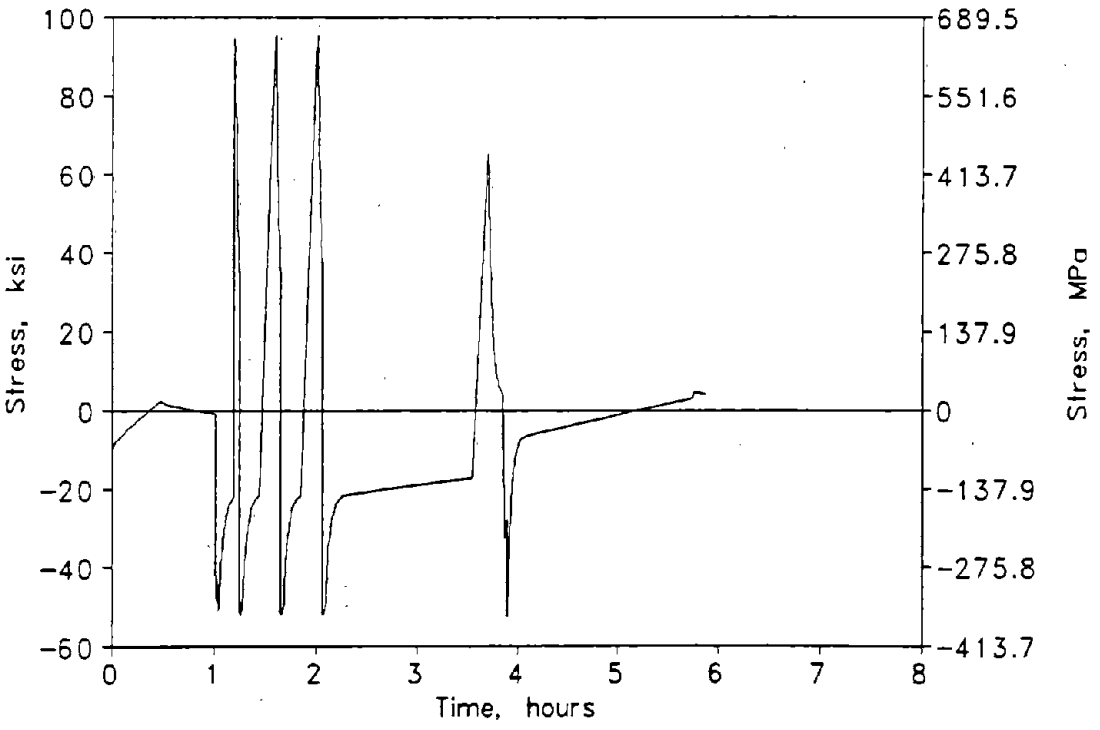

b) Design Shutdown Transient

Figure 5-11. Comparison of Predicted Feedwater Nozzle Safe-End Stresses During Shutdown for Actual Versus Design Data.

5.3 References

5.1 S.R. Gosselin and E.A. Siegel, "A Method for Monitoring and Evaluation of Thermal Transient Fatigue Usage in a Nuclear Power Plant," Presented at Pressure Vessel and Piping Conference, American Society of Mechanical Engineers, 1986.

5.2 J.H. Santander and S.R. Gosselin, "Analysis and Program to Extend the Design Life of the Charging Nozzle in a First Generation Nuclear Power Plant," American Society of Mechanical Engineers, PVP-Vol. 238, 1992.

5.3 A.Y. Kuo, S.S. Tang, and P.C. Riccardella, "An On-Line Fatigue Monitoring System for Power Plants: Part I - Direct Calculation of Transient Peak Stress Through Transfer Matrices and Green's Functions," 1986 Pressure Vessel and Piping Conference, Chicago, Illinois, July 1986.

5.4 A.Y. Kuo, S.S. Tang, and P.C. Riccardella, "An On-Line Fatigue Monitoring System for Power Plants: Part II - Development of a Personal Computer Based System for Fatigue Monitoring," 1986 Pressure Vessel and Piping Conference, Chicago, Illinois, American Society of Mechanical Engineers, July 1986.

5.5 "FatiguePro: On-line Fatigue Usage Transient Monitoring System," Electric Power Research Institute, EPRI NP-5835M, May 1988.

5.6 H.O. Fuchs and R.I. Stephens, "Metal Fatigue in Engineering," John Wiley and Sons, New York, 1980.

5.7 J. Novak and A. Deardorff, "Fatigue Monitoring Program for Susquehanna, Unit 1 Reactor Pressure Vessel," *Damage Assessment/Reliability Life Prediction of Power Plant Components*, American Society Mechanical Engineers, PVP-Vol. 193, 1990.

6. EVALUATION OF ENVIRONMENTAL EFFECTS

An issue related to the adequacy of the margins in the ASME Code Section III fatigue design has recently been identified. Research has shown that under certain conditions, the fatigue resistance of reactor materials in LWR water environments is less than the fatigue resistance of comparable materials in air. As a result, the Nuclear Regulatory Commission has instituted a program to perform additional research and evaluation of the adequacy of the fatigue analysis of operating nuclear power plants [6.1].

6.1 Research Results on Fatigue S-N Curves

The effects of LWR environments on the allowable cycles to fatigue initiation are described in References 6.2 and 6.3. There are three primary parameters that have been identified as important to environmental effects:

- Increased dissolved oxygen content of the water tends to reduce the number of allowable stress cycles.
- Increased temperature, especially above 200°C [392°F], tends to reduce the number of allowable stress cycles.
- Low strain rates, especially at high strain amplitudes, cause a significant reduction in the number of allowable stress cycles.

Carbon steels are most highly affected, followed by low alloy steels. The effect on stainless steels is believed to be minimal [6.4].

These conclusions are based on results of laboratory testing and the effects are quantified in the following equations derived from Reference 6.3, for carbon steel.

$$\varepsilon_{water} = 0.231(N_{water}(\dot{\varepsilon})^{-P})^{-0.472} + 0.00108 \quad (1)$$

$$\text{or} \quad N_{water} = \left[\frac{\varepsilon_{water} - 0.00108}{0.231}\right]^{-\frac{1}{0.472}} (\dot{\varepsilon})^{P} \quad (2)$$

where:

ε	=	strain amplitude, m/m [in/in]
$\dot{\varepsilon}$	=	strain rate, %/sec
N_{water}	=	number of cycles to failure in LWR environment
P	=	environmental factor = $C(0.1 + \eta M)$
C	=	1.0 for water and 0.0 for air

M is a factor to account for dissolved oxygen (DO2) content

DO2	M
DO2 ≤ 0.1 ppm	0
0.1 ≤ DO2 ≤ 0.2 ppm	(DO2-0.1)/0.1
DO2 ≥ 0.2 ppm	1.0

η is the factor to account for temperature (T)

η	Temperature (°C [°F])
0.2T/100	T < 100 [212]
0.2	100 [212] ≤ T ≤ 200 [392]
0.2 + 0.4 (T-200)/100	T > 200 [392]

The environmental parameter *P* is shown in Figure 6-1. The effect of the parameter *P* on the fatigue curves, in a comparison to the ASME Code fatigue curves for carbon steel, is shown in Figure 6-2 for four values of P (0.3, 0.5, 0.1, 0.2). With decreasing dissolved oxygen content, metal temperature, and increasing strain rate, the environmental effect is significantly decreased. The "air curve" in Figure 6-2 is from P = 0 in equation (2), the Higuchi and Iida "air curve."

The above results appear to be reasonable. However, the testing represents a laboratory situation with relatively constant test conditions that probably will not represent the more random conditions that exist in an actual plant.

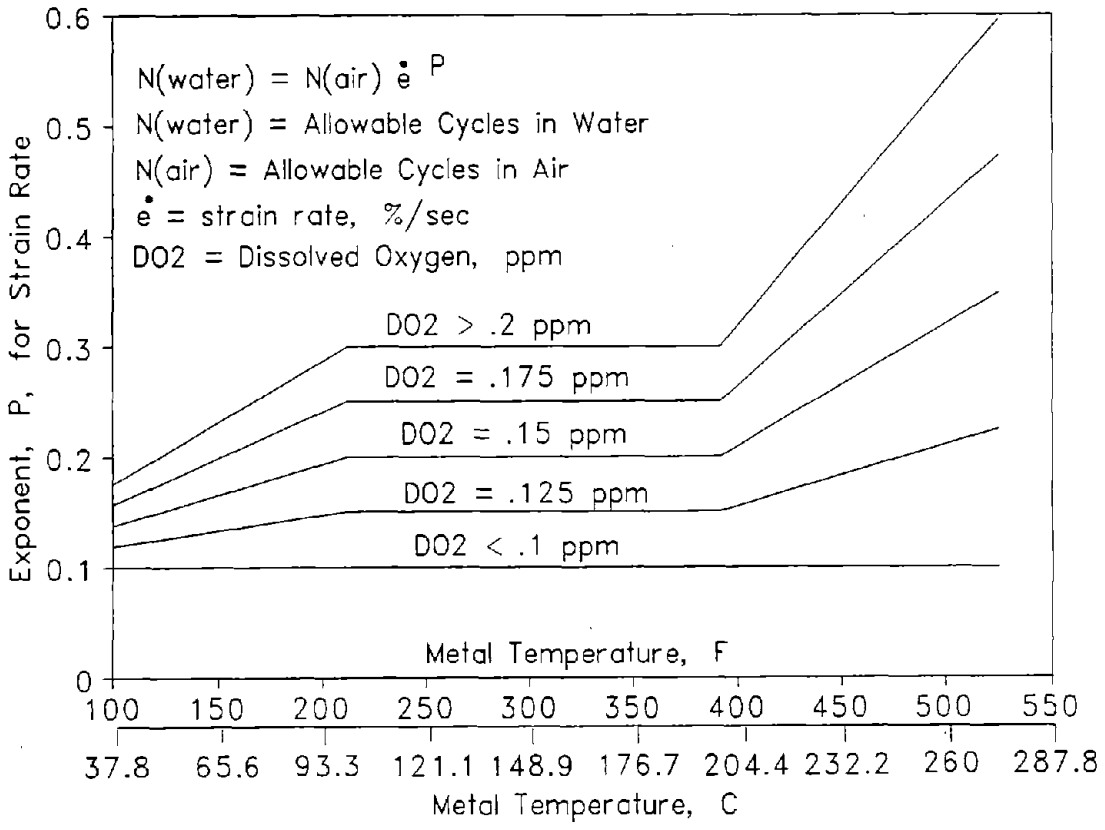

Figure 6-1. Effect of Environment Parameter *P* on Strain Rate Exponent (Carbon Steel).

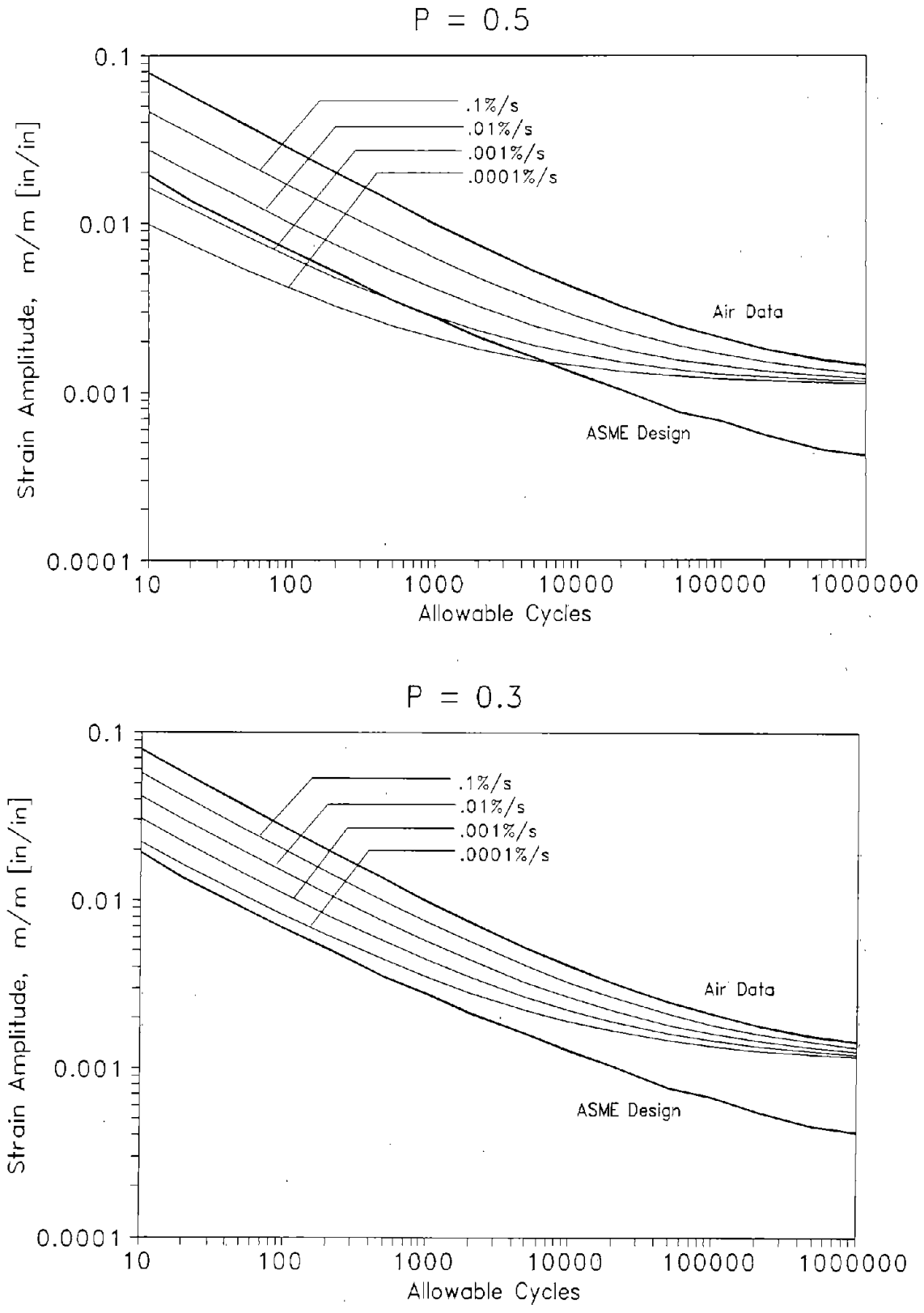

Figure 6-2(a). Effect of Parameter P on Carbon Steel Fatigue Curves (P = 0.5 and 0.3).

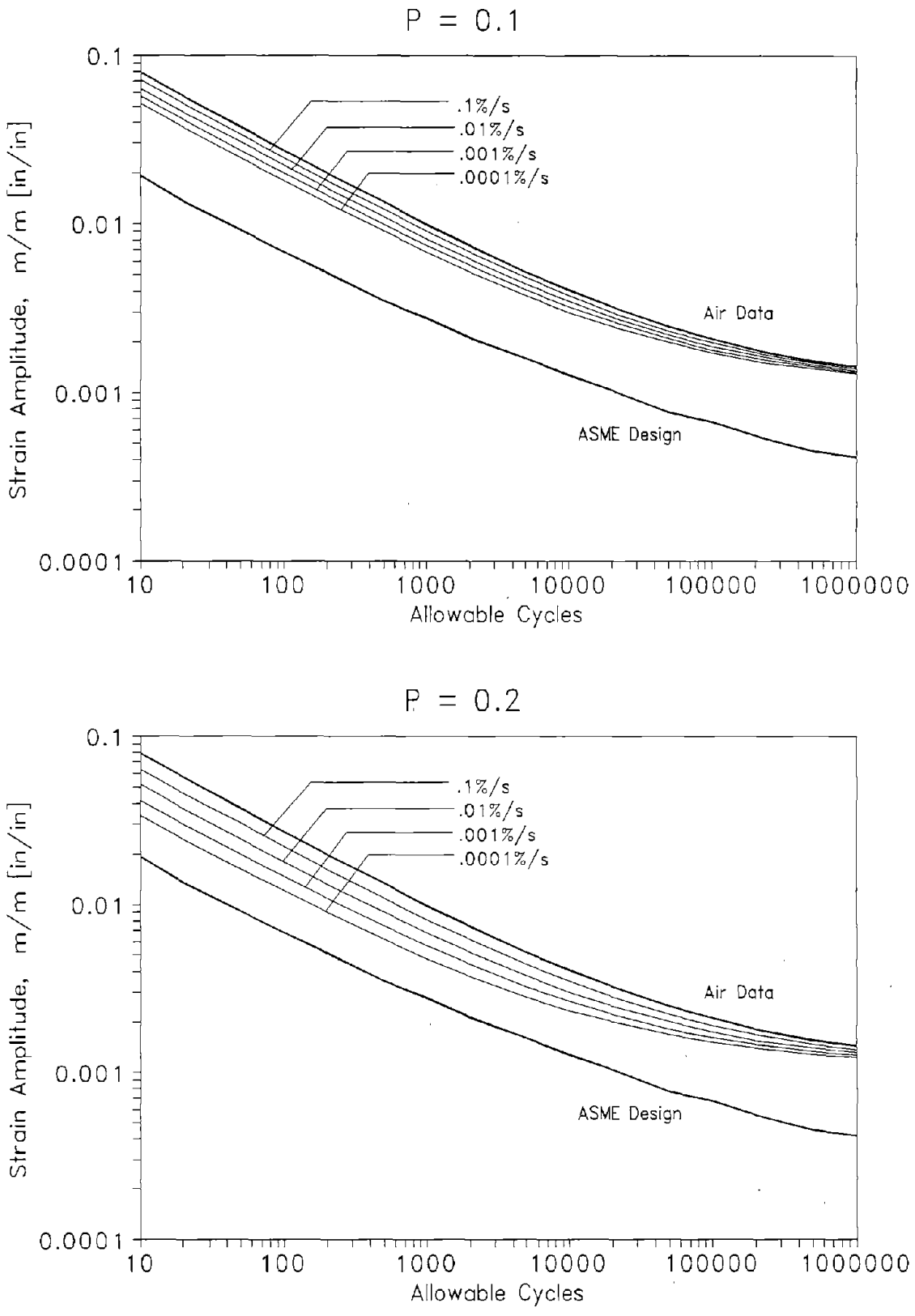

Figure 6-2(b). Effect of Parameter P on Carbon Steel Fatigue Curves (P = 0.1 and 0.2).

Review of the mechanisms associated with corrosion and fatigue provides some insight into why there may be an environmental effect. At high strain rates, the "damage" which occurs is purely mechanical. If there is some breakdown of the oxide film that exists on the material surface, there is not enough time for the oxygen in the water to significantly attack the underlying iron.* For slower strain rates, oxygen is able to diffuse through microcracks in the oxide layer while the surface is in tension, providing further corrosion of the underlying material. This indicates that the strain rates during the tensile portion of the cycle are most important. There would be no break in the oxide film during the compressive portion of the stress cycle. A similar conclusion is reached in Reference 6.5.

Reference 6.2 suggests a correction factor ϕ (T) to account for an effect of temperature on fatigue life, even in air. This correction factor could be used to modify equation (2) as follows:

$$N_{water} = \Phi(T) \left[\frac{\varepsilon_{water} - 0.00108}{0.231} \right]^{-\frac{1}{0.472}} (\dot{\varepsilon})^{P} \qquad (3)$$

where:

$$\Phi(T) = \alpha e^{\frac{\beta}{(T + 273)}}$$

T in °C, $\alpha = 0.6$, $\beta = 148.5$

For a temperature of 150°C [302°F], $\Phi(T) = 0.85$; for a temperature of 290°C [554°F], $\Phi(T) = 0.70$. Because these correction factors are not significantly different than 1.0, and because a more significant effect was the determination of the correct temperature to use (i.e., metal temperature versus water temperature), the $\Phi(T)$ correction factor was not used in this study.

According to Reference 6.2, "the resulting expression for the strain-rate exponent P for high-sulfur steels differs slightly from that given by Higuchi and Iida" and "the coefficients for low-sulfur steel are identical to those given by Higuchi and Iida . . . ." The revised coefficients that can be used to calculate P are given in Table 2 of Reference 6.2. Because large effects were being evaluated in this study, the modified values of P were not used.

6.2 Discussion of Applicability to Actual Plant Components

The applicability of the previously described laboratory data correlation to actual plants has not yet been adequately quantified. Consider the following factors with respect to the high-usage-factor locations in plants:

- For fatigue sensitive locations identified in component stress reports, the major contributor is almost always thermal transients. Stress ranges for the controlling

* The oxygen does not actually "attack" the underlying iron, but it prevents dislocations from filling in a newly formed slip band, thus allowing more slip or less fatigue strength in the material.

transient pairs may or may not be associated with the same transient and peak and valley portions of the cycles may be separated in time. In laboratory testing, the fatigue S-N curves are developed from constant strain amplitude testing, generally with a sinusoidal or triangular wave shape.

- In order to have a significant effect on the design fatigue life of components exposed to water, high thermal stress amplitudes must exist. In order for these to exist, a thermal shock generally has to occur. The thermal strain rate for these thermal shocks is relatively high, and will therefore produce less of an environmental effect. Low strain amplitude transients, that may have more of an environmental effect due to their low strain rates, are generally not a significant contributor to the fatigue life of LWR components.

- As previously discussed, only the strain rate associated with the "tensile" part of severe stress cycles is important. This conclusion is also reached in Reference 6.4. For the thermal stress at an inside surface to be tensile, the surface must be cold-shocked. Thus, the environmental effect due to decreasing temperature would tend to reduce the overall environmental effect. The only exception might be the top portion of a pipe with stratified flow.

- For actual locations in plants where fatigue damage has been observed, the mechanism is generally one of high cycle fatigue due to vibration or local fluid thermal cycling [6.6]. In these cases, the frequency is relatively high and the strain amplitudes are relatively low.

The above arguments show some of the limitations that might exist when applying the laboratory data correlation directly to actual fatigue analysis. More development would be required before the environmental effect can be implemented into a code analysis procedure.

6.3 Evaluation of Environmental Effects Using Actual Plant Conditions

To evaluate the effects of the environment using actual plant data, the fatigue monitoring software described in Section 5.2 was modified so that both stress amplitude and strain rate could be derived from actual plant data. For the revised software, the strain rate associated with each stress tensile peak was calculated along with the stress peak and valley history that is created during plant data analysis. Then, a rainflow cycle counting analysis was conducted, classifying each cycle in the stress range spectrum with a strain rate for the tensile portion of the cycle [6.7]. The fatigue analysis was conducted using the modified spectrum table and the environmental fatigue equation described in the previous section as well as the ASME Code fatigue design curve for carbon steel.

In evaluating real plant data for assessment of environmental effects, several key assumptions had to be made with respect to determining strain rate. The stresses predicted for real transients are not pure ramps or sinusoids, so strain rate is not well defined. In addition, the temperature of the metal surface is not constant (and is the major source of the stresses). The following approach was used:

- Since metal temperature is not required when using the Green's Function approach for transient thermal stress analysis, metal temperature at the time of each stress peak was not available. Instead, a sensitivity evaluation was conducted based on several different temperature conditions to evaluate temperature effects.

- The strain rate for each stress range was based only on the portion of the transient when the dominant principal stress was tensile. Since the critical location was on the inside surface, the stress peaks occurred as a result of rapid decreases in surface temperature or due to stratification changes that induced tension. In calculating the strain rate, no consideration was given to the compressive end of the stress range.

- An average strain rate was computed between the peak of the stress history and each of the preceding points. This is believed to be an adequate characterization of the strain rate associated with a stress peak.

The latter point is illustrated in Figure 6-3. A typical surface stress time history is shown with stress points at 10 second intervals. The question is how should the stress (or strain) rate be computed for the tensile stress peak shown at 220 seconds.

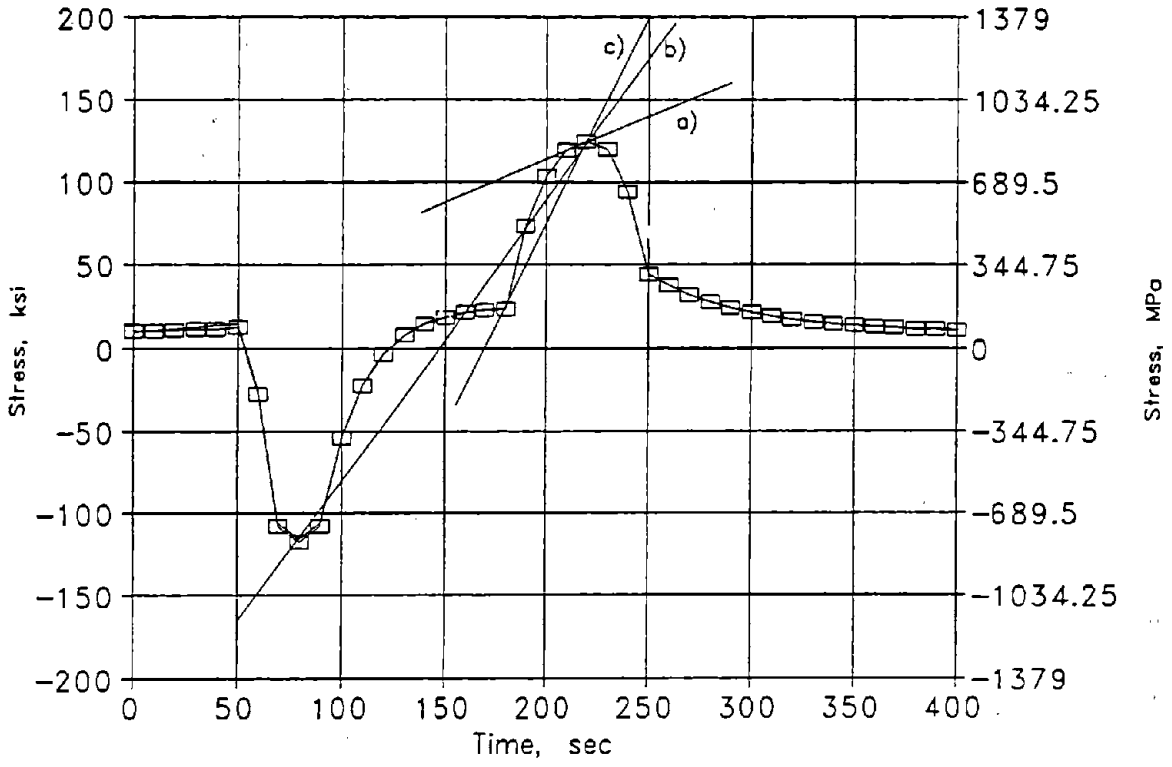

Legend:

Curve a:	Local Strain Rate at Peak	-	Too Conservative
Curve b:	Valley-to-Peak	-	Could be Highly Variable
Curve c:	Average Strain Rate for Local Transient	-	Used for this Evaluation

Figure 6-3. Peak Stress Evaluation for Strain Rate Determination.

- The minimum rate of change of stress occurs for 10 to 20 seconds just prior to the peak, as indicated by line (a). This rate would be conservative and is not representative of the overall rise to the peak tensile stress. Moreover, if the stress history were to be evaluated at smaller and smaller time increments, the rate would go to zero. A strain rate computed using this approach is not consistent with environmental effects testing where strain rate has most likely been calculated based on the overall strain cycle time.

- An alternate method to determine the strain rate is to compute the average stress rate between adjacent stress peaks and valleys as in line (b). For the example shown, this would appear to be realistic. However, for actual plant situations, it is not realistic because there may be days or months between significant stress peaks or valleys. Also, there are many small stress excursions between the major stress peaks and valleys.

- The line shown as (c) shows the average stress rate associated with the tensile portion of the stress peak at 220 seconds. The strain rate may be determined using this approach by "attaching the line to the peak point" and "stretching the bottom of the line until it touches a point on the previous stress history." This is the approach used to determine the stress (strain) rate in the current study, except that stress points removed by more than 200 seconds were arbitrarily not considered. Sensitivity studies showed that the computed strain rates did not change when this time was varied between 50 and 200 seconds since all significant stress peaks occur over a period of less than 50 seconds.

Another issue was how to assess strain rates when K_e must be included in performing a simplified elastic-plastic stress analysis. Application of K_e requires that a higher stress amplitude be used from the fatigue curve. If so, this would imply that the strain rate would also have to increase to produce the equivalent higher stress range. Although K_e may be as high as 5.0 for carbon steel, no correction was made to account for this apparent increase. For this study, the strain rate was conservatively determined from the raw, unmodified stress time history with no increase of strain rate if K_e was required in the fatigue evaluation.

Actual plant transient data from two different plants was used to perform the assessment of environmental effects.

6.3.1 Evaluation of BWR Plant Data

The BWR plant data described in Section 5.2 was used to evaluate environmental effects. For this plant, the critical location is actually located on the stainless steel weld buildup adjacent to the feedwater sparger inlet seals. However, the stress at this location is not much different than the adjacent carbon steel locations and was judged to be similar enough to that at the adjacent carbon steel locations so that a separate stress analysis was not required. Thus, the stress computed for the stainless steel was used to determine the effects of the previously described carbon steel environmental curves on the fatigue usage.

Using the specially developed cycle-counting algorithm, a rainflow cycle spectrum was developed for the data from November 1987 to June 1989. The rainflow analysis produced the stress amplitude and tensile peaks strain rate spectrum as shown in Table 6-1.

A set of simulated design transients was then constructed to evaluate the same transient period. In this case, the design transients described in Section 5.2 were used for each of the startups and shutdowns, based on the limiting feedwater and reactor temperatures and the associated step or design rates of change of temperature. For each of the actual transients, the actual number of feedwater injections following shutdown were used instead of the design number of five per shutdown (resulting in a average number of injections of 3.7 per shutdown for the series).

Table 6-2 shows the strain amplitude spectra developed from the simulated design analysis. The spectra show a significant difference between the design transients and the actual transients of Table 6-1. The BWR design data exhibited significantly higher strain rates for a large number of cycles, in addition to the maximum strains being higher. Both sets of transients exhibited approximately the same number of transients with magnitude above 0.00042 m/m [in/in] strain (the approximate endurance limit for the ASME design fatigue curve).

Table 6-3 shows the fatigue usage calculated for each case. Usage is shown for the air curve (P = 0), environmental curves for P = 0.1 to P = 0.6, and for the ASME fatigue curve. As expected, the actual usage is much less than the design-based usage. In addition, the usage associated with the environmental curves is always much less than that associated with the ASME Code design fatigue curve. This is better shown in Table 6-4 where the results are normalized to the BWR design evaluation based on the ASME Code design fatigue curve.

The tensile stress peaks in the evaluation are the result of significant decreases in temperature. Based on Figure 6-1, the bounding value of P should be on the order of 0.3 since actual metal temperatures at the time of the stress peaks in the transients would be less than 205°C [400°F]. In this case (P = 0.3), actual plant data fatigue usage shown in Table 6-4 is approximately one percent of the design analysis usage based on the ASME Curve.

6.3.2 Evaluation of PWR Plant Data

Similar data were obtained from a fatigue monitoring system at an operating PWR. For this plant, the monitoring system is configured for a number of reactor coolant system locations and is also being used to monitor the steam generator feedwater nozzle to feedwater nozzle safe-end welds. Although this location does not typically require design to the Class 1 requirements of the ASME Code, the monitoring system has been set up to specifically evaluate stratification-induced stresses and the effects of on-off auxiliary feedwater flow cycling that occurs during plant startup and shutdown.

Transients and computed stresses for a typical heatup and cooldown are shown in Figures 6-4 and 6-5. For both startup and cooldown, the most significant stresses are those due to the stratification that exists in the nozzle during periods when auxiliary feedwater flow occurs. At auxiliary feedwater flows of less than about 45 to 57 m^3/hr [200 to 250 gpm], the top of the nozzle experiences hot water recirculation from the steam generator. As auxiliary feedwater flow

Table 6-1. Strain Amplitude Spectrum for Actual BWR Data

Strain Amplitude	Strain Rate, %/sec (× 1000)																SUM
in/in	0.1	0.2	0.4	0.7	1	2	4	7	10	20	40	70	100	200	400	700	
0.00230									1								1
0.00225																	
0.00221																	
0.00215																	
0.00209							1										1
0.00204																	
0.00198									2								2
0.00192									1								1
0.00186									1								1
0.00178									1								1
0.00167						1			1								2
0.00155					1	1	1		4								7
0.00144					1			1	1	1							4
0.00132			1						4								5
0.00121					2	1	1		4								8
0.00109			1		1		1	3	2	1							9
0.00098							2	6									8
0.00086						1		1									2
0.00075		2		1	1			2									6
0.00063			1			1	3										5
0.00052		3															3
0.00040		2	9				3										14
0.00029		2	9	3		1											15
Sum		9	21	4	6	6	12	13	22	2							95

Notes:

1) Strain rate grouping includes all cycles between given strain rate and next higher value.

2) Strain amplitude groupings show mean of ranges except for first entry, which is peak of range.

Table 6-2. Strain Amplitude Spectrum for BWR Design Transients

Strain Amplitude	Strain Rate, %/sec (× 1000)																SUM
in/in	0.1	0.2	0.4	0.7	1	2	4	7	10	20	40	70	100	200	400	700	
0.00344										1	8						9
0.00312																	
0.00293																	
0.00285											1						1
0.00277																	
0.00270																	
0.00262										28							28
0.00255										9							9
0.00247																	
0.00236																	
0.00221									10								10
0.00206										1							1
0.00190																	
0.00175																	
0.00160																	
0.00145																	
0.00130																	
0.00114																	
0.00099																	
0.00087																	
0.00069			21														21
0.00053		11	1														12
0.00038							1										1
0.00026		1															1
Sum		12	22				1		10	39	9						93

Notes:

1) Strain rate grouping includes all cycles between given strain rate and next higher value.

2) Strain amplitude groupings show mean of ranges except for first entry, which is peak of range.

Table 6-3. BWR Fatigue Usage Calculation Results

Fatigue Curve	BWR-Design	BWR-Actual
Higuchi-Iida Air Curve	0.001608	0.000082
Environmental Curves		
$P = 0.1$	0.002320	0.000135
$P = 0.2$	0.003399	0.000227
$P = 0.3$	0.004917	0.000377
$P = 0.4$	0.007188	0.000636
$P = 0.5$	0.010453	0.001073
$P = 0.6$	0.015299	0.001817
ASME Design Curve	0.052700	0.007488

Table 6-4. Normalized Fatigue Usage Results for BWR Analysis

Fatigue Curve	BWR-Design	BWR-Actual
ASME Design Curve	1.000	0.142
Environmental Curves		
$P = 0.6$	0.289	0.034
$P = 0.5$	0.198	0.020
$P = 0.4$	0.136	0.012
$P = 0.3$	0.093	0.007
$P = 0.2$	0.065	0.004
$P = 0.1$	0.044	0.003
Higuchi-Iida Air Curve	0.030	0.002

Note: Usage normalized to BWR-Design with ASME Fatigue Curve

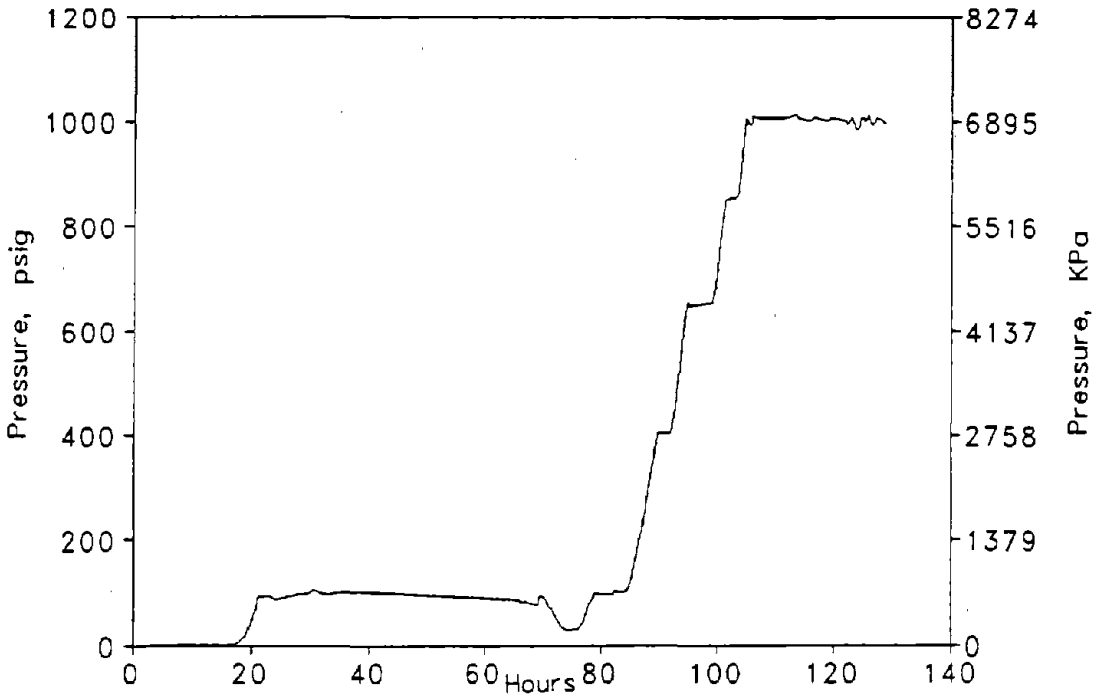

(a) Steam Generator Pressure

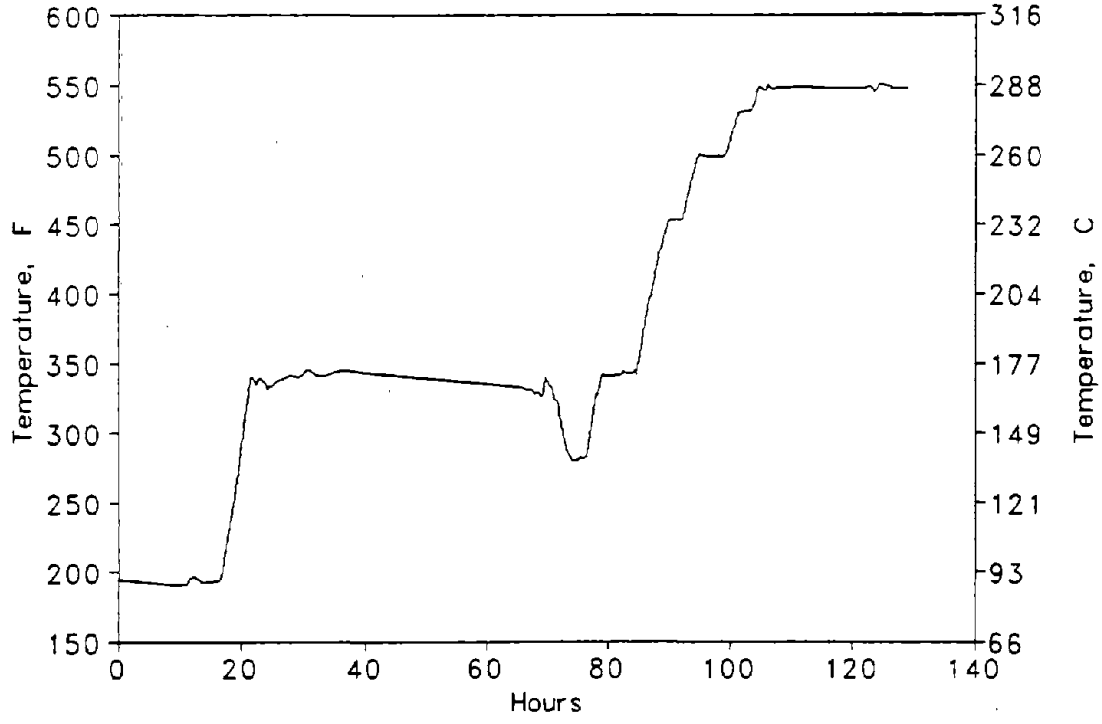

(b) Reactor Coolant Loop Temperature

Figure 6-4. Actual PWR Startup Transient Data.

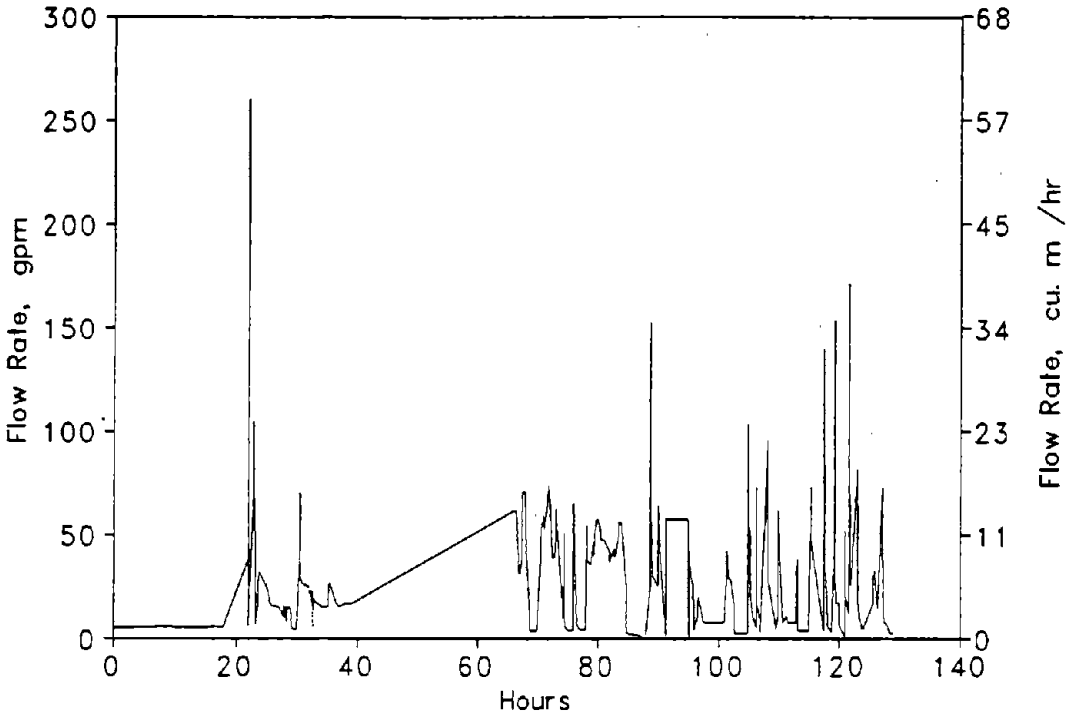

(c) Auxiliary FW Flow

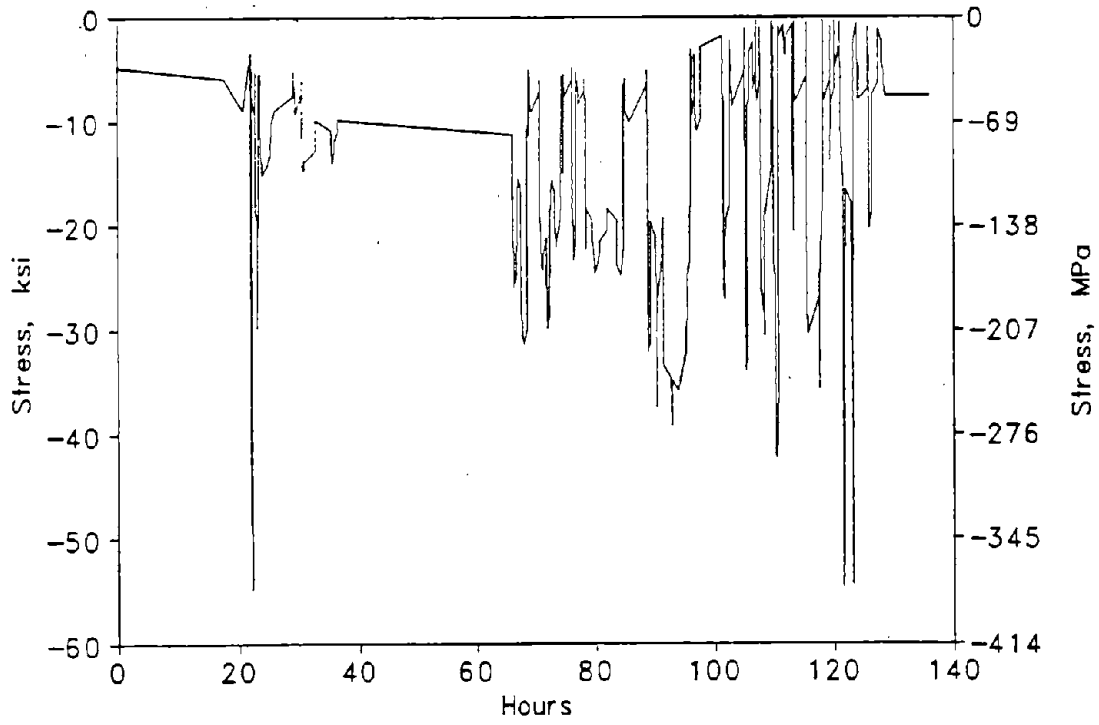

(d) Computed Stress

Figure 6-4. Actual PWR Startup Transient Data - Continued.

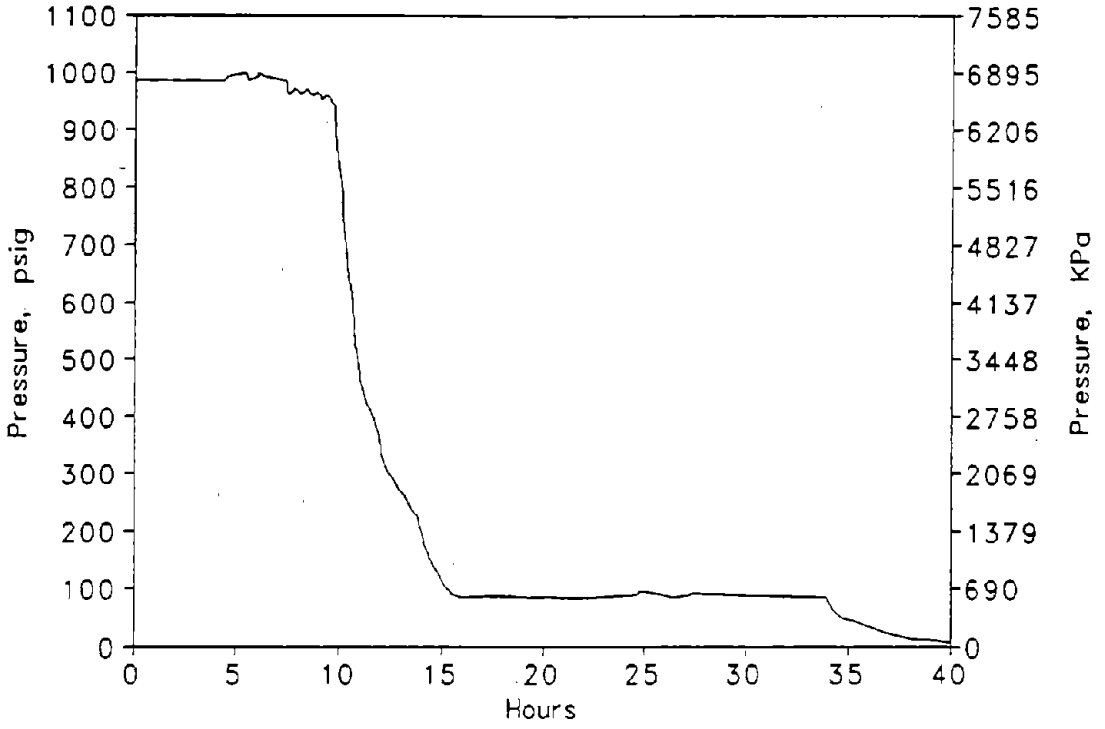

(a) Steam Generator Pressure

(b) Reactor Coolant Loop Temperature

Figure 6-5. Actual PWR Cooldown Transient Data.

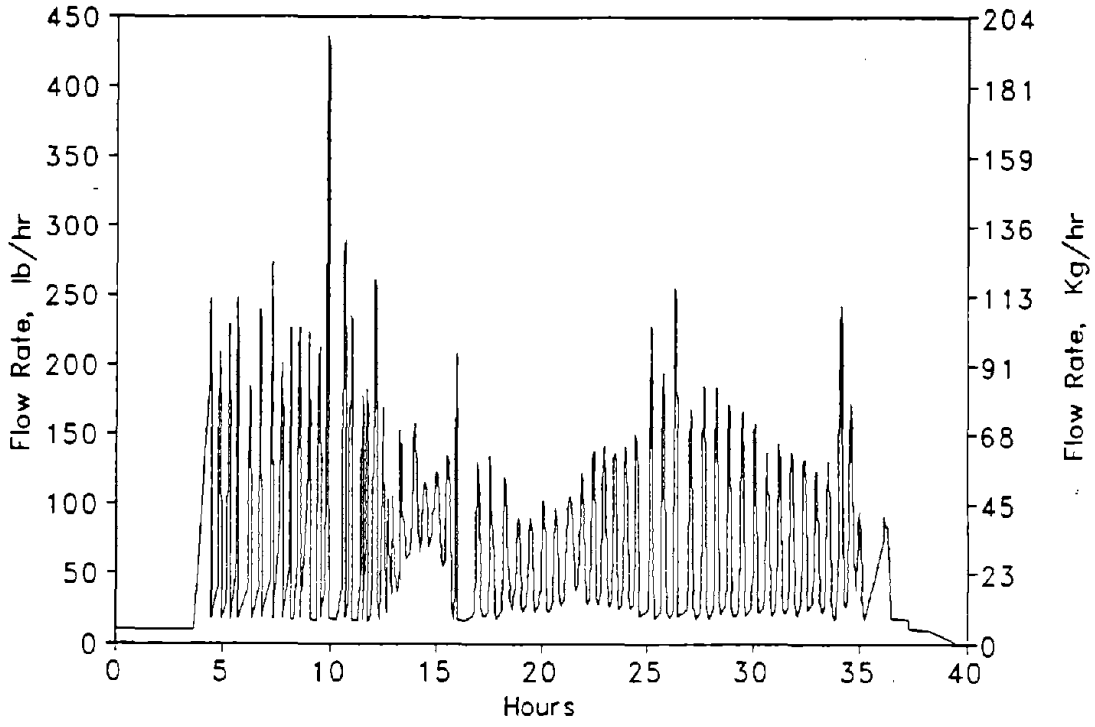

(c) Auxiliary Feedwater Flow

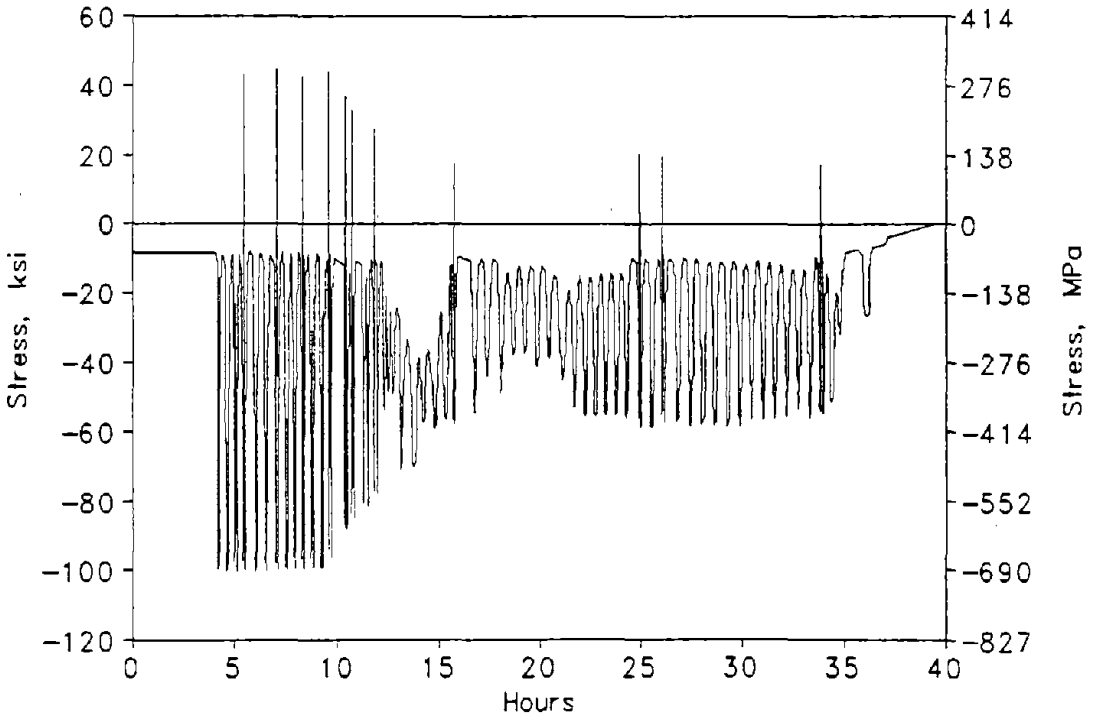

(d) Computed Stress

Figure 6-5. Actual PWR Cooldown Transient - Continued.

rate is changed, the stratification level in the nozzle also changes, causing a stress redistribution across the vertical cross-section. Since plant instrument data was not available to determine the temperature of the auxiliary feedwater flow, a temperature of 13.9°C [57°F] is conservatively assumed in the fatigue monitoring system to predict the stratification temperature difference (ΔT).

Figure 6-5 shows that the most significant cycling occurs at hot standby conditions immediately following shutdown where significant auxiliary feedwater flow is required to maintain steam generator level and to remove core decay heat. Table 6-5 shows the strain amplitude spectrum developed for the actual plant data. Note that the strain amplitudes and rates are not unlike those demonstrated by the similar BWR data. On the other hand, the number of cycles on a per startup-shutdown basis are considerably greater than experienced for the similar BWR location. Table 6-6 shows the computed fatigue usage for the single heatup and cooldown of the plant. As can be seen, for $P = 0.3$ the computed usage from actual plant data is about 8.5% of the design curve value.

6.3.3 Discussion of Temperatures in Regions of Tensile Stress

Prior to continuing the comparisons of the plant data, it is important to develop an understanding of the fluid and metal temperatures that exist in regions of components where high cyclic tensile stresses occur. As presented in the evaluations above, the cyclic tensile stresses occur because of thermal transients with decreasing temperature and during stratification level changes.

To develop a correlation between stress and temperature for thermal shock conditions, a simple model was developed. A transient thermal stress analysis was conducted on a 13-inch OD by 10-inch ID alloy steel cylinder. The outside was insulated and the inside was exposed to fluid with a relatively high convective heat transfer coefficient of 11,356 W/m^2°C [2,000 Btu/hr-ft^2-°F]. A second case was evaluated with a lower heat transfer coefficient of 1,703 W/m^2°C [300 Btu/hr-ft^2-°F]. The fluid temperature at the inside surface was subjected to a step change from 287.8°C [550°F] to 37.9°C [100°F] and then back to 287.8°C [550°F]. Figure 6-6 shows the response of the surface temperature and stress to the transient. When the fluid temperature is stepped, the temperature of the inside surface of the pipe follows. With the higher heat transfer coefficient, the surface temperature closely follows the fluid temperature. Due to the temperature distribution across the pipe wall, surface stresses result, with the tensile stress occurring during periods of decreasing surface temperature. The maximum magnitude of the tensile stress increases for a higher heat transfer coefficient.

Figure 6-7 shows the correlation between the surface stress and the surface temperature. It is observed that the peak thermal shock tensile stress occurred at approximately 93° to 121°C [200° to 250°F] for the higher heat transfer coefficient and at about 177° to 205°C [350° to 400°F] for the lower heat transfer coefficient. Since relatively high magnitudes of temperature drops must occur to create high thermal shock stresses, the surface temperature will always be relatively low at the time of peak tensile thermal stress, and environmental effects should be mitigated. As shown in Figure 6-1, the environmental factor P would be in the mid-temperature range (less than 205°C [400°F]), where a maximum value of $P = 0.3$ is observed.

Table 6-5. Strain Amplitude Spectrum (Actual PWR Data)

Strain Amplitude	Strain Rate, %/sec (x 1000)															Sum
in/in	0.1	0.2	0.4	0.7	1	2	4	7	10	20	40	70	100	200	400	
0.00255										3						3
0.00250										1						1
0.00245																0
0.00239																0
0.00232										1						1
0.00226																0
0.00220																0
0.00213									1							1
0.00207																0
0.00198									1							1
0.00185																0
0.00172									1							1
0.00160		10	1													11
0.00147		1														1
0.00134		1			1	1			3							6
0.00121		3	1			1										5
0.00109		1				1										2
0.00096		1														1
0.00083		18														18
0.00070		9			1											10
0.00057		3	1													4
0.00045		7			1											8
0.00032		3														3
0.00022			2													2
Sum	0	57	5	0	3	3	0	0	6	5	0	0	0	0	0	79

Table 6-6. Results of PWR Fatigue Usage Calculation

Fatigue Curve	PWR-Actual
Higuchi-Iida Air Curve	0.000153
Environmental Curves	
$P = 0.1$	0.000253
$P = 0.2$	0.000440
$P = 0.3$	0.000788
$P = 0.4$	0.001498
$P = 0.5$	0.002962
$P = 0.6$	0.006052
ASME Design Curve	0.009237

For the actual plant examples, a portion of the stress cycling was due to thermal stratification. Figure 6-8 illustrates the stress distribution that occurs in a pipe with hot fluid in the top and relatively colder fluid in the bottom. Two stress profiles are shown, one for a piping system that is relatively free to move vertically (free end condition) and another that is relatively restrained (fixed end condition). The stress distribution across the pipe section changes as the water level changes.

One of the locations that experiences high cyclic stress ranges is denoted as point P in Figure 6-8. When the stratified flow interface is above point P, it experiences high tensile stresses. When the stratification layer moves below point P, then high compressive stresses occur. During the stress range cycle, the temperature is low when the peak tensile stresses occur; as a result environmental effects would be lessened.

At the top of the pipe, the fluid and the pipe are always relatively hot when the flow is stratified. At this location, there can also be relatively high stress ranges, and the same argument cannot be made relative to mitigation of the environmental effects by lowering the temperature. For this case only, the environmental factor P could increase above that expected for the mid-range plateau as shown in Figure 6-1. For all others, a much lower value would be expected.

6.3.4 Water Chemistry

Water chemistry in operating nuclear plants is controlled to limit the effects of corrosion. For example, guidelines have been prepared for BWRs to assist with control of intergranular stress corrosion cracking [6.8, 6.9]. In these guidelines, specific action is required if the level of dissolved oxygen exceeds 0.2 ppm. These limits apply for all operating conditions, including plant startup and hot standby.

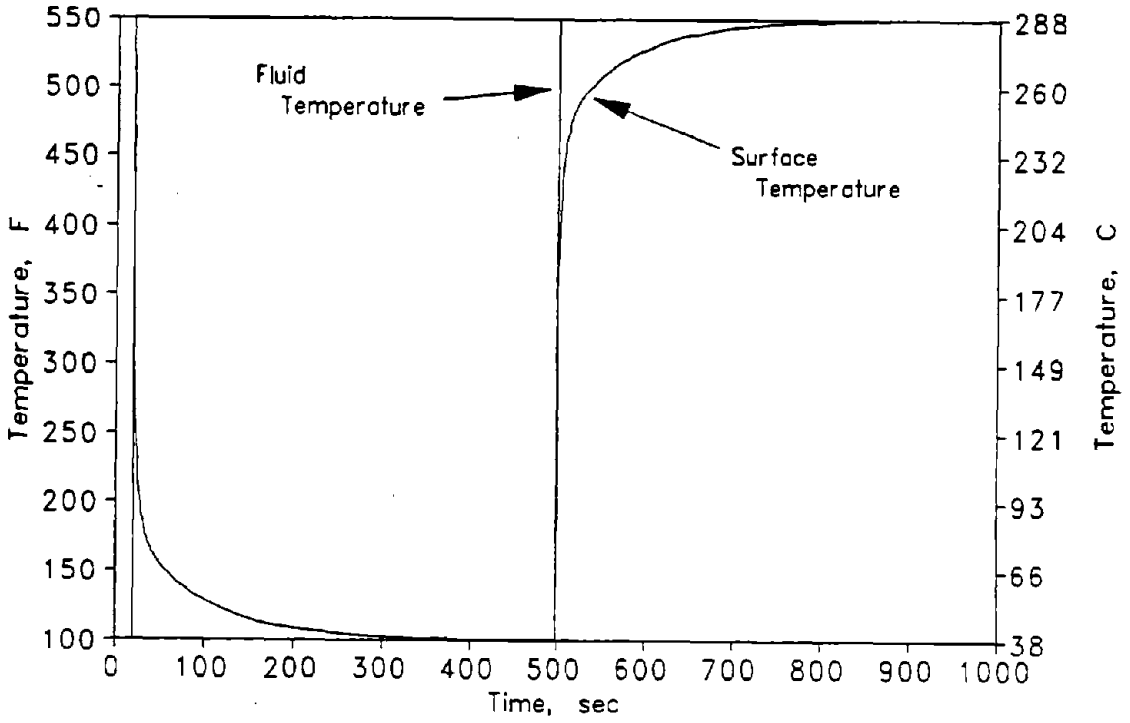

(a) Temperature Response

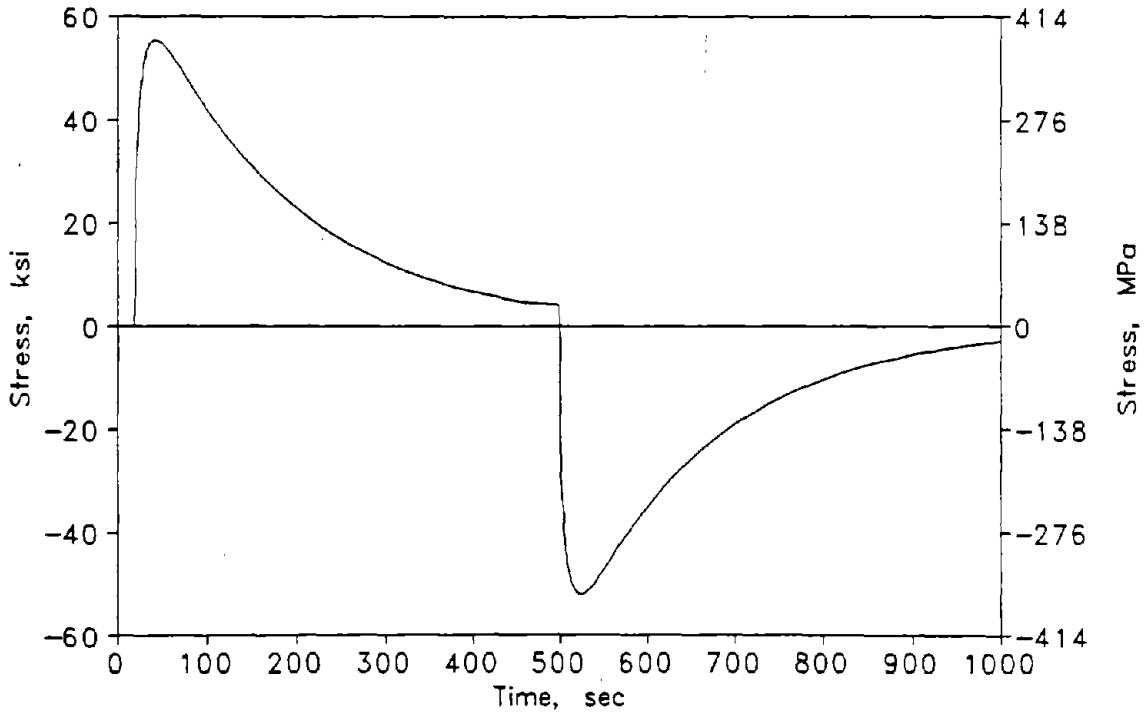

(b) Stress Response

Figure 6-6. Example of Thermal Shock Surface Temperature and Thermal Stress Response.

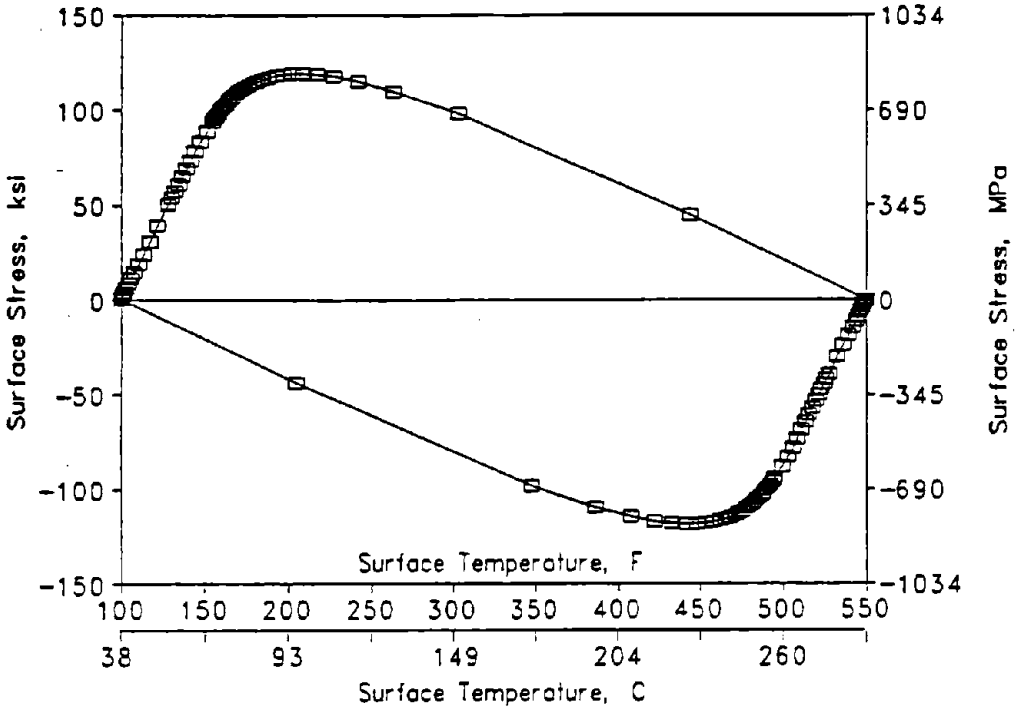

(a) Heat Transfer Coefficient = 11,356 W/m^2-°C [2000 Btu/hr-ft^2°F]

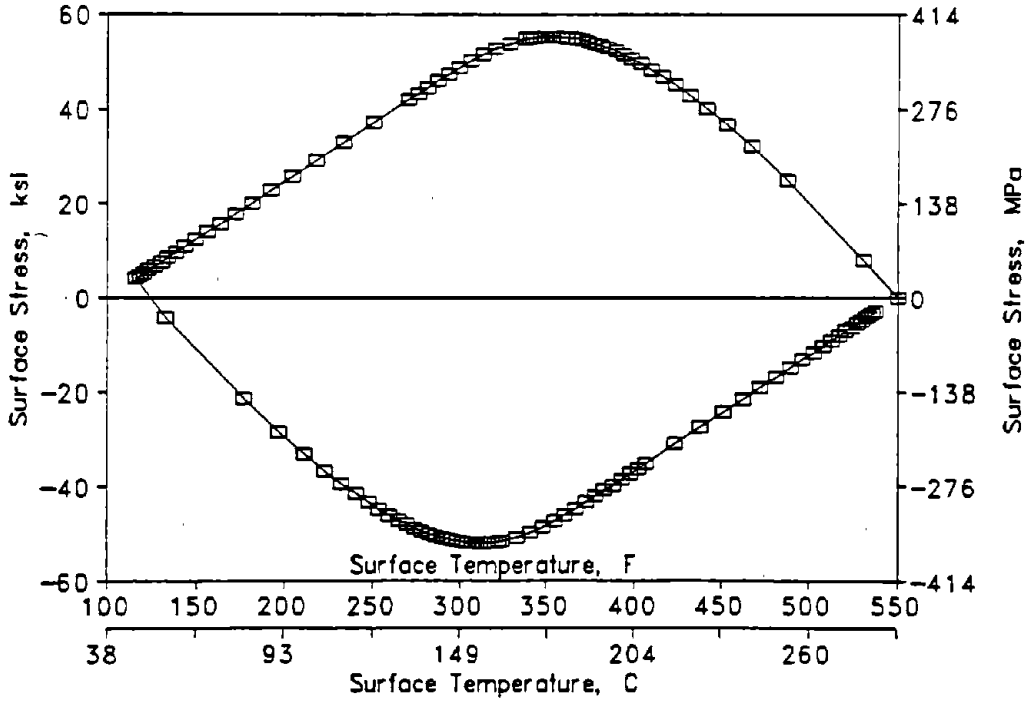

(b) Heat Transfer Coefficient = 1703 W/m^2-°C [300 Btu/hr-ft^2°F]

Figure 6-7. Correlation of Thermal Shock Surface Stress with Surface Temperature.

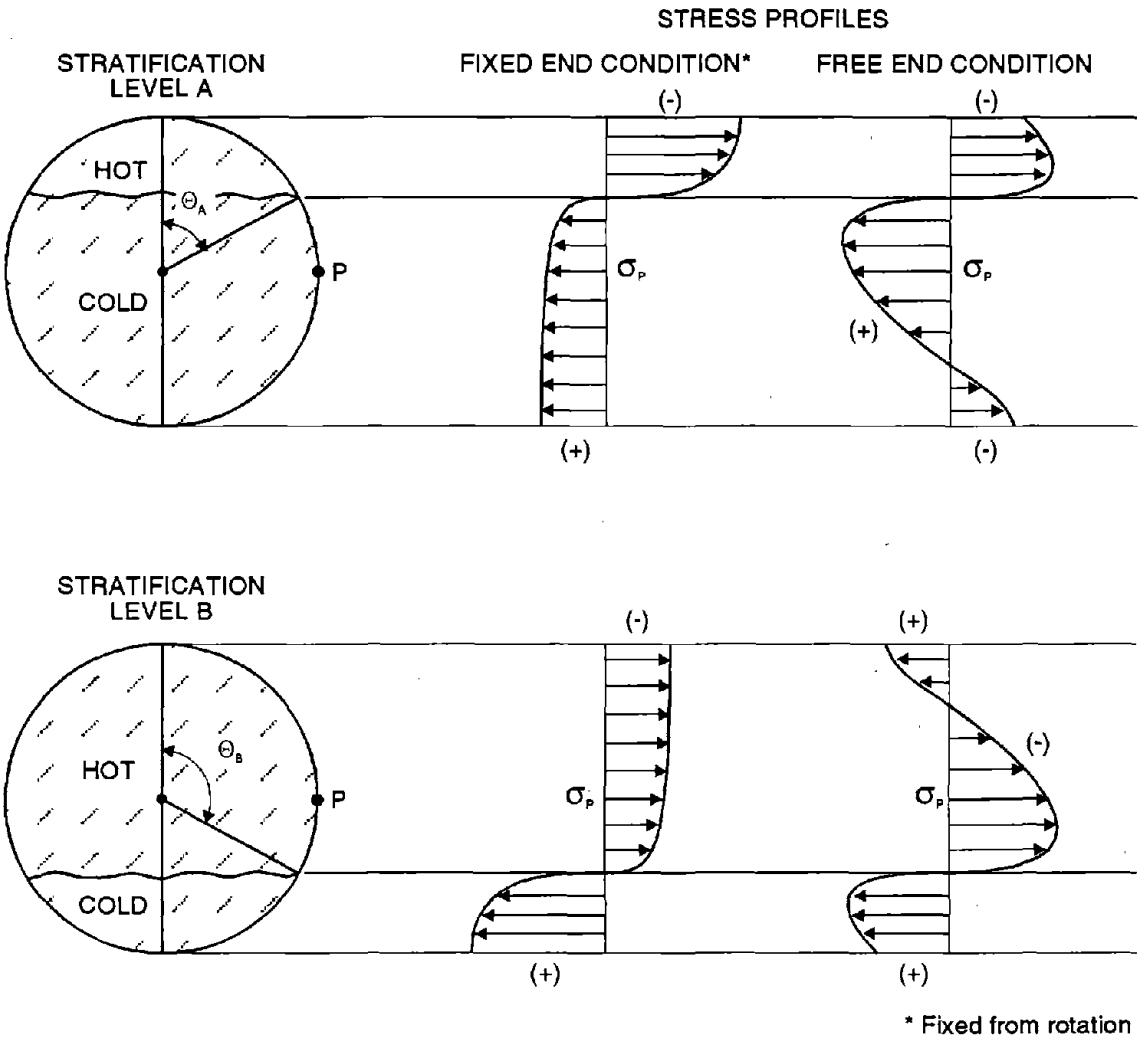

Figure 6-8. Illustration of Top-to-Bottom Bending Stresses Due to Flow Stratification.

Actual reactor coolant system dissolved oxygen content data was obtained from an operating BWR. This data should also be fairly representative of the feedwater which is pumped to the reactor. As shown in Figure 6-9, the dissolved oxygen content typically runs in the range of 0.05 to 0.25 ppm. In each of the startups and shutdowns represented by this data, the dissolved oxygen was less than 0.15 ppm.

Therefore, it is not expected that the bounding curve in Figure 6-1 (for dissolved oxygen = 0.2 ppm) would be representative in assessing the effects of the LWR environment on fatigue usage. Instead, a strain rate exponent (P) on the order of 0.2 or lower would be more representative of a plant's average operating history.

6.3.5 Discussion

Table 6-7 summarizes the evaluations of actual and simulated plant data. The complete range for the parameter P is shown to illustrate sensitivity. A significant observation is that there is considerably more than a factor of 20 between the usage based on the ASME Curve and that derived from the Air Curve. In addition, the usage based on the ASME Curve bounds all of the usages based on the environmental curves.

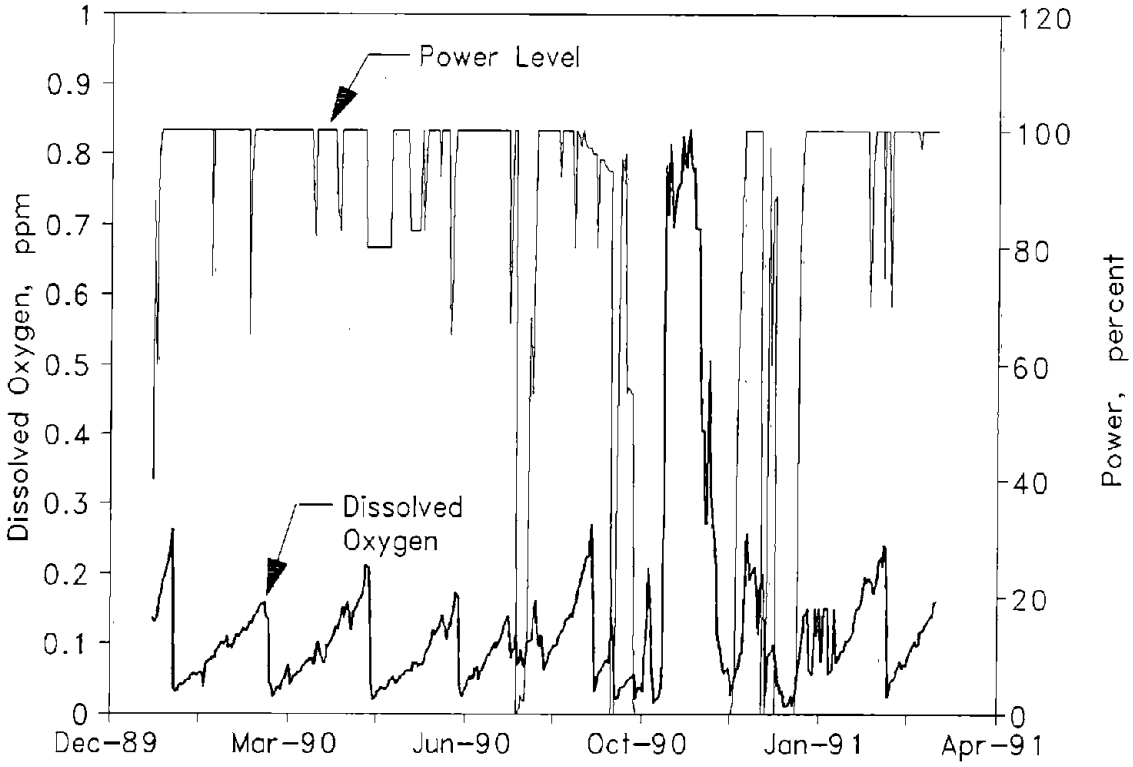

Figure 6-9. Example of Reactor Coolant System Dissolved Oxygen History in an Operating BWR.

One of the major contributions to the margin is that the stresses are relatively low, and much of the usage is derived from that portion of the ASME Curve that is governed by the factor of 2 on stress, not that portion that is governed by the factor of 20 on cycles. For the simulated "design" BWR case where stresses and strain rates were higher, the factor also exceeds 20, but not by such a large margin.

The effect of stress amplitude on the fatigue usage margin is shown in Figure 6-10 where the derivation of the ASME Code fatigue curve is shown. In the region of the curve for less than 50,000 allowable cycles, the ASME design curve is determined by shifting the ASME air curve (corrected for mean stress effects) to the left by a factor of 20 on cycles. Then, to extend the design curve to 10^6 cycles, it was determined that a factor of 2 on the ASME air curve (corrected for mean stress effects) should exist at 10^6 cycles. It is suspected that a French curve was used to extend the ASME Design Curve from approximately 7,000 cycles to 10^6 cycles. Thus, above 7,000 cycles there will be more margin than a factor of 20 on cycles between the air data and the design curve.

Figure 6-10 also demonstrates that the Higuchi-Iida "air" curve is higher than the ASME "air" curve. This is also expected to be a factor in the results of this evaluation. As shown in Figure 6-10, at strain amplitudes of about 0.0016 m/m [in/in], an infinite margin on cycles exists between the ASME design and the Higuchi-Iida "air" curves.

Table 6-7. Computed Usage Ratioed to Usage for Air Curve

Fatigue Curve	PWR-Actual	BWR-Design	BWR-Actual
ASME Design Curve	60.4	32.8	91.4
Environmental Curves			
P = 0.6	39.5	9.5	22.2
P = 0.5	19.3	6.5	13.1
P = 0.4	9.8	4.5	7.8
P = 0.3	5.2	3.1	4.6
P = 0.2	2.9	2.1	2.8
P = 0.1	1.7	1.4	1.6
Higuchi-Iida Air Curve	1.0	1.0	1.0

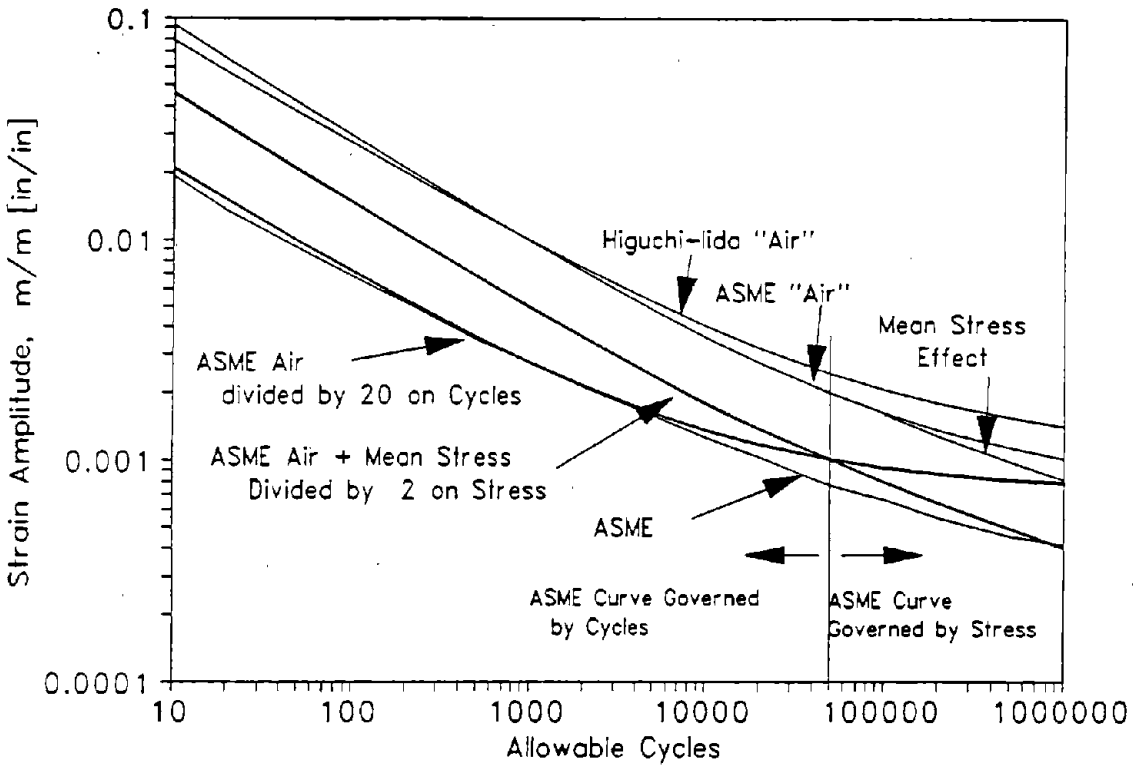

Figure 6-10. Comparison of ASME Design and "Air Data" Fatigue Curves.

In the fatigue analysis performed for this study, there were no specific considerations given to mean stress effects, which can have an effect only at strains less than about 0.00135 m/m [in/in] (corresponding to yield strength). There were two reasons for this. First, the actual plant data exhibits some cases of extreme cycling that will produce shakedown, such that the lower stress ranges will not have high mean stress. Secondly, most of the fatigue usage results from high strain amplitude cycling. A sample analysis for the PWR case was run, which included mean stress effects, and showed that the usage for P = 0.5 increased by about five percent from that shown in Table 6-6. The change was less for lower values of P. This small change does not invalidate the conclusions reached in this study.

If the usage at a location is due to thermal shock transients, the previous discussion has shown that the temperatures will be relatively low, certainly less than 204°C [400°F]. By reviewing Figure 6-1, it can be seen that the parameter P is a maximum of approximately 0.3 for all water chemistry conditions. By reviewing Table 6-7, it is observed that there is approximately a factor of 10 between the ASME Design Curve computed usage and that attributable to the environmental curves with P = 0.3 for two of the cases and a factor of about 20 for the actual BWR case (factor is 60.4/5.2 for PWR-Actual, 32.8/3.1 for BWR-Design, and 91.4/4.6 for BWR-Actual). If water chemistry is favorable, which is certainly expected during a portion of the operations, then the margin further increases.

At the high-cycle end of the design curve, there is a factor of two included as shown in Figure 6-10. The effect of this part of the conservatism was not included in evalutions previously discussed. To show the effect of this factor, a single evaluation was conducted, using the following aproach:

1. To account for mean stress effects, the strain amplitude was increased by the following factor (derived from Equation 4 of Reference 2-6) if the strain amplitude was less than the yield strain:

$$\varepsilon' = \varepsilon \frac{S_u - \varepsilon E}{S_u - S_y}$$

ε' = modified strain amplitude, m/m [in/in]
ε = original strain amplitude, m/m [in/in]
S_u = ultimate tensile strength (assumed to be 552 MPa [80 ksi])
S_y = yield strength (assumed to be 276 MPa [40 ksi])
E = modulus of elasticity (assumed to be 206,850 MPa [30,000 ksi])

2. For each entry in the spectrum table (adjusted for mean strain effects), an allowable number of cycles was determined from the appropriate strain rate curve. This number of cycles was divided by a factor F_c to obtain a number of allowable cycles that included margin. For the current ASME Code, this factor is 20.

3. Also, for each entry in the spectrum table (adjusted for mean strain effects), an allowable number of cycles was determined for a strain amplitude increased by a factor F_s. This number of cycles includes the stress margin, and for the current ASME Code, F_s would be 2.0.

4. The minimum number of allowable cycles was then determined from steps 2 and 3. In the high-cycle part of the fatigue curve, the number of cycles from step 3 was controlling, while the number of cycles from step 2 was controlling for relatively high strain amplitudes.

5. Then, on an iterative basis, the factors F_c and F_s were varied so that the environmental usage predicted by this process was equal to that obtained from the ASME Code fatigue curve analysis.

The previous discussion had indicated that at least a factor of 10 existed between the ASME Code usage factor and that attributed to the environmental curves for P = 0.3. Using the above approach, the margins on stress were determined as follows using the factor F_c = 10:

BWR Design Tansients:	F_s =	2.05
BWR Actual Transients:	F_s =	1.80
PWR Actual Transients:	F_s =	1.41

This shows that for the case of design transients, there was no decrease in the fatigue curve stress factor since almost all of the usage was due to the high stress amplitudes. For the actual transient data, there was a reduction in the stress factor below 2.0 since many of the stress amplitudes were low. However, in each of the cases, not all of the stress margin was used.

For locations where the usage is primarily due to stratification, and the location is at the top of the pipe where it would be at near reactor normal operating temperatures and dissolved oxygen is high, the margins could decrease considerably. **In no case did the environmental effect use up all of the margin in the data evaluated.**

6.4 References

6.1 Letter from W.T. Russell (USNRC) to W. Rasin (NUMARC), "NRC Staff Action Plans Concerning the Issue of Environmental Requalification and Fatigue Analysis of Components," July 30, 1993.

6.2 "Interim Fatigue Design Curves for Carbon, Low-Alloy, and Austenitic Stainless Steels in LWR Environments," NUREG/CR-5999, Argonne National Laboratories Report, ANL-9313, U.S. Nuclear Regulatory Commission, March 1993.

6.3 M. Higuchi and K. Iida, "Fatigue Strength Data of LWR Structural Materials in Japan (Effects of LWR Water Environment on Fatigue Strength)," presented at U.S. NRC - EFD Japan Joint Meeting, Louisville, KY, December 1992.

6.4 S. Yukawa and M. Prager, "PVRC Progress Report on Evaluation of Fatigue Curves in Sections III and XI in the Light of Current Worldwide Data," Pressure Vessel Research Council Special Report, September 29, 1992.

6.5 Yasubide Asada, "Rate Approach for Fatigue Life Reduction Factor in LWR Water Environment," Welding Research Council Progress Reports, Volume XLVIII, No. 9/10, p. 148, September/October 1993.

6.6 "Metal Fatigue in Operating Nuclear Power Plants," Prepared by ASME Section XI Task Group on Fatigue in Operating Plants, TR-100252, Research Project 2688-7, April 1992.

6.7 H.O. Fuchs and R.I. Stephens, "Metal Fatigue in Engineering," John Wiley and Sons, New York, 1980.

6.8 "BWR Normal Water Chemistry Guidelines: 1986 Revision," Electric Power Research Institute, EPRI Report No. NP-4946-SR, 1988.

6.9 "BWR Hydrogen Water Chemistry Guidelines: 1987 Revision," Electric Power Research Institute, EPRI Report No. NP-4947-SR, 1988.

This page intentionally left blank.

7. SUMMARY AND CONCLUSIONS

A number of stress reports for Section III, Class 1 components were reviewed to determine the degree of conservatism that exists in reported fatigue usage factors. The components were selected from nuclear power plants with Nuclear Steam Supply Systems (NSSSs) designed by the four domestic suppliers; General Electric (GE), Combustion Engineering (CE), Babcock & Wilcox (B&W) and Westinghouse. The stress reports were reviewed in order to investigate the potential conservatisms in the fatigue analysis of components. In addition, the methodology included in Section III for Class 1 component evaluation was reviewed to identify inherent conservatisms in the Code itself. Conservatisms were identified due to the following sources:

- Transient Grouping
- Analytical Methods for Heat Transfer and Stress Evaluation
- Conservatisms Related to Simplified Elastic-Plastic Analysis
- Conservatisms in Material Property Selection
- Conservatisms in Code Edition

This study found that each of these sources contributed significantly to conservatisms in the fatigue evaluation of at least one of the Class 1 component stress reports that were reviewed. Of particular importance in almost all of the fatigue evaluations reviewed is the influence of the "penalty" factor K_e, which is calculated as part of the simplified elastic-plastic analysis and is triggered by high stresses. Inclusion of a $K_e > 1.0$ has a large effect on the calculation of the fatigue usage factor and generally results in high usage. For piping systems designed prior to 1979, high usage is almost always associated with high K_e. Use of Code rules after 1979 would significantly reduce reported usage factors for piping since the rules were changed to remove the excessive conservatism associated with determining K_e.

The most significant conclusion one can make after review of these stress reports is that if the fatigue usage factor is high (i.e., close to the maximum allowable value of 1.0) it is probably high because the designer used simplifying assumptions in showing that minimum code requirements were met. The reported usage could probably be reduced significantly by performing a more detailed analysis. This additional analysis may be a relatively simple activity, such as eliminating very conservative transient grouping, or it may be more complex, such as performing a plastic analysis of the component with the use of a finite element model. Whether the additional analysis is relatively simple or complex, the point remains that high fatigue usage factors reported in the original stress reports can probably be reduced. Although each component must be reviewed on a case-by-case basis, the following are examples of tasks that could be performed to attempt to reduce the calculated usage factor:

1. Eliminate excessively conservative grouping of transients,

2. Use real plant data, in lieu of design transients, to reduce the severity of step changes often postulated when defining design transients,

3. Use elastic-plastic methods to calculate maximum strain, in lieu of using the simplified elastic-plastic analysis (K_e),

4. Use variable convective heat transfer coefficients, rather than constant values,

5. Be precise when defining material property values, (e.g., take the effect of temperature into account when defining the modulus of elasticity and allowable stresses),

6. Reanalyze using a post-1980 code edition, when ΔT_1 term in equation 10 of NB-3650 was eliminated,

7. Recompute stresses using an up-to-date finite element model.

It was also found that fatigue usage for actual plant transients as determined by in-plant fatigue monitoring systems was significantly less than fatigue usage calculated for transients as defined in Design Specifications. For the BWR feedwater nozzle safe-end studied in detail, the design analysis conservatism was primarily due to the use of step changes in temperature transients and temperature ranges that were considerably larger in the Design Specification than those observed during actual plant operation. This evaluation supports the general conclusion that much of the high fatigue usage documented in stress reports is due to the definition of operating transients in Design Specifications that are significantly more severe than those occurring in operating plants.

It has recently been identified that LWR environmental effects might invalidate the fatigue curves included in the ASME Code. Research has shown that strain rate, temperature and dissolved oxygen content all have significant effects on the allowable cycles to crack initiation of steel. To evaluate the significance of these factors, the environmental effects on the calculation of cumulative usage factors were evaluated for both a BWR feedwater nozzle/safe-end and a PWR steam generator feedwater nozzle/safe-end. Using both actual plant data and design data (for the BWR case), it was shown that there should be at least factors of 10-15 on cycles remaining after consideration of environmental effects. This is primarily due to the fact that actual tensile stresses in plant components exposed to the LWR environment result because of reduced local temperatures which tend to mitigate environmental effects. Less margin may exist for the top of stratified piping, but environmental effects still should be enveloped by the ASME design curve. Limited data shows that consideration of actual dissolved oxygen levels may provide additional mitigation. The potential lack of conservatism due to environmental effects is more than offset by general conservatisms found in most component analyses, and in some cases the environment effect may not be significant. When actual plant data were considered and compared to design basis transients, the reduction in computed usage was much greater than any increases due to environmental effects.

In the specific cases reviewed as part of this study, fatigue is not a significant issue. Component designers have addressed Code requirements for fatigue only to whatever degree was necessary to prove that the design fatigue usage factors were less than 1.0, which is all that

Section III requires. The calculation of fatigue usage factors is a useful process in design of Section III, Class 1 components because it assures that the designs are fatigue resistant. However, the reported fatigue usage factors should not necessarily be considered as an accurate measure of component life. In all cases reviewed in this study, more analysis could reduce the computed fatigue usage or could show that the components are capable of withstanding more or different transients than were included in the original design.

The following summarizes the major conclusions of this study:

1. ASME Code Section III, Class 1, component fatigue analyses are conservative in two ways. First, the code rules and the allowables contain conservatisms that are intentional, in order to compensate for a variety of uncertainties. Second, component designers and analysts use a number of conservative assumptions when applying the code rules. Because of both types of conservatisms, high fatigue usage factors listed in component stress reports do not necessarily imply that fatigue usage is actually high. Component designers were required only to demonstrate that the fatigue usage factor was less than 1.0; therefore, conservatisms that simplified the analyses within this limit were often taken.

2. High reported fatigue usage can, in most cases, be reduced substantially by recalculation, taking into account two major sources of analytical conservatism — characteristics of design transients and localized elastic-plastic behavior.

    - Design transients are generally very conservative in terms of transient severity, and low-severity transients are often grouped with high-severity transients for simplicity. A useful first step in fatigue usage recalculation is to remove the conservatism associated with grouping low-severity transients with high-severity transients. A second step is often to remove extreme temperature ranges and rates of temperature change in high-severity transients by analysis or by use of actual plant data.

    - High fatigue usage is almost always associated with simplified elastic-plastic analysis, especially for piping system components designed prior to the 1980 ASME Code edition. A third step in fatigue usage recalculation is often an actual, elastic-plastic analysis of localized high-strain regions or, in the case of older piping system component designs, use of a later Code edition.

3. The conservatism built into the ASME Code Section III fatigue allowables, which is intended to compensate or such factors as surface finish, data scatter, and test specimen size effects, also compensates for moderate environmental effects. Although the effects of the LWR environment on the fatigue resistance of pressure boundary materials, especially carbon steels, can reduce this conservatism in the ASME Code allowables substantially (in particular at high temperatures and high levels of dissolved oxygen), a number of factors combine to limit these reductions.

    - Detailed stress analyses show that significant tensile stresses at the component surface in contact with the LWR water environment are associated with reduced temperatures, tending to mitigate the environmental effects.

- The effect of lower strain rates associated with actual plant operating transients is more than compensated for by the lower strain ranges that occur as a result of these transients.

- The overall influence of the LWR environment was shown to be bounded by the conservatism built into the ASME Code fatigue design allowables. Conservatism remains to compensate for test specimen surface finish and size effects, and data scatter.

4. Although severe LWR environmental effects may require special treatment, it does not appear that consideration of these effects would cause any component in existing plants to have a recalculated fatigue usage factor greater than 1.0. The reduction of the fatigue usage factor that can be demonstrated by recalculation with less conservative assumptions seems to more than compensate for any increased fatigue usage recalculated with LWR environment effects.

APPENDIX A
ACRONYMS

ANSI	American National Standards Institute
ASME	American Society of Mechanical Engineers
B&W	Babcock & Wilcox Company
BTP	Branch Technical Position
BWR	Boiling Water Reactor
CE	Combustion Engineering Company
CLB	Current licensing basis
CRDM	Control rod drive mechanism
CS	Core Support
DO2	Dissolved oxygen
DOE	U.S. Department of Energy
ECCS	Emergency core cooling system
EPRI	Electric Power Research Institute
GE	General Electric Company
IR	Industry Report
LPI	Low Pressure Injection
LWR	Light Water Reactor
MC	Metal containments
NEI	Nuclear Energy Institute
NRC	U.S. Nuclear Regulatory Commission
NSSS	Nuclear Steam Supply System
NUMARC	Nuclear Management and Resources Council
OOR	Ordered overall range
PVRC	Pressure Vessel Research Council
PWR	Pressurized Water Reactor
RCS	Reactor coolant system
RPV	Reactor pressure vessel
RTD	Resistance temperature device
S-N	Stress-number of cycles
SNL	Sandia National Laboratories
SRV	Safety relief valve
WRC	Welding Research Council

Distribution for Fatigue Report:

Category UC-523 (91 copies)

DOE

Dennis Harrison (2 copies)
U.S. Department of Energy, NE-451
19901 Germantown Road
Germantown, MD 20874

Sterling Franks, III
U.S. Department of Energy, NE-451
19901 Germantown Road
Germantown, MD 20874

Charles Thompson
U.S. Department of Energy, NE-451
19901 Germantown Road
Germantown, MD 20874

EPRI

John Carey (2 copies)
Electric Power Research Institute
3412 Hillview Avenue
Palo Alto, CA 94303

Joe Gilman
Electric Power Research Institute
3412 Hillview Avenue
Palto Alto, CA 94303

Steve Gosselin (5 copies)
Electric Power Research Institute
1300 Harris Blvd.
Charlotte, NC 28262

Robert Carter
Electric Power Research Institute
1300 Harris Boulevard
Charlotte, NC 28262

EPRI LCM Subcommittee

Barth Doroshuk
Baltimore Gas & Electric
Calvert Cliffs, Route 4 South
Lusby, MD 20657

Deborah Staudinger
B&W Nuclear Technologies
3315 Old forest Road
Lynchburgh, VA 24506

Richard Remshaw
Consolidate Edison Co. of New York
4 Irving Place, Rm. 1238
New York, NY 10003

Greg Robinson
Duke Power Company, EC09F
422 South Church Street
P.O. Box 1006
Charlotte, NC 28201-1006

Willis F. Mashburn
Entergy Operations, Inc.
P.O. Box 31995
Jackson, MS 39286-1995

Roger Murgatroid
Crystal River Nuclear Plant (MAC-NA2G)
15760 West Power Line Street
Florida Power Corp.
Crystal River, FL 34428-6708

Robert Locke
GPU Nuclear
1 Upper Pond Road
Parsippany, NJ 07054

Karl Jacobs
New York Power Authority
123 Main Street
White Plains, NY 10601

Francis Feng
Niagara Mohawk Power Corp.
301 Plainfield Road
Syracuse, NY 13212

Tim Bailey
Northern States Power Co.
Monticello Nuclear Generating Plant
2807 W. Highway 75
Monticello, MN 55362

Distribution for Fatigue Report, Continued:

Robert McDevitt
Nuclear Operations Support Dept.
Pacific Gas & Electric Co.
77 Beale Street, Rm. 1414
San Francisco, CA 94106

Ray McNamara
Pennsylvania Power & Light Company
Two North Ninth Street
Allentown, PA 18101

Jim Perrin
Public Service Electric & Gas Co.
P.O. Box 236, N32
Hancocks Bridge, N.J. 08038

Jose Perez
Southern California Edison
9975 Toledo Way, Suite 102
Irvine, CA 92718

John Giddens
Southern Nuclear Operating Co.
P.O. Box 1295
Birmingham, Al 35201-1295

Jim Chardos
Tennessee Valley Authority
Watts Bar Nuclear Plant
P.O. Box 200
Spring City, TN 37381

John Swailes
Washington Public Supply Power System
P.O. Box 968
3000 George Washington Way
Richland, Washington 99352-0968

Chuck Krause
Wisconsin Electric Power Company
231 West Michigan
P.O. Box 2046
Milwaukee, WI 53201

Institute of Nuclear Power Operations

Tom Mitchell
Institute of Nuclear Power Operations
700 Galleria Parkway
Atlanta, GA 30339-5967National Labs

National Laboratories

William Shack
Argonne National Laboratory
Building 212
9700 S. Cass Ave.
Argonne, IL 60439

Omesh Chopra
Argonne National Laboratory
Building 212
9700 S. Cass Ave
Argonne, IL 60439

Sharif Rahman
Battelle Columbus Labs
505 King Avenue
Columbus, OH 43201

Spencer H. Bush
Battelle Pacific Northwest Labs
P.O. Box 999
Richland, WA 99352

F.A. Simonen
Battelle Pacific Northwest Labs
P.O. Box 999
Richland, WA 99352

Vikram N. Shah
Idaho National Engineering Lab.
EG&G Idaho, Inc.
P.O. Box 1625, MS 2406
Idaho Falls, ID 83415-2406

Thomas A. Auten
Knolls Atomic Power Laboratory
P.O. Box 1072
Schenectady, NY 12309-1072

Distribution for Fatigue Report, Continued:

Bill Pennell
Oak Ridge National Labs
P.O. Box 2009
Oak Ridge, TN 37831-8056

NSSS Owners Group Liaisons

Phil Richardson
ABB-CE Owners Group
P.O. Box 500
1000 Prospect Hill Road
Windsor, Conn 06095

Edward Siegel
ABB Combustion Engineering, Inc.
P.O. Box 500
Windsor, CT 06095-0500

William Gray
B&W Nuclear Technologies
3315 Old Forest Road
P.O. Box 10935
Lynchburg, VA 24506-0935

Tony McConnell
B&W Nuclear Technologies
3315 Old Forest Road
P.O. Box 10935
Lynchburg, VA 24506-0935

Chuck Pierce
BWR Owners Group GLRP Liaison
Southern Nuclear Operating Co.
P.O. Box 1295
Birmingham, AL 35201-1295

Kathy Berry
General Electric Nuclear Energy
175 Curtner Ave., MC 789
San Jose, CA 95125

Don Eggett (8 copies)
Chairman, BWR-POLR Committee
Commonwealth Edison Co.
1400 Opus Place, Suite 300
Downers Grove, IL 60515

Roger Newton
Westinghouse Owners Group GLRP Liaison
Wisconsin Electric Power Co.
231 West Michigan, P.O. Box 2046
Milwaukee, WI 53021

Ted Meyer
Westinghouse Electric Corp.
P.O. Box 355
Pittsburgh, PA 15230-0355

Nuclear Energy Institute

Kurt Cozens (5 copies)
Nuclear Energy Institute
1776 Eye Street, NW, Suite 300
Washington, DC 20006-2496

Dave Modeen
Nuclear Energy Institute
1776 Eye Street, NW, Suite 300
Washington, DC 20006-2496

NEI Fatigue AHAC

Robin Dyle
Southern Nuclear Operating Co.
P.O. Box 1295
Birmingham, AL 35201-1295

Ken House
Tennessee Valley Authority
Sequoyah Access Road
Soddy-Daisy, TN 37379

Matt Kupinski
Northeast Utilities
P.O. Box 270
Hartford, CT 06141

T. H. Liu
Westinghouse Electric Corporation
P.O. Box 355
Pittsburgh, PA 15230-0355

Distribution for Fatigue Report, Continued:

Paul Manbeck
Baltimore Gas & Electric Co.
Calvert Cliffs Nuclear Power Plant
1650 Calvert Cliffs Parkway
Lusby, MD 20657

Robert Nickell
SGI International
1400 Prospect, Suite 325
La Jolla, CA 92037

Sampath Ranganath
General Electric Nuclear Energy
MS MC747
175 Curtner Avenue
San Jose, CA 95125

Larry Rinaca
Tennessee Valley Authority
1101 Market Street, LP4F-C
Chattanogga, TN 37402

John F. Shepard
B&W Nuclear Technologies
P.O. Box 109355
Lynchburg, VA 24506-0935

Sumio Yukawa (3 copies)
4925 Valkyrie Drive
Boulder, CO 80301

Nuclear Regulatory Commission

Terence Chan (2 copies)
U.S. Nuclear Regulatory Commission
11555 Rockville Pike, MS7E23
Rockville, MD 20852

Mike Mayfield
U.S. Nuclear Regulatory Commission
MS 217C NL/S
Washington, D.C. 20555

Ron Parkhill (2 copies)
U.S. Nuclear Regulatory Commission
11555 Rockville Pike
Rockville, MD 20852

Keith Wichman
U.S. Nuclear Regulatory Commission
MS 7D4
Washington, DC 20555

Utilities

Arizona Public Service Co.

Helmut Miyahara
Arizona Public Service Co.
411 N. Central
Phoenix, AZ 85072

Mark Radspinner
Arizona Public Service Co.
411 North Central Avenue
P.O. Box 53999
Phoenix, AZ 85072-3999

James B. Mahoney
Arizona Public Service Company
411 North Central Avenue
Phoenix, AZ 85072-2034

Baltimore Gas & Electric Co.

Scott A. Henry
Baltimore Gas & Electric Co.
1650 Calvert Cliffs Parkway
Lusby, MD 20657

Boston Edison Co.

Steve Roberts
Boston Edison Co.
Braintree Hill Office Park
Braintree, MA 02184

Carolina Power & Light Company

Steve Bertz
Carolina Power & Light Co.
Brunswick Steam Electric Station
Southport, NC 28461

Distribution for Fatigue Report, Continued:

Grant Chappell
Carolina Power & Light Co.
P.O. Box 1551
Raleigh, NC 27602

Robert Cooper
Carolina Power & Light Co.
H. B. Robinson Unit 2, P.O. Box 790
Hartsville, SC 29550

Bill Peavyhouse
Carolina Power & Light Co.
Shearon Harris Plant, P.O. Box 1551
Raleigh, NC 27602

Richard G. Robinson
Carolina Power & Light Co.
H. B. Robinson Plant, P.O. Box 790
Hartsville, SC 27602

Cleveland Electric Illuminating Co.

Paul Crider
Cleveland Electric Illuminating Co.
Perry Station, Mail Zone E150
P.O. Box 97
10 N. Center Road
Perry, OH 44081

H. S. Thornton
Cleveland Electric Illuminating Co.
Nuclear Engineering Dept.
Perry Nuclear Power Plant
P.O. Box 97
Perry, OH 44081

Commonwealth Edison Co.

Robert L. Scott
Commonwealth Edison Co.
1400 Opus Place, Suite 400
Downers Grove, IL 60515

Alex G. Panaos
Commonwealth Edison Company
1400 Opus Place, Suite 400
Downers Grove, IL 60515

Thomas D. Spry
Commonwealth Edison Co.
1400 Opus Place, Suite 400
Nuclear Maintenance Services
Downers Grove, IL 60515

Paul Donavin
Commonwealth Edison Company
Nuclear Eng. & Tech. Services
1400 Opus Place, Suite 400
Downers Grove, IL 60515

Consolidated Edison Co. of New York, Inc.

Sam Sinha
Consolidated Edison Co. of New York
4 Irving Place
New York, NY 10003

Joseph Madia
Consolidated Edison Co. of New York
4 Irving Place
New York, NY 1003

Connecticut Yankee Atomic Power Co.

Robert Morris
Connecticut Yankee Atomic Power Co.
107 Seldon St.
Berlin, Conn 06141-0270

Consumers Power Company

Rolfe Jenkins (2 copies)
Consumers Power Company
Palisades Station
27780 Blue Star Highway
Covert, MI 49085

Detroit Edison Co.

Michael S. Williams
Detroit Edison Co.
Enrico Fermi Plant
6400 N. Dixie Hwy.
Newport, MI 48166

Distribution for Fatigue Report, Continued:

Allen Lim
Detroit Edison Co.
Enrico Fermi Plant
6400 N. Dixie Hwy.
Newport, MI 48166

Duke Power Company

Mike Davis
Duke Power Company
422 South Church Street
P.O. Box 1006
Charlotte, NC 28201

Jeff Gilreath
Duke Power Company
526 South Street, MC EC09O
P.O. Box 1006
Charlotte, NC 28201

W. Gallman
Duke Power Company
P.O. Box 33189
422 South Church Street
Charlotte, NC 28242

Bill Taylor
Duke Power Company
Mail Code MG02CE
13225 Hagers Ferry Rd.
Huntersville, NC 28078

John Rowe
Duke Power Company
422 S. Church St.
Charlotte, NC 28242

David Whitaker
Duke Power Company
P.O. Box 1006 EC 090
Charlotte, NC 28201-1006

Bob Morgan
Duke Power Company
McGuire Nuclear Station - MG02CE
13225 Haggers Ferry Road
Huntersville, NC 28078-89

Duquesne Light Company

Mike Testa
Duquesne Light Company
Beaver Valley Nuclear Station
P.O. Box 4
Shippingport, PA 15077

Greg A. Kammerdeiner
Duquesne Light Co.
Beaver Valley Nuclear Station
P.O. Box 321
Shippingport, PA 15077

Entergy Operations, Inc.

Jagdish Barat
Entergy Operations
Grand Gulf Generating Station
P.O. Box 756
Port Gibson, MS 39150

Rajesh Gupta
Entergy Operations
Waterford 3 Station
P.O. Box B, Highway 18
Killona, LA 70066

John Martin
Entergy Operations
Arkansas Nuclear One
Route 3, Box 137G h
Russellville, AR 72801

James S. Rowe
System Engineer
Entergy Operations
Arkansas Nuclear One-Unit 2
Route 3 Box 137 G h
Russellville, AR 72801

K. R. Rao
Senior Staff Engineer
Entergy Operations
P.O. Box 31995
Jackson, MS 38286-1995

Distribution for Fatigue Report, Continued:

Florida Power Corp.

Mike Clary
Florida Power Corporation
Crystal River Power Plant
P.O. Box 219
15760 W. Powerline Street
Crystal River, FL 34428-6708

Tony Petrowsky
Florida Power Corporation
Mail Code NA1E, P.O. Box 219
15760 W. Powerline Street
Crystal River, Fla 34428-6708

Florida Power & Light Co.

Tom Luke
Florida Power & Light
700 Universe Boulevard
P.O. Box 14000
Juno Beach, FL 33408

Harry Paduano
Florida Power & Light
700 Universe Boulevard
P.O. Box 14000
Juno Beach, FL 33408

Steve Collard
Florida Power & Light
700 Universe Boulevard
Juno Beach, Florida 33458

R. Scott Boggs
Florida Power & Light
700 Universe Boulevard
Juno Beach, FL 33408-0420

Georgia Power Co.

Sang Lee
Southern Nuclear Operating Co.
Vogtle Units 1 and 2
P.O. Box 1295
Birmingham, AL 35201

Lewis Sumner (2 copies)
Edwin Hatch Units 1 & 2
P.O. Box 439
Baxley, GA 31513

Kerry Walton
Georgia Power Co.
Vogtle Units 1 & 2
P.O. Box 1600
Waynesboro, GA 30830

GPU Nuclear Corp.

George L. Lehmann
GPU Nuclear
1 Upper Pond Road
Parsippany, NJ 07054

Stephen D. Leshnoff
GPU Nuclear
1 Upper Pond Road
Parisppany, NJ 07054

Gulf State Utilities

Amir Shahkarami
River Bend Station
P.O. Box 220
St. Francisville, LA 70775

Houston Lighting & Power Co.

Sam Kannan
Houston Lighting & Power Co.
South Texas Project, EGS
P.O. Box 289
Wadsworth, TX 77483

Samuel B. Patel
Houston Lighting & Power Co.
South Texas Project, EGS
P.O. Box 289
Wadsworth, TX 77483

Distribution for Fatigue Report, Continued:

Illinois Power Co.

J. Puzauskas
Illinois Power Co.
RR3, Box 522
Bloomington, IL 61704

David Thuston
Illinois Power Co.
Clinton Power Station
P.O. Box 678
Clinton, IL 61727

Indiana/Michigan Power Co.

Tapan Chatterjee (2 copies)
Indiana/Michigan Power Co.
D.C. Cook Plant
One Cook Place
Bridgeman, MI 49106

Iowa Electric Light & Power Co.

David Dedic
Iowa Electric Light & Power Co.
Duane Arnold Energy Center
3277 DAEC Road
Palo, IA 52324

Michael McDermott
Iowa Electric Light & Power Co.
Duane Arnold Energy Center
3277 DAEC Road
Palo, IA 52324

Maine Yankee Atomic Power

Charles Eames
Main Yankee Atomic Power
P.O. Box 408
Wiscasset, ME 04578

Howard Jones
Main Yankee Atomic Power
P.O. Box 408
Wiscasset, ME 04578

Nebraska Public Power District

Ken Done
Nebraska Public Power District
1414 15th Street
Box 499
Columbus, NE 68602-0499

Edwin Brown
Nebraska Public Power District
Cooper Power Station
P.O. Box 98
Brownville, NE 68321

New York Power Authority

H. Y. Chang
New York Power Authority
123 Main Street
White Plains, NY 10601

Richard Drake
New York Power Authority
123 Main Street
White Plains, NY 10601

Bob Penny
New York Power Authority
123 Main Street
White Plains, NY 10601

Niagara Mohawk Power Corp.

Yang Soong
Niagara Mohawk Power Corp.
300 Erie Blvd West
Syracuse, NY 13202

Lee A. Klosowski
Niagara Mohawk Power Corp.
300 Erie Blvd. West
Syracuse, NY 13202

Distribution for Fatigue Report, Continued:

North Atlantic Energy Services Corp.

Brian Brown
Seabrook Generating Station
P.O. Box 300
Seabrook, NH 03874

Northeast Utilities

Prem Godha
Northeast Utilities
P.O. Box 270
Hartford, CT 06141

J. Ely
Northeast Utilities
P.O. Box 128
Waterford, CT 06385-0128

Tom Mawson
Northeast Utilities
P.O. Box 270
Hartford, CT 06141-0270

Northern States Power Co.

Terry Pickens
Northern States Power Co.
414 Nicollet Mall
Minneapolis, MN 55401

Jeffery H. Gehlhar (2 copies)
Northern States Power Co.
Prairie Island Plant
1717 Wakonade Dr. East
Welch, MN 55089

Omaha Public Power

Randy Lewis (FC-2-4ADM)
Omaha Public Power District
Ft.Calhoun Nuclear Station
P.O. Box 399
Ft.Calhoun, NE 68023

Ralph L. Phelps
Omaha Public Power District
444 S. 16th Street Mall
Omaha, NE 68102

Pacific Gas & Electric Co.

Henry Thailer
Pacific Gas & Electric Co.
P.O. Box 770000
33 Market-Rm. 1205 (Zip-94105)
Mail Code A10T
San Francisco, CA 94177

Paul Hirschberg
Pacific Gas & Electric Co.
333 Market Street.
Mail Code A1205
San Francisco, CA 94105

Mike Wright
Pacific Gas & Electric Co.
Diablo Canyon Power Plant
P.O. Box 56
Avila Beach, CA 93424

Pennsylvania Power & Light Co.

John Novak
Pennsylvania Power & Light Co.
Susquehanna Steam Electric Station
P.O. Box 467
Berwick, PA 18603

Lew Willertz
Pennsylvania Power & Light Co.
Two N. Ninth Street
Allentown, PA 18101

Jeffrey Weik
Pennsylvania Power & Light Co.
Two N. Ninth Street, M/S A6-3
Allentown, PA 18101

Distribution for Fatigue Report, Continued:

Philadelphia Electric Company

Bob Zong (4 copies)
965 Chesterbrook Blvd., M/C 63C-9
Wayne, PA 19087-5691

Public Service Electric & Gas Co.

Don Longo
Public Service Electric & Gas Co.
P.O. Box 236, N32
Hancocks Bridge, NJ 08038

Dilip Bhavnani
Public Service Electric & Gas Co.
P.O. Box 236
Hancocks Bridge, NJ 08038

C. P. Lashkari
Public Service Electric & Gas Co.
Salem Units 1 and 2
P.O. Box 236
Alloway Creek Neck Road
Habcocks Bridge, NJ 08038

Bill Maher
Public Service Electric & Gas Co.
Hope Creek Generating Station
Hancock's Bridge, NJ 08038

Rochester Gas and Electric Corp.

Jerry Bettle
Rochester Gas & Electric Corp.
89 East Avenue
Rochester, NY 14649-0001

John Fisher
Rochester Gas & Electric Corp.
89 East Avenue
Rochester, NY 14649-0001

Michael Saporito
Supervisor Materials Engineering
Rochester Gas & Electric Corp.
89 East Avenue
Rochester, NY 14649-0001

South Carolina Electric & Gas Co.

Bob Waselus
South Carolina Electric & Gas Co.
V.C. Summer Station
P.O. Box 88
Jenkinsville, SC 29065

Al Paglia
South Carolina Electric & Gas Co.
V.C. Summer Station
P.O. Box 88
Jenkinsville, SC 29065

Southern California Edison

Jennifer Hedrick
Southern California Edison Co.
23 Parker St.
Irvine, CA 92718

Riyad Qashu
Southern California Edison Co.
23 Parker St.
Irvine, CA 92718

Southern Nuclear Operating Co.

Kenneth Maynard
Southern Nuclear Operating Co.
42 Inverness Parkway Bin B456
Birmingham, AL 35242

Larry Matthews
Southern Nuclear Operating Co.
P.O. Box 1295
Birmingham, AL 35201-1295

Jerry Sims
Southern Nuclear Operating Co.
Farley Units 1 and 2
P.O Box 1295
Birmingham, AL 35201

Distribution for Fatigue Report, Continued:

Tennessee Valley Authority

Robert Phillips (3 copies)
Tennessee Valley Authority
Browns Ferry Nuclear Station
P.O. Box 2000
Decatur, AL 35602

Williams Goins (2 copies)
Tennessee Valley Authority
Sequoyah Power Station
P.O. Box 2000
Soddy-Daisy, TN 37865

R. W. Bibb
Tennessee Valley Authority
Watts Bar Nuclear Plant
10B-1A, P.O. Box 2000
Highway 68
Spring City, TN 37381

TU Electric

Craig Harrington
TU Electric
Comanche Peak Power Station
P.O. Box 1002
Glenn Rose, TX 76043

Paul Passalugo
TU Electric
Comanche Peak Power Station
Mail Zone C39
P.O. Box 1002
Glen Rose, TX 76043

Toledo Edison Co.

K. C. Prasad
Toledo Edison Co.
Davis-Besse Nuclear Generating Station
M/S 3045
5501 N. State Route 2
Oak Harbor, OH 43449

Theo Swim
Toledo Edison Co.
Davis-Besse Nuclear Generating Station
5501 North State Route 2
Oak Harbor, OH 43449

Union Electric Co.

Tim Herman
Union Electric Co.
Callaway Power Station
P.O. Box 620
Fulton, MO 65251

Richard Lutz
Engineer/NSSS Design
Union Electric Co.
P.O. Box 620
Fulton, MO 65251

Vermont Yankee Nuclear Power Corp.

Mike Metall
Vermont Yankee Nuclear Power Corp.
RD 5, Box 169, Old Ferry Road
Brattleboro, VT 03301

Virginia Power Co.

John Harrell
Virginia Power Co.
Innsbrook Technical Center, M/S IN3SW
5000 Dominion Blvd.
Glenn Allen, VA 23060

Keshab K. Dwivedy
Virginia Power Co.
5000 Dominion Blvd.
Glenn Allen, VA 23060

Joe Hegner
Virginia Power Co.
Innsbrook Technical Center, M/S IN2E
5000 Dominion Blvd.
Glenn Allen, VA 23060

Distribution for Fatigue Report, Continued:

David Roth
Virginia Power Co.
Innsbrook Technical Center, 3NW
5000 Dominion Boulevard
Glen Allen, VA 23060

Washington Public Power Supply System

C. R. Noyes
Washington Public Power Supply System
Mail Drop PE 23
3000 George Washington Way
Richland, WA 99352

Richard Moen
Washington Public Power Supply System
3000 George Washington Way
MD PE 22
Richland, WA 99352-1617

Wisconsin Electric Power Co.

Mike Woznicki
Wisconsin Electric Power Co.
231 W. Michigan Street
Milwaukee, WI 53201

Ken Arneson
Wisconsin Electric Power Co.
231 W. Michigan Ave.
Milwaukee, WI 53201

Wisconsin Public Service Corp.

Chuck Tomes
Wisconsin Public Service Corp.
600 N. Adams
P.O. Box 19002
Green Bay, WI 54307-9002

Wolf Creek Nuclear Operating Corp.

Glenn Neifef
Wolf Creek Nuclear Operating Corp.
P.O. Box 411
Burlington, KS 66839

Zarif Botros
Wolf Creek Nuclear Operating Corp.
P.O. Box 411
Burlington, KS 66839

Yankee Atomic Electric Co.

Enrico J. Betti
Yankee Atomic Electric Company
580 Main Street
Bolton, MA 01740

NSSS Vendors, Consultants and Universities

Chris L. Hoffman
ABB CE Nuclear Service Co.
1000 Prospect Hill Road
P.O. Box 500
Windsor, CT 06095-0500

Owen Hedden
ABB CE Nuclear Service Co.
1000 Prospect Hill Road
Windsor, CT 06095-0500

S. Weinman
American Society Mechanical Engineers
345 East 47th Street
New York, NY 10017

Janek S. Porowski
AEA O'Donnell Inc.
241 Curry Road
Pittsburgh, PA 15236

John Hechmer
Babcock & Wilcox
91 Stirling Avenue
(BW562A)
Barberton, OH 44203

A. Van Der Slys
Babcock & Wilcox Research Center
1562 Beeson Street
Aliance, OH 44601

Distribution for Fatigue Report, Continued:

James Williams
B&W Nuclear Technologies
P.O. Box 10935
Lynchburg, VA 24506-0935

David Church
General Dynamics
Electric Boat Division
Eastern Point Road
Groton, Conn. 06340

F. P. Ford
General Electric CR&D
1 River Road, Bldg. K-1, Rm 3A37
Schenectady, NY 12301

Wayne A. Pavinich
Grove Engineering
9040 Executive Park Dr., Suite 218
Knoxville, TN 37923

F.L. (Bill) Cho
IL Dept. of Nuclear Safety
1035 Outer Park Drive
Springfield, IL 62704

Tsuguyasu Wada
Michigan Advanced Materials
5141 Platt Road
Ann Arbor, MI 48108

Bill O'Donnell (3 copies)
O'Donnell Consulting Engineers, Inc
3611 Maplevue Drive
Bethel Park, PA 15102

Robert L. Cloud & Assoc.,Inc.
2150 Shattuck Ave., Suite 1200
Berkeley, CA 94704

Ralph Hill
Science Applications International Corp.
20300 Century Blvd., Suite 200-B
Germantown , MD 20874

Art Deardoff (5 copies)
Structural Integrity Associates
3150 Almaden Expressway, Suite 145
San Jose, CA 95118-1217

Jay Smith (2 copies)
Structural Integrity Associates
3150 Almaden Expressway, Suite 145
San Jose, CA 95118-1217

Peter C. Riccardella
Structural Integrity Associates
3150 Almaden Expressway, Suite 145
San Jose, CA 95118-1217

Lynn Connor
STS
3 Metro Center, Suite 610
Bethesda, MD 20814

Don Landers
Teledyne Engineering Services
10 forbes Road
Woburn, MA 01801-2103

Peter K. Liaw
Dept. of Material Science & Eng.
University of Tennessee
Knoxville, TN 37996-2200

S. Chattopadhyay
Dept. of Mechanical Engineering
University of Vermont
Burlington, VT 05405-0156

Martin Prager
Welding Research Council
345 E. 47th Street
New York, NY 10017

Warren H. Bamford
Westinghouse Energy Center
Energy Systems
STC 701-207
P.O. Box 2728
Pittsburgh, PA 15230-2728

Distribution for Fatigue Report, Continued:

A.K. Dhalla
Westinghouse Electric Corp. NATD
P.O. Box 355
Pittsburgh, PA 15230-0355

D. P. Jones
Westinghouse Bettis
P.O. Box 79 (ZAP 34E)
West Miflin, PA 15122-0079

Wayne C. Kroenke
Westinghouse Bettis
P.O. Box 79/ZAP35C
West Miflin, PA 15122

Mark Gray
Westinghouse Electric Corp. NATD
BAY EC511 East
P.O. Box 355
Pittsburgh, PA 15230

Hong Gong
Westinghouse Electric Corp.
Machinery Apparatus Operation
P.O. Box 1021
Schenectady, NY 12301

Foreign Contacts

M. T. Flaman
Ontario Hydro Research
800 Kipling Ave., KB223
Toronto, Ontario M8Z554
Canada

Richard Barnes
ANRIC Enterprises
38 Primrose Ave.
Etobicoke, Ontario M8V1P8
Canada

Denis Acker
C.E.A/CEN Saclay
Service d'Etudes Mecaniques
et Thermiqies
91 191 Gif/Yvette
Cedex France

Claude Faidy
E.D.F - septen-ms
12 Av. Dutrievoz
69628 Villeurbanne
Cedex France

Suren Bhandari
Framtome
Tour Fiat. CEDEX 16
92084 Paris-LA Defense
France

Dr. Klaus Rahka
VTT, Technical Research Centre of Finland
- Metals Laboratory
Kemistintie 3, P.O. Box 26
SF-02151 ESPOO, Finland

John Hickling
MPA Stuttgart
Pfaffenwaldring 32
D-7000 Stuttgart 80 (Vaigingen)
Germany

Professor Yasuhide Asada
University of Tokyo
Mechanical Engineering Dept.
7-3-1 Hongo, Bunkyo-ku
Tokyo 113
Japan

Makkoto Higuchi
Ishujawajima-Harima
Heavy Industries Co., Ltd.
1. Shin-Nakahara-Cho
Isoho-Ku, Yokohamaa 235
Japan

Kunihiro Iida
Dept of Mechanical Engineering
Shibaura Inst of Technology
3-9-14, Shibaura, Minato-Ku
Tokyo, 108
Japan

Distribution for Fatigue Report, Continued:

Ishujawajima-Harima
Heavy Industries Co., Ltd
1. Shin-Nakahara-Cho
Isogo-Ku. Yokohama 235
Japan

Kazuo Kishida
Ishikawajima-Harima
Heavy Industries Co., Ltd.
1, Shin-Nakahara-Cho
Isogo-Ku, Yokohama 235, Japan

Hitoshi Nakamura
CRC Research Institute,Inc.
Section Manager, Sec. No.3, Structural Engineering Dept.
1-3-D16, Nakase, Mihama-ku
Chiba-shi, Chiba 266-01
Japan

Dr. Hioshi Sakata
Hitachi, Ltd. Mech. Eng. Research Lab
1-1 Saiwai-cho 3-chome, Hitachi-shi
Ibaraki-ken, 317 Japan

Dr. Wataru Sagawa
Mgr., Nuclear Plant Maintance Tech.
Hitachi
1-1, Saiwai-cho 3-chrome, Hitachi-shi
Ibaraki-ken, 317 Japan

T. Shoji
Tohoku University
Faculty of Engineering
Aramaki Aoba, Aobaku
Sendai 980
Japan

Michiaki Yoshino
CRC Research Institute, Inc.
Manager, Structural Engineering Dept.
1-3-D16, Nakase, Mihama-ku
Chiba-shi, Chiba 266-01
Japan

David Worswick
AEA Industrial Technology
Risley laboratory
Risley
Warrington WA36AT
United Kingdom

Sandia (Internal)

MS 0736 N. R. Ortiz (6400)
MS 0744 W. A. von Riesemann (6403)
MS 0741 A. K. Moonka (6471)
MS 0741 J. M. Clauss (6471) (2 copies)
MS 0741 J. T. Nakos (6471) (15 copies)
MS 0741 S.T. Rosinski (6471)
MS 0899 Technical Library (7141) (5 copies)
MS 0619 Technical Publications (7151)
MS 9018 Central Technical Files (8523-2)
MS 0100 Document Processing for DOE/OSTI (7613-2) (10 copies)